Titre: Title:	Stall Margin Prediction and Improvement for Mixed Flow Compressors
Auteur: Author:	Noureddine Djeghri
Date:	2016
Type:	Mémoire ou thèse / Dissertation or Thesis
Référence: Citation:	Djeghri, N. (2016). Stall Margin Prediction and Improvement for Mixed Flow Compressors [Thèse de doctorat, École Polytechnique de Montréal]. PolyPublie. https://publications.polymtl.ca/2280/

URL de PolyPublie: PolyPublie URL:	https://publications.polymtl.ca/2280/
Directeurs de recherche: Advisors:	Huu Duc Vo
Programme: Program:	Génie mécanique

UNIVERSITÉ DE MONTRÉAL

STALL MARGIN PREDICTION AND IMPROVEMENT FOR MIXED FLOW COMPRESSORS

NOUREDDINE DJEGHRI

DÉPARTEMENT DE GÉNIE MÉCANIQUE

ÉCOLE POLYTECHNIQUE DE MONTRÉAL

THÈSE PRÉSENTÉE EN VUE DE L'OBTENTION

DU DIPLÔME DE PHILOSOPHIAE DOCTOR

(GÉNIE MÉCANIQUE)

AOÛT 2016

UNIVERSITÉ DE MONTRÉAL

ÉCOLE POLYTECHNIQUE DE MONTRÉAL

Cette thèse intitulée :

STALL MARGIN PREDICTION AND IMPROVEMENT FOR MIXED FLOW COMPRESSORS

présentée par : DJEGHRI Noureddine

en vue de l'obtention du diplôme de : Philosophiae Doctor

a été dûment acceptée par le jury d'examen constitué de :

M. REGGIO Marcelo, Ph. D., président

M. VO Huu Duc, Ph. D., membre et directeur de recherche

M. GUIBAULT François, Ph. D., membre

M. GHALY Wahid, Ph. D., membre externe

ACKNOWLEDGEMENTS

First of all, I would like to express my deep gratitude to my advisor Huu Duc Vo, who gave me the chance to work with him on this very exciting but complex topic about rotating stall inception and its control. Without his guidance, support, and help, this project would not be possible.

I am also grateful to our industrial sponsor for their financial support.

I also thank *Calcul Canada* for allowing me to run most of the unsteady simulations, presented in this thesis, on their cluster computer *Cottos* as well as the assistance received from *Calcul Québec'* team on many occasions when it was needed.

I would also, like to express my appreciation for my thesis committee, consisting of Dr. Marcelo Reggio, Dr. Francois Guibault, Dr. Wahid Ghaly, and Dr. Richard Gourdeau, for the time they have devoted to reading and evaluating my thesis.

Finally, the unconditional, financial and moral, support of my parents is without doubt the main impetus for advancing in my studies.

RÉSUMÉ

Les instabilités aérodynamiques dans les compresseurs sous la forme du décrochage tournant (rotating stall) et du pompage (surge) sont des phénomènes connus qui limitent l'enveloppe d'opération des turbines à gaz. Le décrochage tournant est caractérisé par la formation d'une cellule d'écoulement de vitesse déficiente qui tourne à une fraction de celle du compresseur alors que le pompage est une oscillation axisymétrique de l'écoulement à travers la turbine à gaz. Ce dernier mène à une chute soudaine de la puissance du moteur et entraîne souvent des dommages au moteur. Une marge de sécurité doit être mise entre le point d'opération et le point de pompage à la même vitesse de rotation, et est connue sous le nom de 'surge margin'. Comme le décrochage tournant dans le compresseur est souvent à l'origine du pompage dans le moteur, le surge margin est l'équivalent du 'stall margin' (ou marge au décrochage tournant) lorsqu'on considère le compresseur tout seul. Vu son importance, on a besoin de pouvoir prédire le point de décrochage (tournant) durant la phase de conception du compresseur afin de pouvoir déterminer avec précision le stall margin. Il est aussi nécessaire de développer des stratégies efficaces pour retarder le point de décrochage afin d'augmenter un stall margin insuffisant sans pénaliser la performance du compresseur au point de design. Au niveau de la prédiction du décrochage tournant, la recherche récente a proposé des critères prometteurs liés à l'écoulement de jeu d'aube pour prédire pour des compresseurs axiaux le décrochage tournant de type pip initié par des perturbations à courte longueur d'onde, qui est le type le plus commun dans les compresseurs modernes. Les traitements de carter, sous la forme de fentes dans le carter au-dessus des rotors, ont été étudiés depuis plusieurs décennies comme une technologie de suppression passive du décrochage tournant. Cependant, leurs conceptions ont été empiriques et augmentent souvent le stall margin au dépend du rendement optimal du compresseur. Bien que certain travaux récents ont indiqué la possibilité d'obtenir des traitements de carter par fentes axiales qui peuvent prévenir la perte du rendement optimal dans les compresseurs axiaux, il n'existe aucune règle de conception systématique pour permettre d'optimiser l'augmentation du stall margin tout en prévenant la perte du rendement optimal. De plus, la grande majorité de la recherche sur ces deux aspects a été faite pour le compresseur axial, qui est le type le plus utilisé dans les moteurs d'avion. Toutefois, presqu'aucun travail n'a été fait sur le compresseur à écoulement mixte qui commence à retrouver son chemin dans les nouveaux petits moteurs d'avion. Ce type de

compresseur est un hybride entre le compresseur axial et le compresseur centrifuge et donne une augmentation de pression par étage plus importante que celui des compresseurs axiaux.

Les objectifs de la présente recherche consistent à déterminer des critères pour prédire le décrochage tournant de type pip dans les compresseurs à écoulement mixte et d'établir des règles de conception préliminaires pour produire un traitement de carter qui augmenterait significativement le stall margin sans pénaliser le rendement optimal pour ce type de compresseurs. Les résultats de cette recherche aideront le processus de conception des compresseurs à écoulement mixte. Une approche numérique sur un rotor de compresseur à écoulement mixte de moteur d'avion a été choisie pour rencontrer les objectifs. Pour le premier objectif, des simulations numériques de l'écoulement (CFD) ont été faites jusqu'à la limite de convergence de la caractéristique du rotor. Selon le montage numérique, ce point représenterait le point de décrochage tournant de type pip. L'analyse de ce point démontre qu'un des deux critères de prédiction du décrochage tournant de type pip récemment proposés pour les compresseurs axiaux peut être utilisé pour prédire ce type de décrochage tournant dans les compresseurs à écoulement mixte. Ce critère est l'alignement de l'interface entre l'écoulement d'entré et l'écoulement de jeu d'aube avec la plaine du bord d'attaque au bout du rotor et peut être évalué avec des simulations CFD à un passage d'aube de bas coût souvent utilisées durant la phase de conception. Des simulations avec micro-injection au bout du rotor démontrent aussi que le retardement de ce critère augmente le *stall margin*.

Une étude numérique plus complexe a été ensuite faite pour déterminer les règles de conception préliminaires pour un traitement de carter optimisé pour des compresseurs à écoulement mixte. En se basant sur la revue de littérature pour les compresseurs axiaux, un traitement de carter composé de fentes axiales semi-circulaires inclinées a été choisi comme configuration partante ayant un potentiel d'augmentation signifiant du stall margin avec un minimum de perte du rendement optimal. Partant de cette configuration de base, une nouvelle stratégie de calcul a été conçue pour permettre de faire l'étude paramétrique la plus étendue à date de traitements de carter en terme du nombre de paramètres de design, tous compresseurs confondus. Cette stratégie implique un grand nombre de simulations CFD en régime permanent à bas coût couplé à un nombre très limité de simulations CFD en régime transitoires à haut coûts pour valider quelques points d'opération importants. Cette étude a identifié las paramètres géométriques les plus importants et a produit un design avec une grande amélioration du stall margin sans perte du

rendement optimal. Les résultats montrent que les paramètres de design du traitement de carter avec le plus grand impact sur la stall margin et le rendement optimal sont: rapport d'ouverture, angle d'inclinaison, longueur axiale des fentes et leur position axiales. De plus, il est fortement possible que ces règles de conception préliminaires s'appliqueraient aussi pour les compresseurs axiaux.

ABSTRACT

Compressors are known to exhibit aerodynamic instabilities in the form of rotating stall and surge that limit the operational envelope of gas turbine engines. Rotating stall is characterized by the formation of a flow cell with a velocity deficiency that rotates at part of the compressor speed while surge is an axisymmetric flow oscillation across the entire engine. The latter leads to a sudden drop in engine performance and often to engine damage. A safety margin, often referred to as 'surge margin' is provided between the compressor operating point and the surge point at the same rotating speed. Since compressor rotating stall usually leads to engine surge, surge margin is really equivalent to 'stall margin' (or rotating stall margin) when considering the compressor alone. Given its importance, there is a need to be able to predict the (rotating) stall point at the compressor design stage, in order to accurately predict the stall margin. It is also necessary to develop effective stall suppression technologies that can delay the stall point to extend insufficient stall margin and do so without degrading compressor performance near its design point. In terms of stall prediction, recent research proposed promising criteria for axial compressors linked to tip clearance flow to predict short length-scale (spike) stall inception, which is the most commonly found route to rotating stall in modern compressors. Casing treatments, in the form of grooves and slots placed on the shroud over the rotors, have been studied for several decades as a passive stall suppression technology. However, their designs have been arbitrary and often trade compressor peak efficiency for stall margin improvement. While some recent works have shown the possibility of obtaining slots casing treatments that prevent loss in efficiency on axial compressors, there are no systematic design rules to optimize stall margin improvement while preventing peak-efficiency loss. Furthermore, the large majority of the researches on both of these aspects have so far been conducted on axial compressors, which is the most widely used type in aero-engines. However, virtually no such research has been carried out on mixed flow compressors that have found their way into recent small aero-engines. This type of compressor is a hybrid between an axial and a centrifugal compressor, providing higher stage pressure ratio than axial compressors.

The objectives of this research are to determine predictive criteria for spike stall inception for mixed flow compressors as well as to establish preliminary design rules to produce a casing treatment for this type of compressor that can improve stall margin significantly without

penalizing peak efficiency. The results from this will help the design phase of mixed flow compressors. A computational approach on an aero-engine mixed flow rotor was chosen to reach these objectives. To address the first objective, CFD simulations were carried out up the speedline to the convergence limit which, based on the computational setup, represents the predicted spike stall inception point. Analysis of this point shows that one of the two recently proposed stall criteria for axial compressors can be used to predict spike stall inception in mixed flow compressors. This criterion is the alignment of the incoming/tip clearance flow interface with the rotor leading edge plane at the blade tip and can be evaluated with low-cost single blade passage CFD simulations commonly used in the design phase. Micro tip injection simulations also show that the delay of this criterion improves stall margin.

A more complex computational study was then carried out to determine preliminary design criteria for optimized casing treatment on mixed flow compressors. Based on the literature review for axial rotors, a semi-circular axial skewed slot casing treatment was chosen as the starting configuration with the best potential for stall margin improvement with low peak efficiency loss. Using this baseline configuration, a new computational strategy was set up to allow for carrying out the most extensive slot casing treatments parametric study so far in term of number of design parameters considered for any type of compressor. It involves large numbers of inexpensive steady-state CFD simulations coupled with a very limited number high-cost unsteady CFD simulations for validation of important operating points. This study identified the most important geometrical design parameters and arrived at a design with large stall margin improvement without loss in peak efficiency. The results show that the design parameters with the largest impact on stall margin improvement and peak efficiency are: open area ratio, slot skew angle, slot axial length and slot axial position. Moreover, these casing treatment preliminary design rules may likely be applicable to axial compressors as well.

TABLE OF CONTENTS

LIST OF TABLES

LIST OF FIGURES

LIST OF SYMBOLS AND ABBREVIATIONS

Abbreviations

SM	Stall margin
OAR	Open Area Ratio
CGCT	Circumferential Groove Casing Treatment
BTLV	Blade Tip Leakage Vortex
EAR	Entire Annular Recess

Symbols

p	Static pressure
Pt	Stagnation (or total) pressure
Tt	Stagnation (or total) temperature
$\dot{m}_{corr}$	Corrected mass flow
η	Total-to-total isentropic efficiency

LIST OF APPENDICES

CHAPTER 1 INTRODUCTION

1.1 Introduction

It is well known that the operational envelope of a gas turbine engine is constrained by the compression system air-flow instability which can lead to a severe drop in engine power and incur engine damage. Therefore, compressor aerodynamic stability is a major concern for the gas turbine industry.

The operating range of a compressor is described by a plot of the pressure rise characteristic versus mass flow rate, called a *speedline*, at different speeds, often referred to as a compressor map, as shown in figure 1.1. At a particular speed, if the mass flow rate is reduced, the pressure rise across the compressor increases until a point, usually called *stall point*, where an aerodynamic instability called *rotating stall* occurs. This instability is described by the formation of a cell of stalled fluids with meridional velocity deficiency, called a *rotating stall cell*, which rotates at a fraction of the compressor rotor speed, and which is usually accompanied by a sudden drop in pressure rise. When coupled to the other main components of a gas turbine, namely the combustor and the turbine, the resulting failure to maintain the pressure rise across the compressor mean that the high-pressure gas in the combustor volume can flow backward toward the front of the compressor [1]. This leads to an axisymmetric flow oscillation across the entire engine called surge, which is much more damaging in terms of performance and hardware than rotating stall itself. Since rotating stall is usually the trigger for surge, research in compressor aerodynamic instabilities, including the present one, focus on rotating stall control.

As shown on the compressor map depicted in figure 1.1, the line joining the stall point of each compressor speed is often referred to as the *surge line*, while the line that runs through the design point along which the compressor operates as the engine accelerates or decelerates is called the *running line* or *operating line*. The position of this line is set by the turbine. Since the shape of the running line changes with the rate of acceleration and that of the surge line changes with operational wear and with any flow non-uniformity in the incoming airflow, such as cross-wind or during aircraft maneuvers, a safety margin called *surge margin*, is left between the running and surge lines. However, the presence of the surge margin often means that the compressor is not

operating at the point of optimum pressure rise and/or optimum efficiency which can lie close to the stall point. Delaying stall inception to lower mass flow rate also means that the operating point could approach or reach this point while maintaining the same stall margin resulting in reduction in the engine weight (by reducing the number of compressor stages) and fuel consumption.

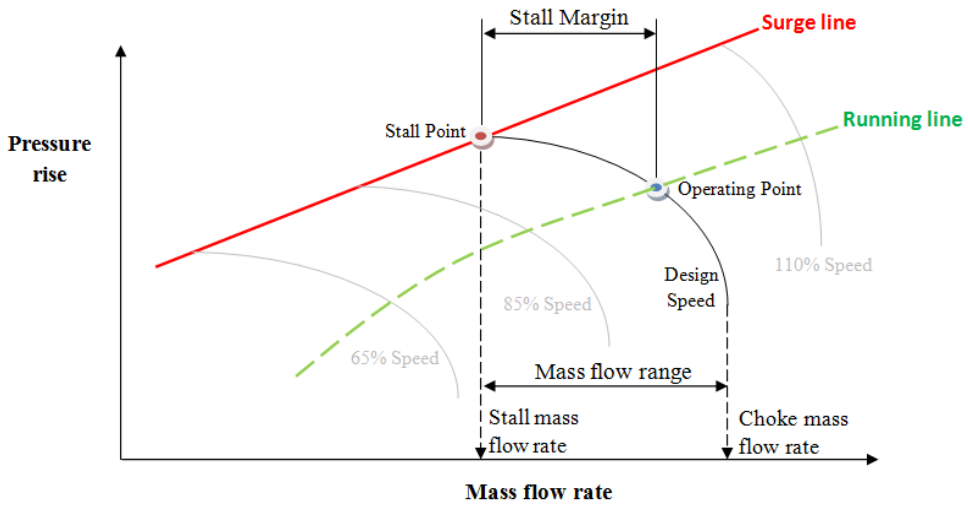

Figure 1.1: Compressor map

A good understanding of the physical processes responsible for the rotating stall contributes greatly to the development of optimal stall inhibition technology. Research into stall suppression technologies have been carried out for several decades. However, the development of these technologies has mostly been empirical. In fact, although there has been significant progress into rotating stall inception research, the phenomenon it still not fully understood yet. As a result, the existing stall suppression technologies often involves a trade-off between stall margin improvement and efficiency penalty at the design point, where the engine spends most of its operating time, and there are at present no general rules for their design to limit or eliminate this trade-off.

The idea behind the current research is to use the latest understanding in rotating stall inception and results from past stall suppression research to come up with general design rules to increase

stall margin without losing efficiency, especially around the design point. As illustrated in figure 1.2, the flow in even an axial compressor rotor blade passage is highly three-dimensional and quite complex. The first feature is the boundary layers on the blade and endwall surfaces that migrate normal to the streamwise direction under the effects of the blade passage turning and the centrifugal and coriolis forces to create *secondary flows*. Unlike the flow in a turbine blade passage, the positive pressure gradient and possible presence of shock (sudden pressure increase) can cause these boundary layers to separate either on the blade (blade stall) or in the corner (corner stall) both of which can in theory lead to rotating stall. The second feature is the flow through the clearance between the rotor tip and casing, called *tip clearance flow* or *tip leakage flow*, which interacts with the incoming flow to form a three-dimensional vortex with both low streamwise velocity and low relative total pressure in the tip region, producing a blockage that reduces the flow area and limits the diffusion of the flow through the blade passage. Research have pointed to tip clearance flow as the first responsible for the rotating stall inception, in which case the compressor is usually referred to as a *tip critical* compressor. Modern compressor blade design technology usually insures that boundary layer separation is not an issue, such that most modern compressor seem to be tip critical compressors. The current research will focus on stall suppression technologies as applied to tip critical compressors.

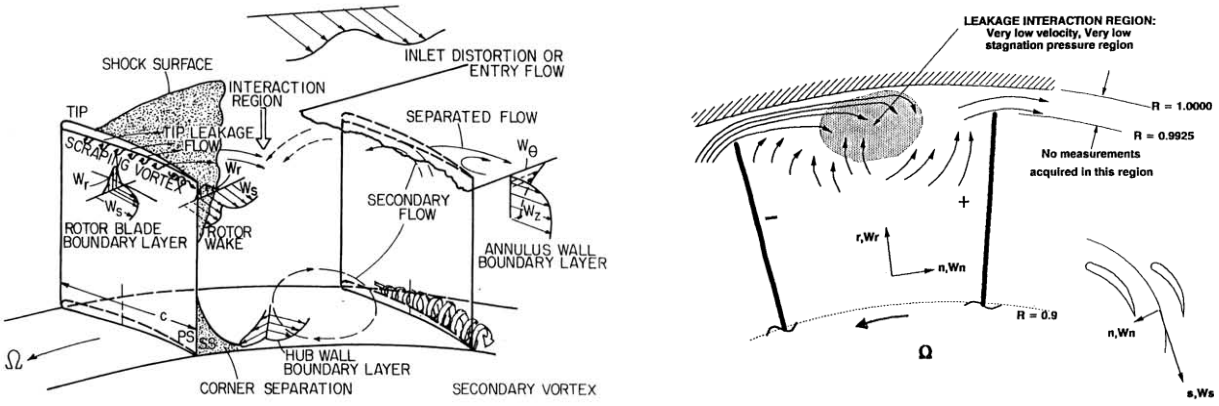

Figure 1.2: Axial compressor flow field: (a) three-dimensionality of the flow, (b) tip clearance flow (Lakshminarayana's book [2])

1.2 Compressor rotating stall inception

There are two known types of rotating stall inception: long length-scale (*modal*) and short length-scale (*spike*) stall inception. First theorized by Moore and Greitzer [3] and later shown experimentally, modal stall inception is characterized by the relatively slow growth of a small usually full-span disturbance of long circumferential wavelength into a fully developed rotating stall cell within 10 to 40 rotor revolutions. This disturbance rotates at roughly half the rotor speed without changing speed till the final establishment of the rotating stall cell. This is illustrated on the left plot of figure 1.3 and shown by stacked velocity traces from equally spaced probes around the compressor circumference. Modal stall has been shown to occur at or slightly past the zero-slope peak of the total-to-static pressure rise characteristics (speedline). Moore and Greitzer [3] showed that a positive slope of the total-to-static speedline means negative damping of naturally occurring perturbations causing them to grow into rotating stall. It is thus basically an instability of the entire compression system and seems to be only related to the compressor rotor tip clearance flow in so as much as how it affects the shape of the speedline through mixing losses and tip blockage [4]. The relatively slow growth of the perturbations into rotating stall implies that they can be detected and low-power counter perturbations can be applied in real time to negate their growth while their amplitude is still small. Several experiments [5, 6] have shown success for this concept, at least for a single or a small number of axial stages. Since this technology is only applied at the stall point there should be no effect on the design point performance.

However, most modern compressors stall through spike stall inception, which was discovered by Day [7] in 1993. It is characterized by the appearance of a large amplitude short length-scale disturbance (‘spike’) at the rotor tip, as illustrated on the left plot of figure 1.4, which grows very rapidly into a fully developed rotating stall cell within two to five rotor revolutions. Spike stall inception occurs at the negative slope of the total-to-static speedline, before the conditions (zero-slope) associated with modal stall inception. The short time scale involved in spike stall inception renders real-time detection and suppression virtually impossible with current technology and one must thus rely on passive techniques. However, these techniques are also active away from the stall point and may thus adversely affect compressor performance near the design point, which underlines the importance of studying and optimizing these techniques. While the true

mechanism behind spike stall inception is not yet known, a promising explanation was provided by Vo et al. [8] based on tip clearance flow. They postulate that two threshold flow events must be both present for spike disturbances to form and thus spike stall inception to occur. These are tip clearance flow spillage below the leading edge (LE) rotor blade tip, and flow reversal ("backflow") of tip clearance fluid below the rotor trailing edge (TE) blade tip. Although other recent research tend to support this hypothesis, it has not been fully confirmed and is too recent to be taken into consideration for most of the literature on stall suppression technologies. This hypothesis will provide the starting point for the current research into optimizing suppression technologies for spike stall inception.

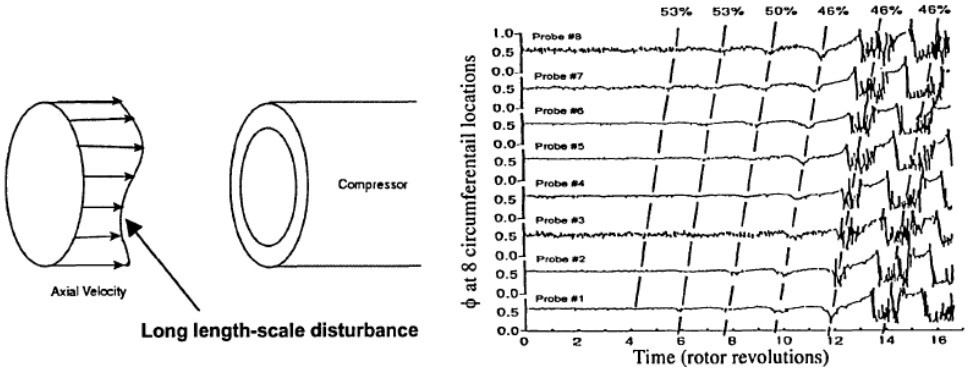

Figure 1.3: Modal stall inception and associated hot-wire (axial velocity) trace [7]

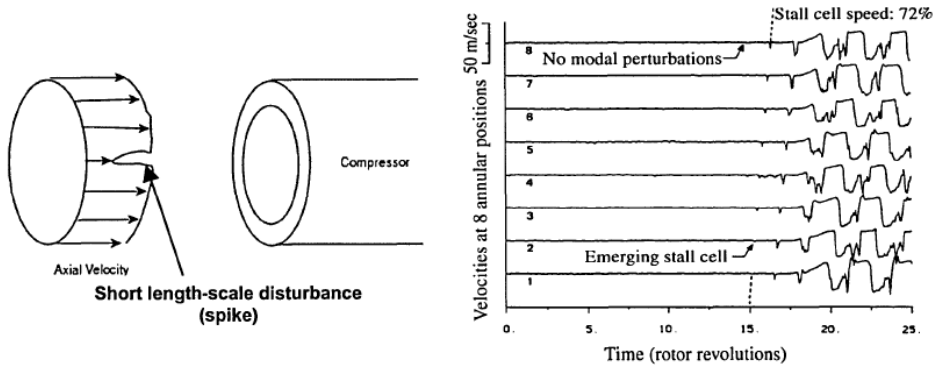

Figure 1.4: Spike stall inception and associated hot-wire (axial velocity) trace [7]

1.3 Stall suppression technologies

The two most promising technologies for suppressing rotating stall in tip-critical compressors are casing treatment and tip injection. Casing treatment is the most commonly applied technique and involves putting slots, grooves or recessed vane in the outer casing, above the tips of compressor rotor blades. Over the last 40 years, various forms of casing treatment have been tested for improving endwall flow and enhance compressor stability as depicted in figure 1.5. Slots and circumferential grooves casing treatments afford a path for flow to recirculate in both axial direction from the rear to the front near blade leading edge guided by the streamwise pressure gradient and in circumferential direction from the pressure side to suction side while tip injection provides additional streamwise momentum to the endwall flow. While their developments have mostly been by trial and error, it is now recognized that all casing treatments forms (slots, grooves or tip injection) energize the endwall flow field. For example slots casing treatments remove low momentum fluid at the rear and blow it at the front. Previously, the main drawback that casing treatments faced was the loss in compressor peak efficiency which is found to be proportional to stall range increase. Recently, some researchers reported that slots casing treatment placed in a more forward position over an axial compressor rotor may operate without loss in efficiency. However, there are no systematic design rules for casing treatment to achieve lossless casing treatment with acceptable stall margin improvement. In the absence of a detailed understanding of the flow mechanisms behind rotating stall and how stall inhibition techniques such as casing treatments affect these mechanisms, such design rules are essential to the effort of designing optimal casing treatment. Since casing treatment usually involve highly unsteady flows that required extensive simulation time and resources, even a computational parametric study to obtain such rules have so far been too expensive to be contemplated. Tip injection involves injection of high-speed flow near the casing of the compressor to delay stall, as illustrated in figure 1.6. While this technique has shown success [9] the amount of air required in traditional tip injection, which would have to be taken from the rear of the compressor, will penalize engine efficiency. This factor and the mechanical integration involve in terms of piping and valves may explain why this technique has been restricted to the laboratory. Recent research into micro-injection [10, 11], in which a very small amount of injected air aimed almost exclusively at the tip clearance region, has shown very promising results and opens the door to

this technology being used with no or negligible engine performance loss. However, the possibility of clogging and associated preventive maintenance requirements remains a hurdle for the practical implementation of micro-injection technology.

Given the practical inconvenience of tip injection technology, this research will place more emphasis on pursuing casing treatment technology.

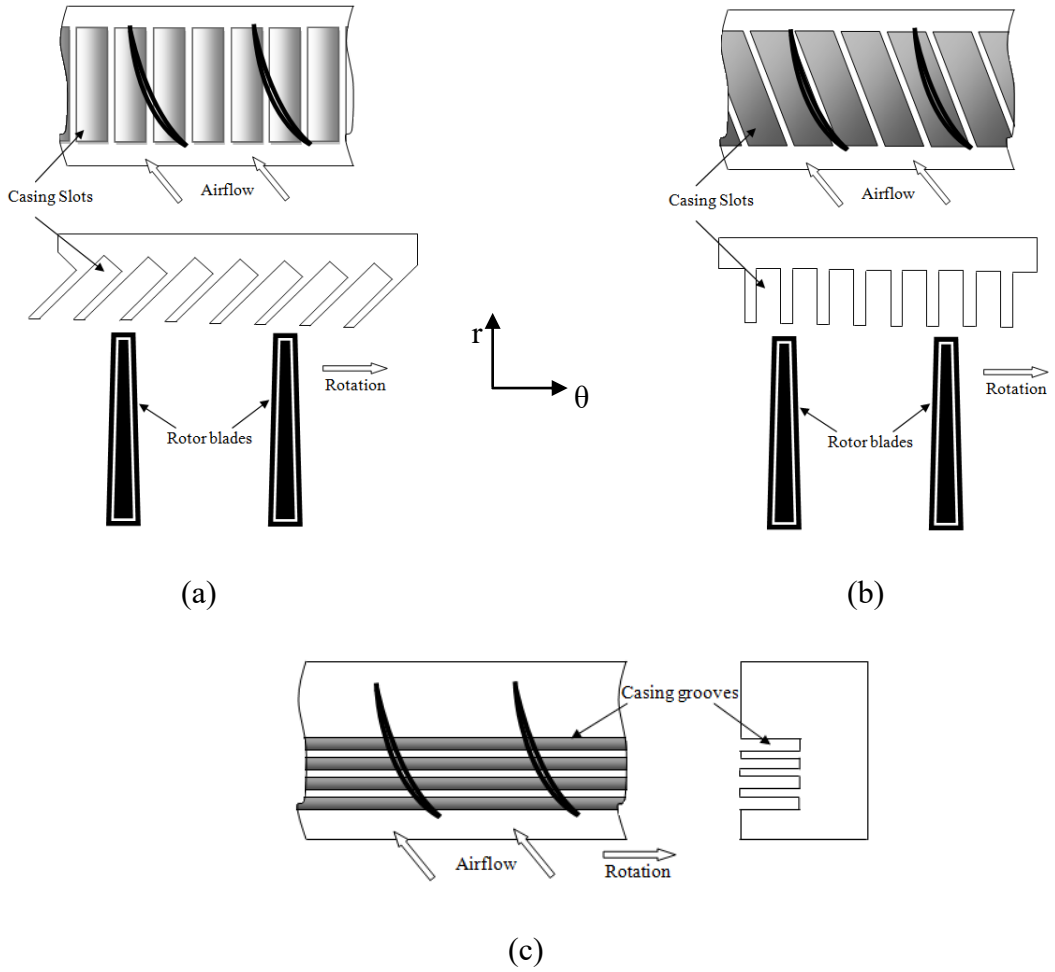

Figure 1.5: Different Casing treatment configurations (a) Axial-skewed slots casing treatment, (b) Blade angle slots casing treatment, (c) Circumferential grooves casing treatment

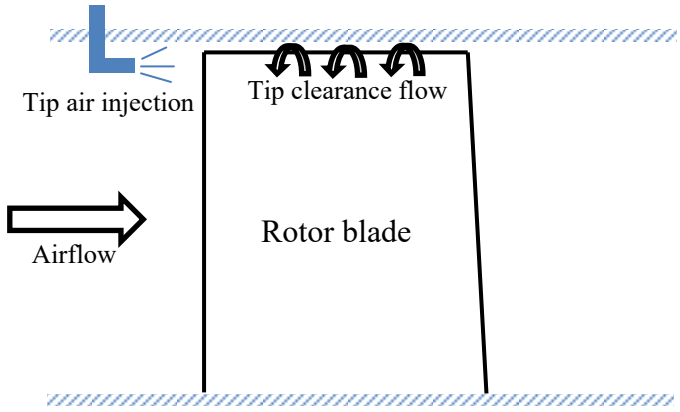

Figure 1.6: Tip air injection principle

1.4 Mixed-flow compressors

Continuous flow (turbomachinery) compressors usually come under two types: axial and centrifugal compressors. The axial compressor stage is composed of a rotor and a stator across which the fluid is mainly flowing in the axial direction with very little change in mean radius. On the other hand, a centrifugal compressor stage is composed of an impeller across which the fluid enters axially but goes through a large change in radius and typically exits in the radial direction with a very large amount of swirl. A diffuser is then used to turn the flow back into the axial direction. The large radius change implies that centrifugal compressors can deliver much higher pressure ratio per stage than axial compressors, but the flow in them is much more complex with higher levels of aerodynamic losses (lower compressor adiabatic efficiency). As such, the axial compressor has so far been widely used in aero-engines for higher efficiency at the cost of using many more stages. The wider aeronautical application of axial compressors coupled with the relatively simpler flow field means that the majority of research into stall inception and stall suppression technologies concentrated on axial compressors.

A hybrid design between the axial compressor and the centrifugal compressor, called *mixed flow compressor*, has found its way into recent small gas turbine engines. As illustrated in figure 1.7, it is similar to an axial compressor with the exception that it has a larger chord with a more

significant change in mean flow radius across the rotor. As such, the rotor would have a much lower aspect ratio and deliver significantly higher pressure ratio per stage than axial compressors, allowing for lower stage count. Inversely, the change in radius renders the flow relatively more complex with more radial displacement of low-velocity blade boundary layer fluid toward the blade tip and as such increases tip loss and lowers efficiency. There is virtually no research carried out on this type of compressor. The only exception is the recent empirical study by Qiang et al. [12] of casing grooves on a mixed flow compressor. Thus, there is a need to establish stall prediction capability and casing treatment design methods/rules for this type of compressor that may, in the latter case, be also applicable to axial compressors.

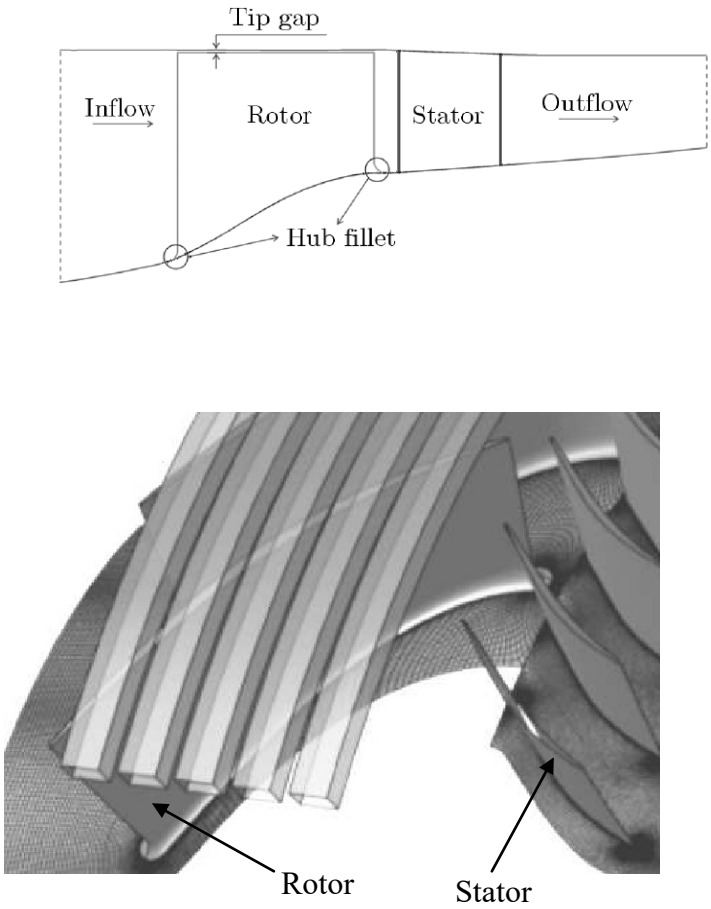

Figure 1.7: Meridional and 3D view of a mixed flow compressor stage [12]

1.5 Research questions

The relevant research questions for the current project are threefold:

- What are the stall criteria for mixed flow compressors?
- Can we design a casing treatment for a mixed flow compressor to increase its surge margin without negative impact on peak efficiency?

1.6 Thesis objectives

Based on the above research questions, the objectives of the current project are:

1) Determine stall prediction criteria for mixed flow compressors
2) Provide preliminary casing treatment design rules for mixed flow compressors to enhance stall margin without loss in compressor efficiency around the design point.

To meet these objectives, a literature review on past research into stall inception mechanism and stall suppression technologies for axial compressors is first carried out and assessed. Simulations are then carried out on a modern aircraft mixed flow compressor rotor geometry to establish the stall criteria for this type of compressor. Finally, a baseline casing treatment geometry is proposed for this compressor rotor based on past research into axial compressors. A new method is then devised to efficiently carry out for this rotor the most complete parametric study of casing treatment design so far (for any compressor) in order to establish preliminary design rules for design of an optimal casing treatment.

1.7 Thesis outline

The structure of the present thesis is described as follows. Chapter 2 contains a literature review on stall suppression techniques that could be separated into five main configurations, namely slots, circumferential grooves, recess-vanes and self-recirculated casing treatments and tip air injection and ends up with important conclusions that constitute the starting point for the current work. Chapter 3 exposes the general methodology. Chapter 4 presents the computational setup and results for the stall criteria study. Chapter 5 presents in detail the methodology and results for the casing treatment study. Finally, the conclusions and proposed future work are given in chapter 6.

CHAPTER 2 LITERATURE REVIEW

2.1 Introduction

This chapter presents a literature review of relevant and recent research on stall inception and passive stall suppression technologies, in particular casing treatments and tip air injection. The chapter starts with a brief review of the research into the mechanisms associated with rotating stall inception. Subsequently, a review on the three main categories of casing treatment technologies, namely slots, circumferential grooves and recirculation endwall casing treatments is presented. Thereafter, the literature review continues with tip air injection technologies. The chapter concludes with a summary of the main findings from the literature review.

2.2 Stall inception research

The first attempt to physically explain the development and evolution of rotating stall dates back to the early 1950's. Emmons [2] was the first to postulate a scenario for rotating stall in axial compressors. He stated that once a blade passage stalls through suction side boundary layer separation due to an instantaneous increase in incidence at the blade LE, a blockage represented by a deficiency in the streamwise velocity will then favour the adjacent blade passage to reduce its incidence and stabilize while the other one, in the opposite direction to the rotor rotation, will see its incidence increase and therefore will subsequently stall in turn as shown in figure 2.1. This process will be sequentially repeated for each blade passage and will move in a direction opposite to rotation in the relative frame, and at part of the rotor speed in the stationary frame.

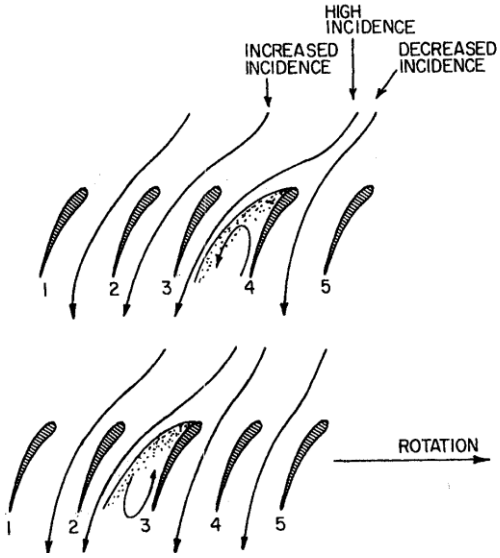

Figure 2.1: Propagation of rotating stall in axial compressors [4]

However, it is well known that compressors can operate with large regions of separated flow over the blade without imminent compressor instability. Moore and Greitzer [3] presented a comprehensive model of the compressor stability by combining 1-D and 2-D compressor instability theories. The 1-D model corresponds to surge-like behaviour which considers the entire compression system which is made up by the compressor, upstream and downstream ducts (flow inertia), plenum chamber (mass storage) and throttle valve as illustrated in figure 2.2. The mechanical analogy in the form of mass-spring-damper is also shown. When the mass flow is reduced, by closing the throttle valve, beyond the zero-slope of the compressor characteristic, the pressure in the plenum does not fall as rapidly as the pressure rise in the compressor. The compressor no longer produces the pressure necessary to contain the air in the plenum which will flow back through the compressor and the system becomes unstable. The presence of ducts leads to internal lag processes in the compression system shifting therefore the occurrence of surge instability to lower mass flow in the positive slope of the compressor characteristic. Furthermore, the 2-D model deals with the non-axisymmetric instabilities associated with rotating stall. The authors demonstrated that the growth of 2-D axisymmetric small amplitude waves appropriate to rotating stall are inherent to the compressor system when the stagnation-to-static pressure rise reaches zero slope. As previously discussed, this route to rotating stall is known as the long-wavelength or modal stall inception characterized by the growth of a small amplitude full-span

perturbation with circumferential wavelength in the order of the compressor annulus within 10 to 40 rotor revolutions into a fully developed rotating stall cell. Modal stall inception was measured and suppressed successfully by real-time feedback control via a set of independent movable inlet guide vanes by Haynes et al., [13] on a three stage low-speed axial compressor.

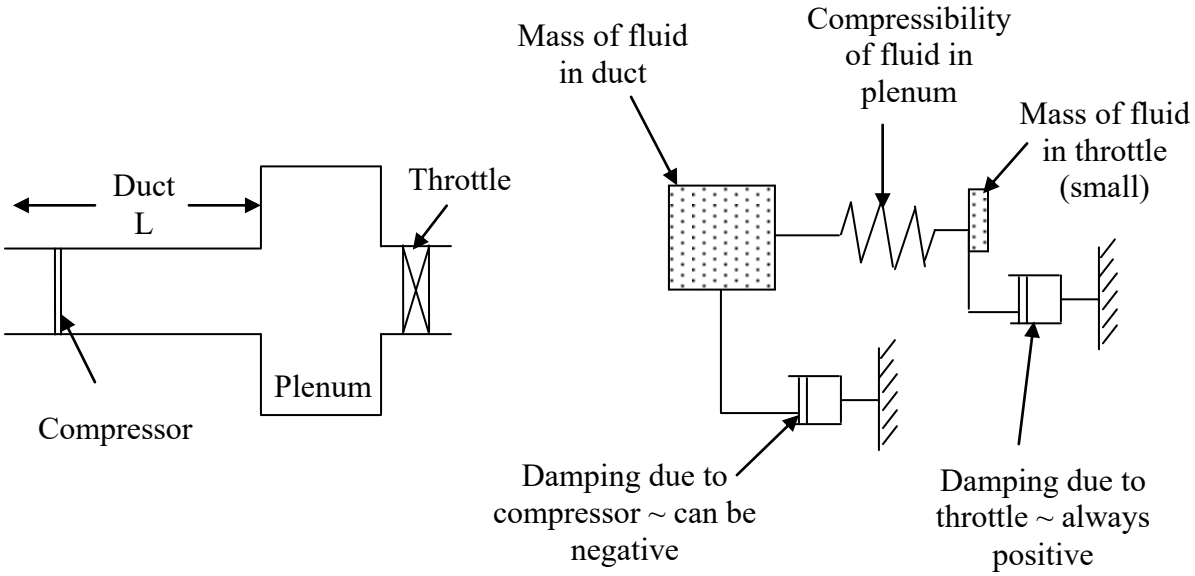

Figure 2.2: Simple compression system with a corresponding mechanical analogue [1]

Less than a decade after the Moore-Greitzer model, Day [7] experimentally investigated rotating stall inception in a low-speed compressor and discovered that it can stall after the formation of a short-length scale, roughly three blade passage wide, large amplitude disturbance at the rotor tip, called ‘spike’, which grows very rapidly within roughly three rotor revolutions into fully developed rotating stall. This new type of spike stall inception is known as short length-scale or spike rotating stall inception, and seems to be the most common type in modern compressors. Unfortunately, their limited circumferential wavelength and very high growth rate makes detection and real-time feedback control practically impossible, thus forcing reliance on passive control techniques such as casing treatment.

Gong et al., [14] extended the Moore-Greitzer model by including 3D nonlinear effects in a multi-stage compressor by means of Euler equations for simulating the development of both long and short wavelength compressor instabilities. Individual blade rows were represented by a body force formulated in terms of the blade's pressure rise and turning characteristic. They successfully simulated a spike stall inception and development of full rotating stall occurring on the negative-slope part of the compressor characteristic in agreement with experimental measurements. The only drawback of their model is the requirement of a localized disturbance of sufficient amplitude to initiate the stall inception process (i.e. the origin of the spike is not given).

However, the results mentioned above do not address the early stall inception, i.e., the spike formation processes. In this context, Hoying et al., [15] looked at the flow physics responsible for the occurrence of spike stall inception in the blade passage and specifically to the tip gap region. With computational simulations, they observed the tip clearance vortex spilling ahead of the leading edge plane of the rotor blade, resulting in spike-type stall in a fraction of the annulus using eight blade passages. Later, Vo et al., [8] refined the previous criterion for spike stall inception by stating that it is tip clearance fluid, rather than the tip vortex, that spills into the adjacent passage as illustrated in figure 2.3-a. They also added a second criterion, shown in figure 2.3-b, which concerns the trailing edge backflow of tip clearance fluid originating from the adjacent blade passage that moves upstream, below the blade tip, and impinges on the rear pressure side surface.

As illustrated in figure 2.3-c, Vo et al. [8] postulated that the movement of the interface between the incoming and tip clearance flows ahead of the leading edge plane opens a low-flow-resistance passage to allow this backflowing fluid (which would otherwise be forced into the adjacent tip clearance or to convect downstream) to continue toward the leading edge and amplify, leading to the formation of a spike disturbance. Thus, they stipulated that spike stall inception can occur only if these two criteria are present and that the last (lowest mass flow) converged solution of inexpensive single blade passage simulations can be used to evaluate these criteria and predict spike stall inception, as shown in figure 2.3-d and 2.3-e. In figure 2.3-d, the leading edge tip clearance spillage criterion is satisfied when the interface at the blade tip plane between the low-entropy incoming flow and the high-entropy tip clearance flow reaches the leading edge plane, especially on the pressure side, marking the onset of tip clearance flow spillage. Figure 2.3-e

plots the spanwise distribution of mass flow at the trailing edge plane, for which a zero value at the blade tip indicates the onset of tip clearance backflow (and impingement) below the blade tip.

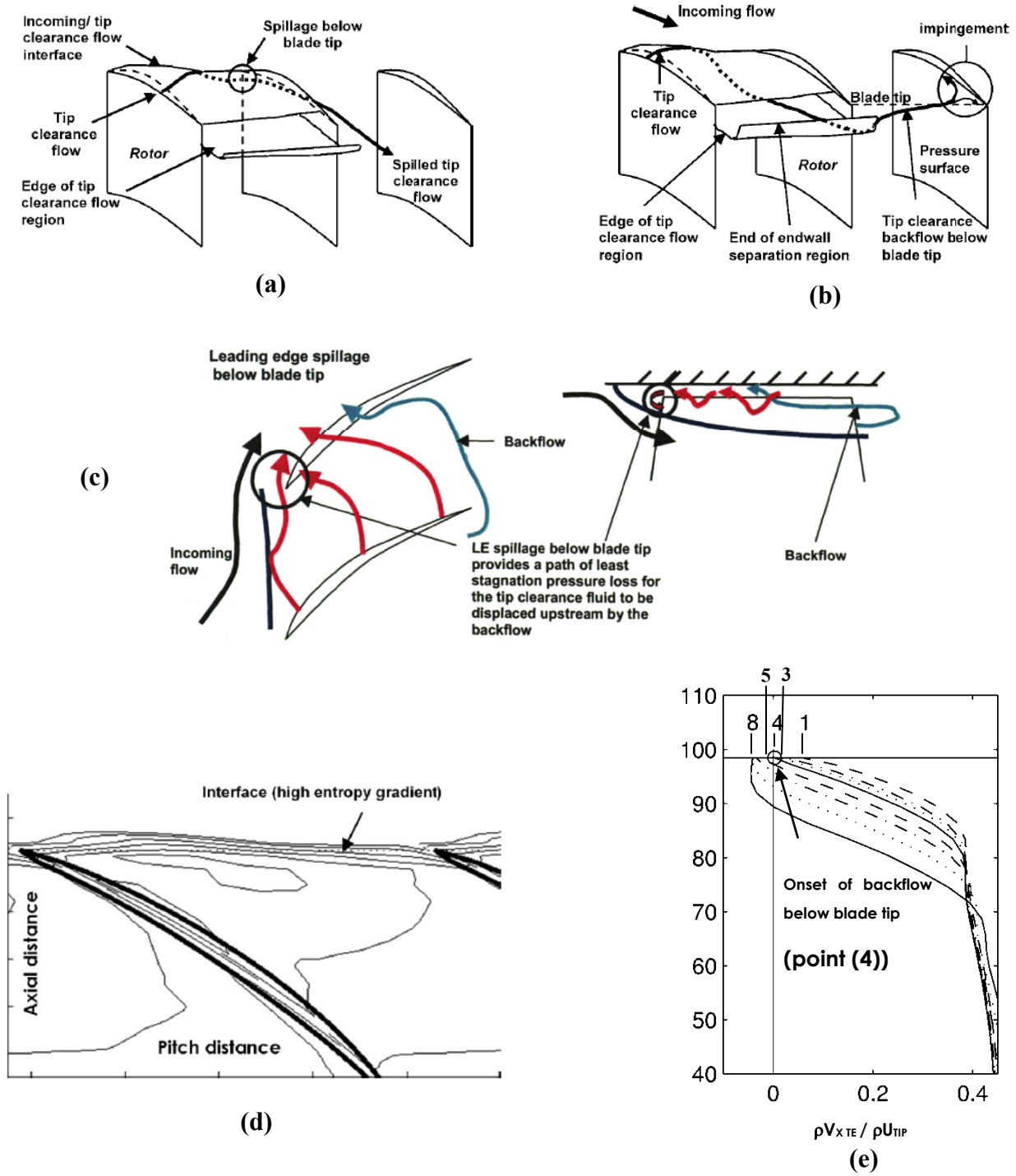

Figure 2.3: Proposed criteria and mechanism for spike stall inception in axial compressors and their quantitative evaluation [4]

Deppe et al. [11] investigated spike stall inception on three low-speed single-stage axial compressors and gave further experimental support to the criteria of Vo et al. [8]. They utilized highly sensitive pressure probes to demonstrate that spike stall inception is characterized by unsteady spill forward of the rotor tip clearance flow ahead of the rotor and is initiated by unsteady spots of axial backward directed flow just downstream of the rotor trailing edge close to the casing. Figure 2.4 illustrates both criteria using oil visualization technique on the outer casing wall of an axial compressor cascade corresponding to the rotor of one of the tested compressor stages at the stall point.

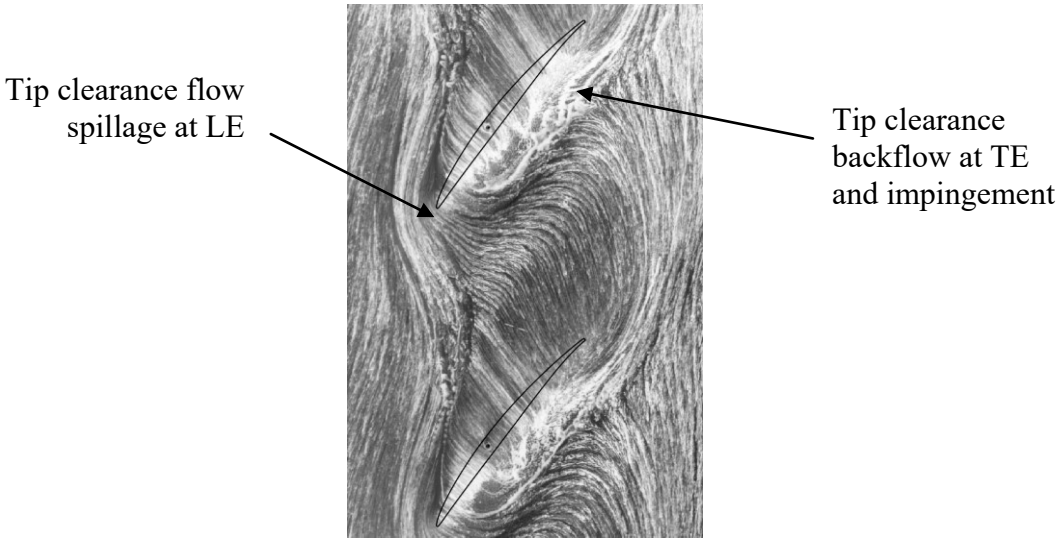

Figure 2.4: Experimental visualisation of the endwall flow in an axial compressor cascade at stall [16]

As for transonic compressors, the leading edge spillage was experimentally evidenced by the work of Cameron [17] as shown in figure 2.5 by using fine particles of chalk to indicate the casing shear. The chalk was continuously transported with the oil by the shear stress at the oil surface while the compressor was operating. From the position of the incoming/tip clearance flow interface at the casing (measured by the upstream zero-shear-stress line) at a point on the verge of stall, they deduced by calculation the position of this interface at the blade tip span and showed

that it is at the blade tip leading edge plane thus confirming the first criterion of Vo et al., [8] in a transonic axial compressor.

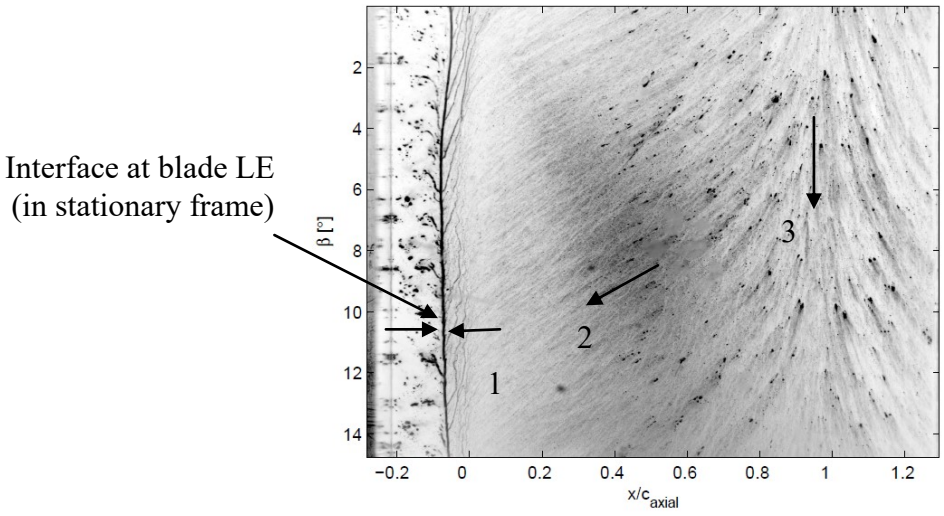

Figure 2.5: Chalk surface visualization on casing of axial transonic compressor rotor at stall point: 1) zero shear stress line (interface), 2) reverse flow region, and 3) trailing ege bifurcation line [16]

More recently, Hah et al., [18] simulated the stall inception of a modern transonic rotor known to stall via spike with full annulus unsteady LES (Large Eddy Simulations) and they demonstrated that the criteria proposed by Vo et al., [8] are still valid for transonic axial compressor.

2.3 Casing treatments stall suppression technologies

Casing treatment consists of incorporating slots or grooves, as shown in figure 2.2, in the rotor shroud (and/or stator hub, if there is a stator hub clearance), to passively add momentum to the endwall flow by air recirculation from high to low-pressure zones within or near the blade passage to improve performance. This section can be divided in three sub-sections dedicated to each one of the following three general types of casing treatment: slots, grooves and recess vanes casing treatments.

2.3.1 Slots casing treatments

Slots casing treatment consists of placing a series of discrete slots on the casing above the rotor. The slots can be axial or rotated with or against the direction of stagger of the rotor. They can also be radial or skewed (inclined circumferentially) in the direction with or against the direction of rotor rotation. The slots can also be of varying shape either in the radial or circumferential plane and their axial position, axial extent, number and open area ratio are all geometric design parameters that can be varied.

Prince et al. [19] initiated the first reported attempts to take a comprehensive, physics-based approach to understanding the mechanism associated with casing treatment effectiveness. Their tests of different configurations of circumferential grooves, skewed slots, and blade angled slot casing treatments showed that compressibility considerations are not essential to the effectiveness of casing treatments. The interesting thing is that when they included a baffle in the middle of the axial skewed slots to prevent recirculation in the axial direction they improved the efficiency or the compressor as shown in figure 2.6. In addition, they reported that radial holes or perforated endwall treatments do not provide any benefit in terms of stall margin improvement.

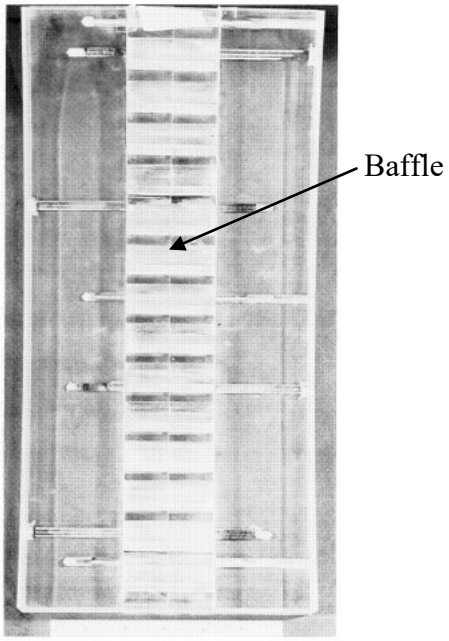

Figure 2.6: Axial skewed casing treatment with baffle in the middle of the slots [18]

Fujita and Takata [20] tested different configurations of axial, skewed, and circumferential groove casing treatments, which had been shown by previous investigators to have the greatest stall range potential or exhibited the least efficiency decrement. Their results, which are consistent with past measurements, clearly show that the more effective the casing treatment is in extending the stable compressor operating range, the greater the efficiency penalty as illustrated in figure 2.7. Takata and Tsukuda [21] were the first to report clear evidence of the importance of the orientation of skewed slots on stall range and performance. Their results indicate that the greatest range extension for skewed axial slots is when the slots are skewed opposite to the rotor rotation as shown in figure 2.8, whereas skewing the slot in opposite direction (i.e. in the direction of rotor rotation) results in a drop in the flow range even when compared to the reference case without casing treatment.

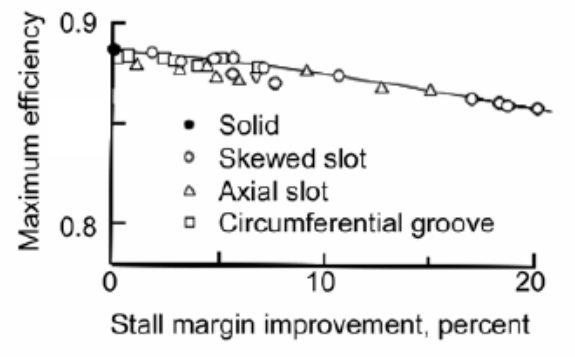

Figure 2.7: Measured trend of decreasing efficiency with increasing stall margin [19]

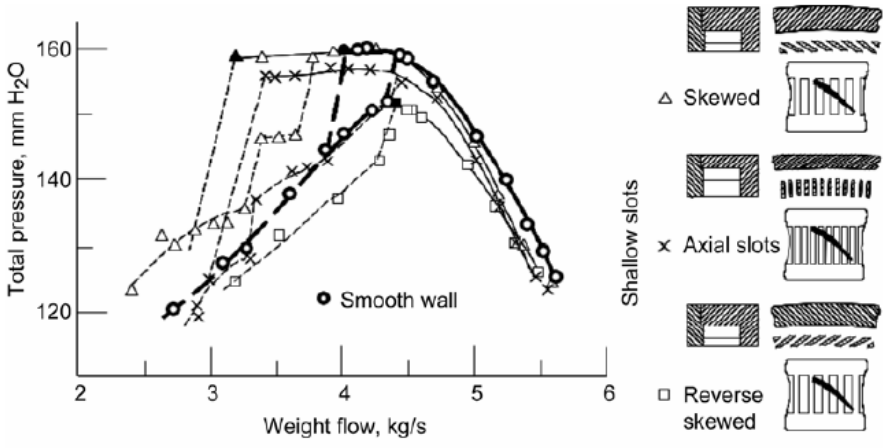

Figure 2.8: Impact of orientation of the skewed slots on the performance of the rotor [21]

Smith and Cumpsty [22] applied axial skewed slots to a low-speed axial compressor with the same skewed slots design as was used by Prince et al., [19]. When they varied the clearance gap from 1% to 6% of tip clearance normalized by the tip chord, they reported that the axial skewed slots appeared to be effective in desensitizing the impact of tip clearance in the stable operating range as depicted in figure 2.9, which is consistent with the finding of Fujita and Takata [20]. Their explanation for stall range improvement was focused on the accumulation of endwall blockage that triggers the stall, with casing treatments, a path for recirculation is provided to low momentum fluid to enter slots but the overriding characteristic of casing treatments is the flow path between the pressure and suction surface.

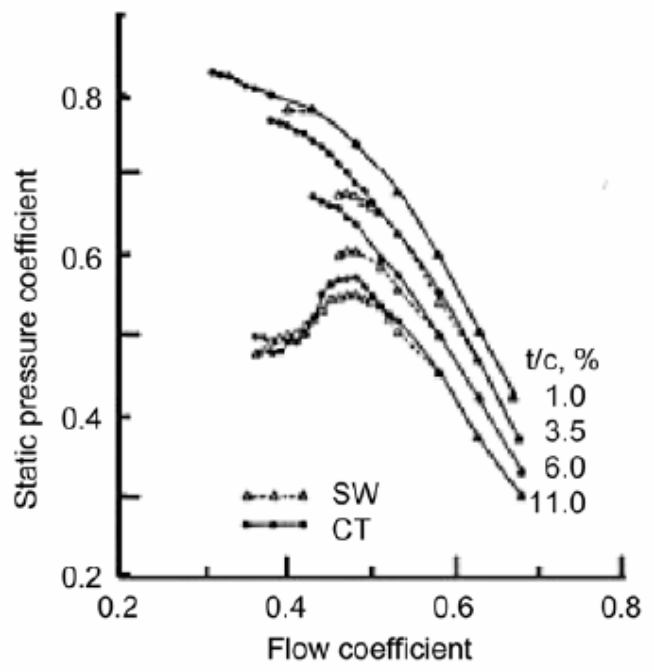

Figure 2.9: Static pressure rise at various tip clearances for the solid wall and the treated builds [22]

Lastly, numerous additional studies of the reliability of casing treatment have emerged with the growth of CFD and the advent of high-speed computing as discussed below.

In an unpublished thesis, Seitz [23] investigated experimentally and numerically axial slot casing treatment for a subsonic compressor exhibiting spike stall inception. He conducted a series of parametric tests for the forward-positioned axial skewed slot casing treatment to assess the effect of varying slot skewed angle from 0º to 60º. He concluded that casing treatment with no loss (or even an increase) in rotor efficiency is possible when axial skewed slots extend well upstream of the rotor leading edge. He found that the maximum stall margin improvement with no loss of efficiency was 28%* for the case of a 60º skew angle when the treatment slots extend 75% axial chord upstream and 25% downstream of the rotor leading edge. For this optimum skew angle an

* Unless indicated otherwise, the stall margin improvement is defined in this report as the reduction in stalling mass flow as a percentage of the stalling mass flow with smooth casing

increase in peak efficiency of 1.1% was recorded when the upstream axial extent was reduced to 55% of axial chord. At this condition stall margin improvement was 20%. He related the gain in efficiency with the forward-positioned axial skewed slots to the reduction of the recirculated mass flow inside slots compared to the conventional axial skewed slots. In addition, he concluded that suction, in the downstream half of the slot, is the primary mechanism for stall delay for axial skewed slots located in the unconventional position while blowing, in the upstream half of the slot, is secondary but neither suction nor blowing are as effective at improving the stall margin as the full treatments are, irrespective of their axial positions. Furthermore, the deleterious effect of blowing is counteracted by the positive effect of suction resulting in no loss in efficiency for the unconventional treatment.

For transonic compressors, Wilke et al. [24] carried out a numerical investigation on Rotor 37 which reveals that the effectiveness of casing treatments depends very much on the aerodynamics of the compressor inflow and the specific flow mechanisms at conditions close to stall. Their simulations with the slots casing treatment as illustrated in figure 2.10 show that axial slots directly impact the flow mechanisms responsible for compressor stall, which were referred to as “blade tip stall” and “tip blockage stall”. The former mechanism refers to suction side boundary layer separation in the blade tip region from high incidence/loading. The latter mechanism refers to increase in tip blockage due perhaps to tip vortex breakdown. The stall margin improvement was approximately 5.5% with a drop in peak efficiency of about 0.4%. Their work indicates that the effectiveness and impact on compressor efficiency of axial slots mainly depend on their axial position over the blade tips. On the one hand, the more upstream the slots are positioned the less their negative impact on the compressor efficiency will be. In the other hand, the more upstream slots the less the extension in stall mass flow.

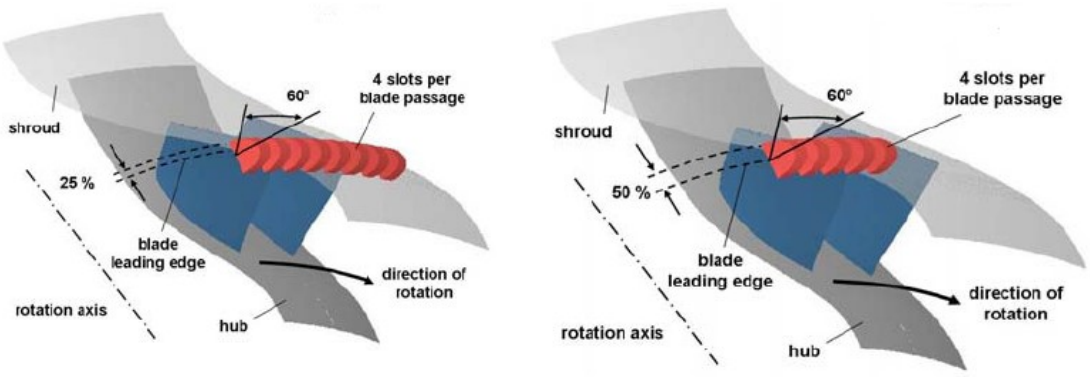

Figure 2.10: Slots casing treatment configuration [24]

Lu et al. [25] examined experimentally and numerically for a subsonic compressor different type of slots casing treatments (blade angle slot, bend skewed slot, axial skewed slot, circumferential grooves), and demonstrated the practicality of employing CFD simulations to expediently and economically conduct an array of parametric studies on the effects of casing treatment design parameters. They used unsteady CFD simulations with axial skewed slot casing treatment to illustrate the intermittent, time-dependent nature of the recirculating flow pattern for discrete slot endwall casing treatments. They found that circumferential grooves are not as effective as the axial skewed slots casing treatment because the circulation inside the slots is much stronger than circumferential grooves. This finding is consistent with other previous works. They also indicated that the mechanism by which the casing treatments postpone the inception of the stall instability is that they prevent an early spillage of low momentum fluid into the adjacent blade passage.

Lin et al, [26] carried out both experimental and numerical investigations of a slot-type casing treatment with a recess chamber on a transonic axial flow compressor rotor, as shown in figure 2.11. Their experiments show that at 60% and 98% of rotor design wheel speeds, approximately 26.5% and 20.16% in stalling mass flow reduction were achieved, respectively. On the other hand, there were about 3.4% and 0.7% drops of efficiencies at 60% and 98% speeds respectively. For the treated casing case, the passage shock near the blade tip is oblique relative to the incoming flow (as shown in figure 2.11) and its strength is reduced, thus, the shock loss and the reversed flow on the endwall behind the shock are reduced. Consequently, the incidence and the

loading at blade tip region are reduced. They concluded that the interactions between the blade passage flow and the casing treatment flow exhibit different behaviour at two rotating speeds. The flow condition in which the rotor operates, i.e., either the subsonic condition at the 60% speed or the transonic condition with passage shock presented at the 98% speed, explains the difference in the improved performances of the rotor since the alteration of the shock strength and its location brings additional improvement in the performances in terms of pressure rise and isentropic efficiency as well.

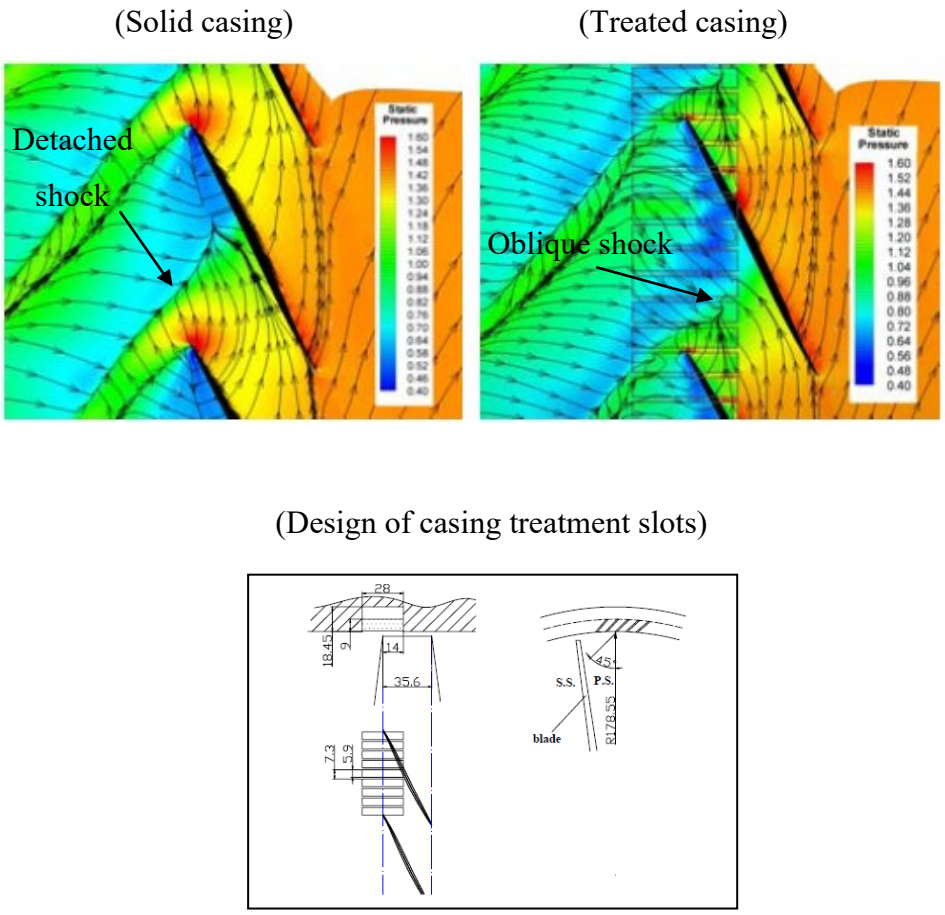

Figure 2.11: Effects of the casing treatment slots on the passage shock structure and the geometrical design of the casing treatment slots [25]

Emmerich et al. [27] investigated numerically and experimentally casing treatment with axial skewed slots ending in a plenum chamber for a highly subsonic compressor similar to Lin et al., [26]. Their experimental results show a stall margin improvement of approximately 18.5 %, while the design efficiency decreases by 1.4 %.

In an extension to the work of Wilke et al., [24], Brignole et al, [28] examined numerically the effects of four different semi-circular axial skewed slots casing treatments on a transonic compressor stage, as shown in figure 2.12, in order to identify correlations between cavity geometries and the passage flow. The tested configurations are; 1) standard skewed slots, 2) narrow skewed slots with a small open area in the casing, 3) curved skewed slots with elliptic shape of the slots with the same open area as for the narrow slots case, and 4) short skewed slots with a small axial extent of the slots. The results showed an improvement in efficiency at design conditions of up to 0.6% for the narrow slots configuration and a raised total pressure ratio at both 100% and 80% speed with reduction of 10.7% in stalling mass flow rate. The gain in efficiency was found to correlate to the relative amount of mass entering the casing treatment and especially to the effectiveness of the geometry to induce a recirculation across the entire cavities. In addition, the simulations showed a decrease in the endwall secondary flow by a reduction of three-dimensional flow phenomena originating in the rotor tip clearance, improving thus the stall margin of the compressor stage. Furthermore the rotor loading was enhanced in the tip region, resulting in a higher pressure ratio.

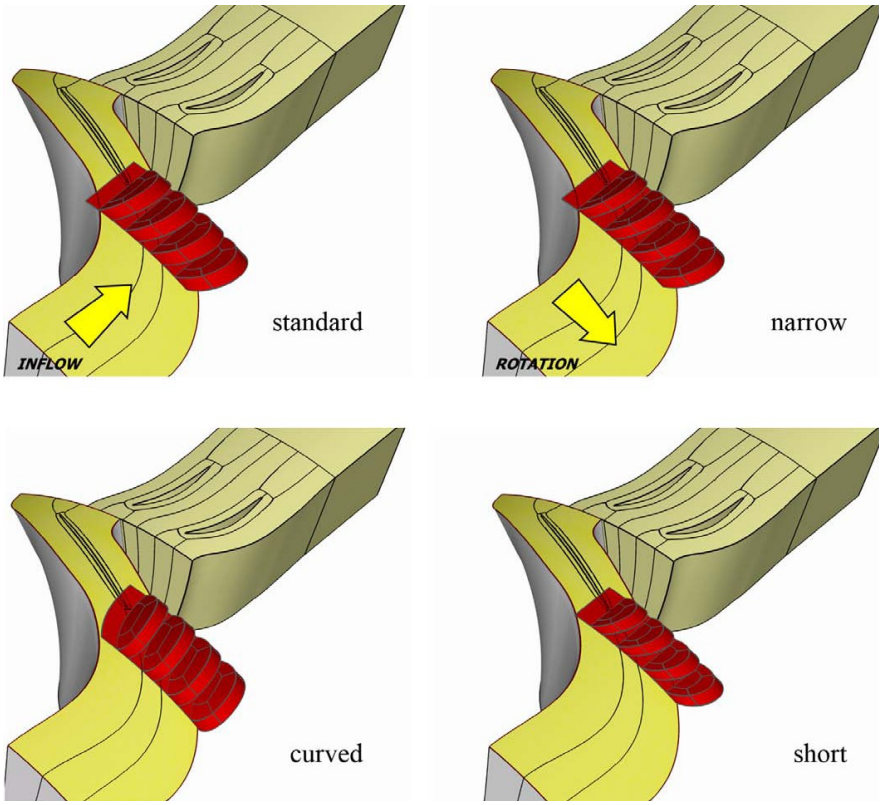

Figure 2.12: Slots casing treatment configuration [28]

2.3.2 Circumferential grooves casing treatments

Circumferential groove casing treatments consist of adding circumferential recesses in the casing above the rotor. The shape of the recess, depth, number, axial location and axial extent are geometric design parameters that can be varied.

In the case of circumferential grooves for subsonic compressors, Nezym [29] carried out a parametric experimental investigation of entire annular recess (EAR) casing treatment over the compressor rotor blades where various forms of grooves were used. He reported on the benefit of using a penetration (figure 2.13a) and rectangular recess extending from the leading edge to the trailing edge of the rotor with the casing radius at the same value as that of the rotor tip (figure 2.13b). He concluded that the larger recess depth and volume, the more the stable operating range. For the former case with a penetration, he could obtain an improvement in the operating

range of 35% when compared to the configuration without treatment, and 22% for the second configuration

(a) (b)

Figure 2.13: Two effective variants of the EAR (Entire Annular Recess) (a) penetrating casing treatment and (b) blade tips coincide with the casing baseline [29]

For high speed compressors, Muller et al. [30] reported on an experimental and numerical investigation of circumferential grooves in a transonic single-stage axial compressor with four different groove configurations characterized by deep and shallow grooves and variable coverage of the projected rotor axial chord, as shown in figure 2.14. The authors demonstrated a significant increase in operating range with all configurations with an improvement of 9.6% in the stall mass flow for the best configuration which corresponds to 6 deep grooves. However, shallow grooves were less effective. They noticed that while deep grooves roughly maintained efficiency levels compared to the smooth wall case, shallow grooves had a beneficial effect in increased stage peak efficiency at design speed by more than one percent. Independently from the groove depth, they proved that a higher coverage of the rotor projected axial chord seems favourable for delaying stall inception to a lower mass flow (six grooves against three grooves, i.e. twice the axial extent, as shown in figure 2.14). For this compressor, spike stall inception was deduced from measurements upstream of the leading edge.

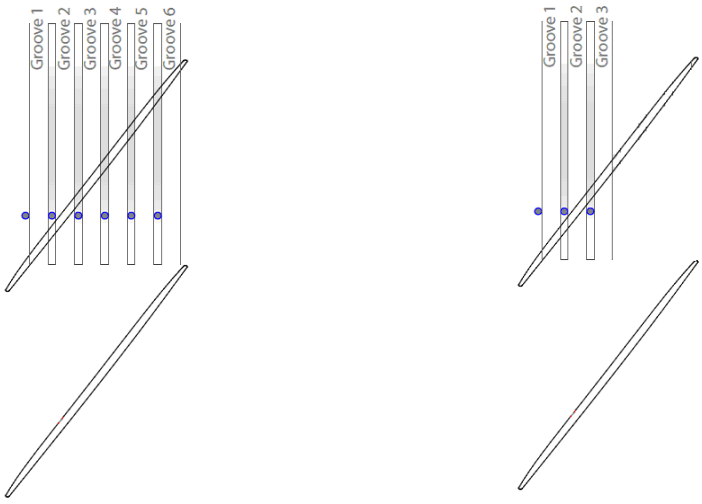

(a) (b)

Figure 2.14: Circumferential grooves position (a) 6 gooves and (b) 3 grooves, deeper shallow for each [30]

Another casing treatment investigation on Rotor 37 transonic has been done by Zhang and Ma [31] using sloped circumferential groove, as shown in figure 2.15. When compared to the smooth casing, the results show that this geometry provides a barrier to minimize the forward flow from the tip clearance vortex, that seems to be associated with spike stall inception. Furthermore, they show the entropy interface which lines up with the leading edge plane at stall which corresponds to one of the two criteria proposed by Vo et al., [8]. Their stall margin improvement is approximately 1% with almost no drop in efficiency (≈ 0.2%).

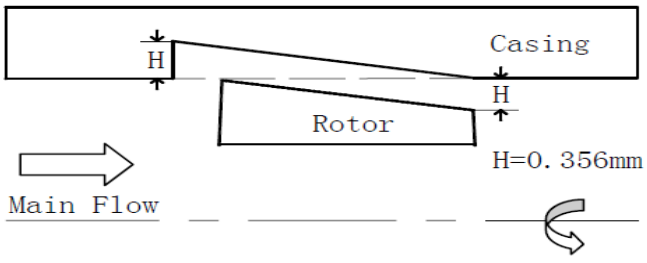

Figure 2.15: Sloped trench casing treatment configuration [31]

Huang et al., [32] studied the performance of Rotor 37 (transonic compressor) with circumferential grooves casing treatment (CGCT). They used different configurations of CGCT using only one groove G1 to all in same time from G1 to G7 as shown in figure 2.16. Two critical flow structures with different tip clearance at near stall condition were revealed. With the designed small tip clearance, the leading edge tip leakage flow driven by the pressure gradient has high momentum to make the leading edge BTLV (Blade Tip Leakage Vortex) strong enough to avoid from breakdown before the occurrence of other unstable structures, for example the trailing edge separation. But if the separation is suppressed by the casing treatment, the leading edge BTLV breakdown happens with a higher back pressure. When the tip clearance increases, the tip leakage flow joined to the BTLV gets weak due to the decreasing of the pressure gradient in the tip clearance. That may lead to the BTLV having not enough energy to get through the passage shock and breakdown before the full development of trailing edge separation. For these two typical stall relating structures, circumferential grooves at the mid-chord or near the leading edge were effective, respectively. Benefit on stall margin has been achieved without obvious efficiency penalty in the present computational results. However, they did not present the compressor's characteristic to extract the stall margin but they obtained 11.75 % in stall margin improvement based on a definition of stall margin given here as:

$$SM = \left(\frac{\dot{m}_{peak}}{\dot{m}_{stall}} \frac{P_{TR_{stall}}}{P_{TR_{peak}}} - 1 \right) \times 100\,\%$$

Where P_{TR} means the total pressure ratio and $\dot{m}$ the mass flow rate.

Mileshin et al., [33] studied numerically the performances of a transonic axial stage, and near-surge rotor tip clearance flow has been performed for small and large rotor tip clearances and for large tip clearance equipped with 8 circumferential grooves used like a casing treatment. They concluded that grooves diminish mass flow in the circumferential direction through tip clearance gap and locate tip leakage vortex trajectory deeply within blade-to-blade channel. It increases surge margin. They got approximately 2% reduction in the stalling mass flow. However, they did not discuss about the gain in efficiency.

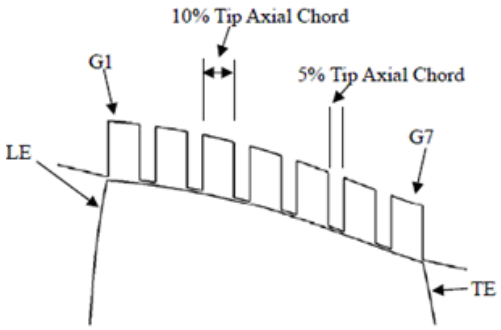

Figure 2.16: Circumferential grooves casing treatment configuration [32]

2.4 Recirculation endwall casing treatments (blowing/suction)

Casing recirculation endwall treatment consists of blowing air with a specific injection port from within the casing treatment slot or groove near the tip front of the rotor (as shown in figure 2.17) using high pressure air bled off through a specific bleed port at the rear stages of the compressor or behind the rotor. This type of casing treatment is attempting to provide a recirculation path to move low momentum fluid out of the passage and then to re-inject it in a beneficial manner back into the passage. In the 1990s, many authors began revisiting similar concepts that attempt to exploit flow removal and re-injection. Most are patented ideas that have not been reported in the open literature [34]. Thus, the results obtained for this type of treatment has so far been limited to numerical studies.

Yang [35] investigated numerically the effects of the recirculation treatment on the stability and performance of a transonic compressor stage at 100% rotational speed through unsteady simulations. The casing treatment consists of nine segments per rotor blade pitch (see figure 2.17b), and each segment is composed of one bleed port, one injection port and one bridge channel connecting the bleed and the injection ports. The author reported a 4.5% improvement in stall margin without loss in efficiency, and he related this improvement to the fact that the low energy tip leakage flow emanating from the vicinity of the rotor blade leading edge has more time to get energized from the mixing process with the injected recirculated fluid before passing by the shock.

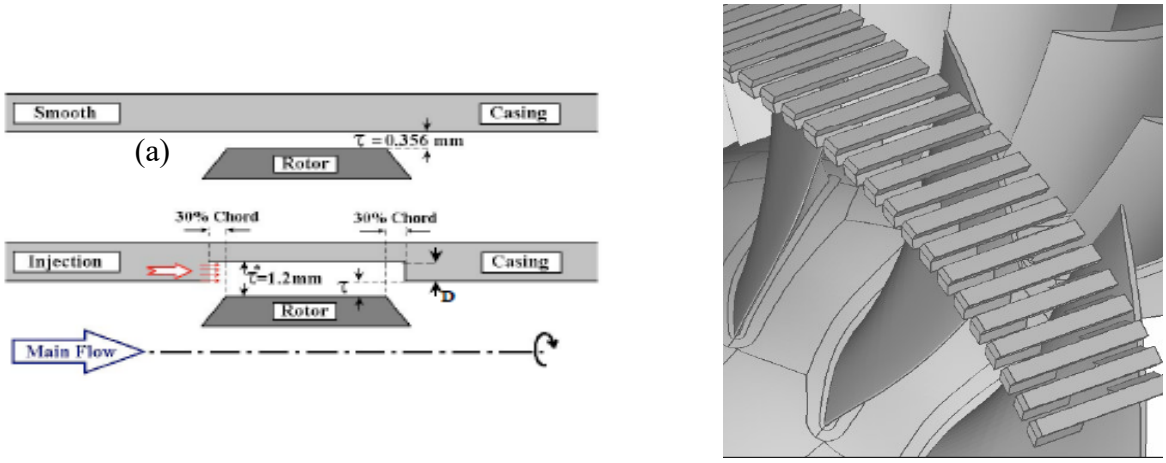

(a) (b)

Figure 2.17: Configuration of casing recirculation with: (a) circumferential groove [35] and (b) segments [36]

In addition, Behesthi et al., [36] have done a parametric study on the circumferential recirculation casing treatments on performance and stability of a transonic axial compressor, as shown in figure 2.17a, and they noticed that this type of casing treatment can be a successful mean to reduce the effects of tip region blockage, resulting in noticeable (0.9%) improvement in peak efficiency and a stall margin improvement of about 4.5 %. Bleed air mass flow rate plays an important role in controlling the tip-induced instabilities. The compressor stability enhancement is reported to be directly related to the injector mass flow rate and exit velocity. The compressor stability margin increase reaches a maximum when the bleed air in the relative coordinates is aligned with the mean camber line of the blade leading edge. Simulations also showed that recirculation casing treatments are able to improve the stall margin without detrimental impact on the compressor efficiency.

Khaleghi et al. [37] investigated numerically by means of steady simulations the endwall recirculation casing treatment using an anti-swirl in the recirculation channel for a transonic compressor (Rotor 67). They obtained a stall margin improvement of 9.95%, which is considerable for a transonic case, by recirculating 1.21% of the main flow with a small penalty in efficiency (about 0.25%). It was found that the anti-swirl vanes used in the passage effectively removes the swirl component of the bled air and turns it into the axial direction for blowing.

2.5 Tip air injection stall suppression technologies

Tip injection is a technique whereby air is injected in the tip region, usually with a set of discrete actuators distributed circumferentially and placed upstream of the rotor, to suppress compressor instabilities. It is well known that the injection of air upstream of compressor rotors enhances their stability. This feature was understood and applied by NASA as early as 1960 when an array of experimental tests was conducted to passively control high hub-tip ratio compressors [38]. At the end 1980's, Epstein [39] was the first to propose coupling injection with feedback control to suppress modal stall inception that resulted in a few experimental demonstrations of this technique. While active stall suppression with injection works for modal stall inception, it does not for spike stall inception due to the much higher response time required. Thus, passive injection techniques would be more realistic in this case. In most of the experimental work, the injected flow is supplied from an external source and involves typical injected mass flow on the order of several percent of compressor mass flow. However, in an engine environment, this flow would be bled from the rear of the compressor, and a passive injection technique that is turned on almost continuously can incur a significant engine cycle efficiency penalty. Thus, there is a strong incentive to minimize the amount of injected mass flow required for a given extension in stable operating range. Thus, a new approach based on steady micro tip injection, has been proposed in recent years to enhance the stability of compressors, so far in low-speed geometries. This technique is referred to as micro tip injection and usually involves injected mass flow below 0.1% of compressor mass flow. The review will first cover the conventional tip injection techniques followed by micro tip injection research.

2.5.1 Conventional tip air injection

Weigl et al. [6] investigated experimentally the benefit of the unsteady discrete tip injection in a high-speed compressor, as shown in figure 2.18, in enhancing the stall margin of a high-speed compressor designated as NASA Stage 35, which exhibits modal stall inception. They achieved 11% and 3.5% in stall margin improvement, at 70% and 100% of design speed, respectively, with injection of 3.6% of the design compressor mass flow. It is reported that the unsteady injection is not only beneficial to the stability but also useful for recovery from a large amplitude disturbance and a fully developed stall. Their results also show that tip injection enhances the stable operating range of compressors by damping the spatial harmonics of the pre-stall perturbations associated

with modal stall inception. At a higher rotational speed (up to 150% speed), the compressor stabilization becomes more difficult due to numerous traveling modes of instabilities. The effect on efficiency was not considered in this work.

In an extension of this work, Spakovszky et al. [40] actively stabilized the same transonic compressor with inlet distortion in both radial and circumferential direction independently, and they were able to improve the stall margin by 17.2% and 15.2%, respectively. They demonstrated that active control of rotating stall with tip injection can be effective even in presence of inlet distortion. Again, the effect on efficiency was not considered in this work.

Later, Suder et al. [9] experimentally and numerically examined the effect of discrete tip injection (figure 2.18) and found that the total stability enhancement is due in large part to steady injection. In contrast to the previous works where 12 injectors were used, they tested a variety of circumferential distribution of casing-mounted injectors (between two and eight) located 200% of axial chord upstream the rotor. They improved the stall margin of the same Rotor 35 by 30% and 6%, using an injected mass flow equivalent to 1% and 2% of the annulus flow, at 70% and 100% speed, respectively. The reduced injector effectiveness at design speed was explained by the choking velocity of the injector, which is fixed in their setup and independent of compressor speed. This implies a decrease of the jet injection momentum relative to the background flow momentum, as the compressor speed increases. In addition, the authors noticed that the range extension is independent of the injector arrangement around the annulus.

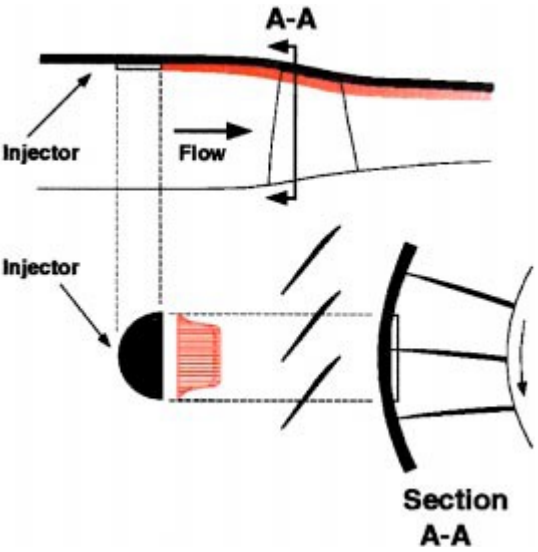

Figure 2.18: Cased-mounted tip-injection casing treatments [9]

Kefalakis and Papailiou [41] conducted an experimental parametric study of steady and pulsating jets injection on a high-speed compressor stage and demonstrated a stall margin improvement on the order of 10% with a jet mass flow of less than 1% of the incoming flow. They concluded that to obtain the same surge margin improvement with fewer nozzles, the injection has to be performed with a higher velocity to achieve an equivalent level of injected momentum. No theoretical explanation was given for this finding. Their experiments to test whether low and high frequency tip injection could be effective in increasing the gain of surge margin without the help of the usual feedback control mechanism was not conclusive. No discussion on efficiency was given.

Cassina et al. [42] carried out a parametric study of the tip injection in a subsonic compressor by the means of 10 circumferentially axisymmetric injectors with different axial position as shown in figure 2.19. Their simulations showed an improvement of the surge margin of 13.25% for an optimum width/length (L/W) ratio of the injectors of 53.3, as shown in figure 9b, with an injection mass flow of 4.27% of the annular mass flow. However, they did not consider the effects of tip injection on the compressor overall efficiency because they believed that results are not comparable to experiments if the stator blades are not considered.

Khaleghi et al. [43] carried out numerical simulations to study the stability increase of a transonic rotor, known as NASA Rotor 67, with air injection at the blade tip. Their simulations predicted a stall margin improvement of 13.23% without efficiency loss, by injecting 1.8% of the main flow rate, which corresponds to the mass flow of choked injectors. They showed that the onset of stall occurs when the diffusion factor near the tip of the blade exceeds a value of about 0.75 as found by Suder et al. [9]. They claimed that the tip injection pushes the shock downstream in the passage and reduces the region of negative axial velocity near the tip of the blade. Furthermore, the tip leakage vortex is pushed towards the suction surface as a result of a weaker passage shock associated with the added axial momentum into the tip of the blade.

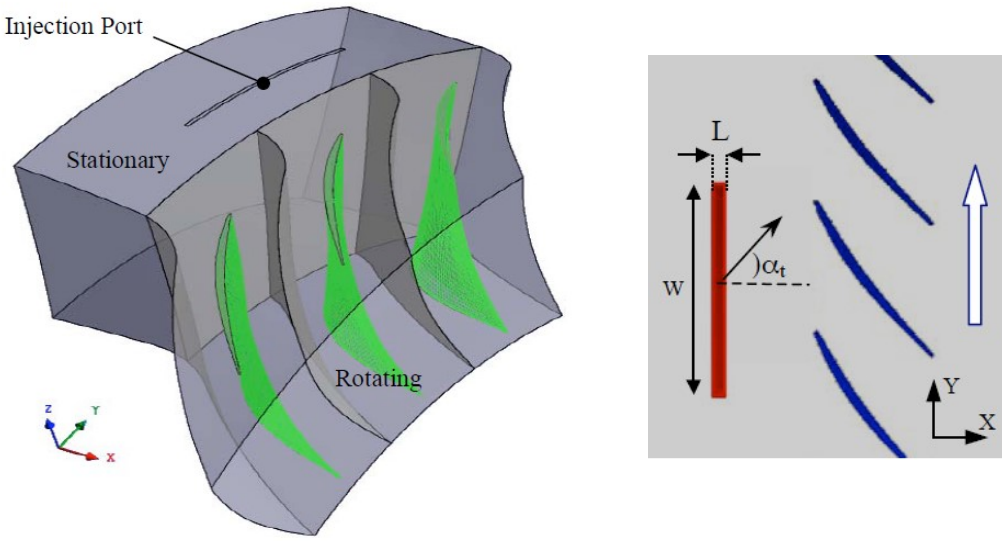

(a) (b)

Figure 2.19: (a) Computation domains used for numerical simulation (b) Schematic of compressor stage and injection port [41]

Roy and Veraarapu., [44] conducted an experimental study of the discrete tip-injection in low speed axial fan test rig. Injection was applied from the casing by varying different parameters e.g. injection angle, number of injection ports, and location of injection ports. They used discrete and distributed injection schemes applied: i) only at the rotor tip mid-chord, and ii) both at the leading edge and at the mid chord of the rotor tip (combined injection). The effect of injection applied has been studied (i) during recovery only, and (ii) during the entire period from unstalled flow to the end of recovery (hysteresis). It was observed that various tip injection schemes were successful, in varying degrees, in alleviating hysteresis. While discrete injection provided more stall margin gain (10.5% reduction in the stalling mass flow), combined injection scheme was better in stall recovery.

Dobrzynski et al., [45] investigated the discrete tip injection for the active flow control on a 1.5 stage low-speed axial compressor, utilizing stage performance measurements, 5-hole probe traverse measurements as well as an oil flow visualization technique. They could reduce by

15.5% the stalling mass flow with almost no loss in efficiency for low mass flow injection and nearly 1.5% loss in efficiency for the highest mass flow injection.

2.5.2 Micro tip air injection

Nie et al., [10] got a stall margin improvement of 16% with injection of 0.045% of the annular mass flow. They looked at the unsteady response of the compressor to the micro injection through three different ways: experiments under various injection configurations, wavelet analysis for unsteady flow disturbances and numerical computation at the near stall condition. The authors claim that the mechanism of unsteady response exist in the compressor when the steady injection acts on the unsteady phenomenon of flow instability; the rotating stall. They drew two consequences from the above argument on the unsteady response. First, since the action really needed for control of the flow instability is only on the unsteady part of the flow, the amount of the injected air for the steady injection can be dramatically reduced. This is perceptible because the behaviour of a highly nonlinear system may be influenced even by a slight variation of boundary condition and this is the case for compression systems operating at near stall conditions. Second, the steady compressor characteristic with no injection should not be influenced by such tiny injected air and thus could keep its shape unchanged. They reason that both of these propositions, if they work well, would make this micro injection approach very attractive for its use in a practical application. Unfortunately, they did not provide any results on efficiency. More recently, Nie et al., [10] reported a comprehensive series of experimental tests with new feature about the sliding of the micro injector along the chord. The main result was about the best location of injection. They find that the best stall margin improvement was recorded when the injector is located between 1/4 and 1/3 of the axial chord.

Another micro tip injection investigation was conducted by Deppe et al. [11] applied an air injection upstream of the rotors through a few micro-injectors whose radial extent is on the order of the tip clearance at the casing wall (as shown in figure 2.20) aiming to delay these criteria and improved the surge margin by approximately 11.6% by injecting 0.096% of the main flow rate. In addition, they also demonstrated the capability of the injection to recover the compressor stages from a stalled condition. However, they did not comment on efficiency in this work.

Last but not least, Lu et al. [46] investigated experimentally and numerically the steady micro tip injection with flush-mounted inclined holes (see figure 2.21) in a low-speed compressor and

demonstrated the potential to significantly extend the operating range of the compressor with minimal or no loss in isentropic efficiency. For the tested rotor, their experimental results showed a reduction of 7.69% in the stalling mass flow using an injected mass flow equivalent to only 0.064% of the annular flow with a gain in the peak efficiency of about 3.5%. They demonstrated that the two criteria for spike-type rotating stall inception of Vo et al., [8] applied to their subsonic compressor, namely a forward spillage of tip-clearance flow just below the tip leading edge and reversed tip-clearance flow at trailing edge plane. They concluded that the physical mechanisms responsible for extending the compressor stall margin incurred by the steady micro-tip injection are linked to delaying the upstream movement of the incoming/tip-clearance flow interface. However, they noted that the injected flow is supplied from an external source whereas in an actual application, the efficiency penalty to the engine cycle incurred by extracting bleed air from rear stages for injection may offset any efficiency benefit to the compressor.

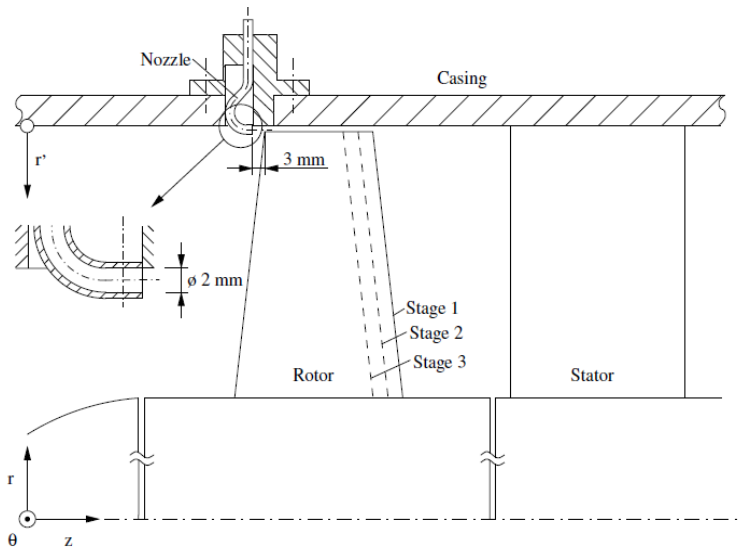

Figure 2.20: Nozzle arrangement of single stage subsonic compressor with different aspect ratio [11]

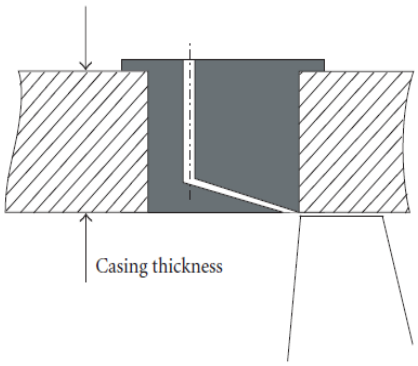

Figure 2.21: Flushed-mounted tip injection [45]

2.6 Mixed flow compressors

With the exception of two papers, there is very little published research on mixed flow compressors given its recent commercial application. Cevik et al. [48] looked at design optimization for the rotor of a mixed flow compressor. In terms of stall research, the only published work is from Qiang et al. [12] who carried out steady and unsteady CFD simulations on a transonic mixed flow compressor stage with five circumferential groove over the rotor, as shown in figure 2.22. Their simulations showed a relatively small 2.7% reduction in stalling mass flow rate at a cost of 1% loss in peak efficiency. There was no attempt at improving the performance of the casing treatment.

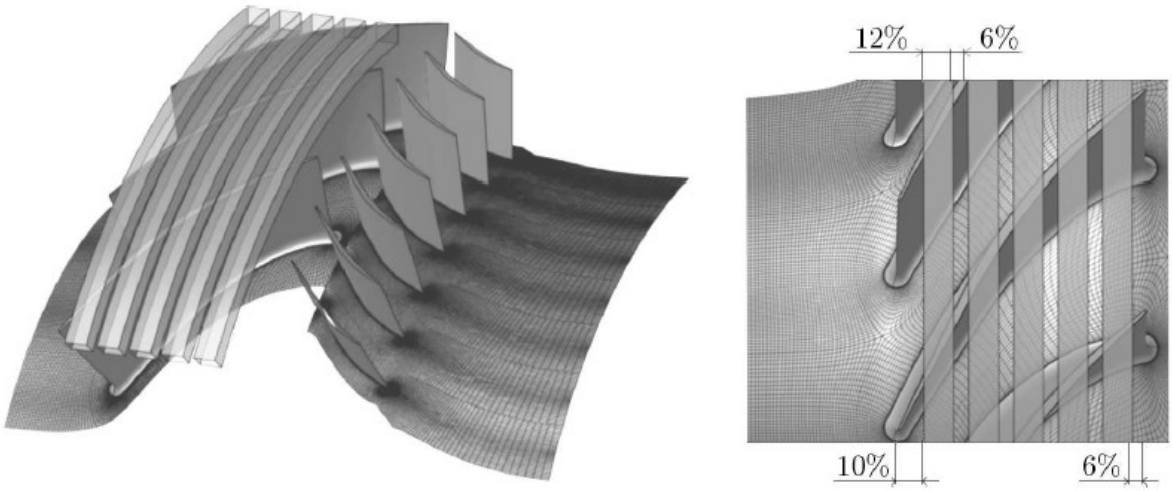

Figure2.22: Circumferential grooves applied to mixed flow compressor rotor [12]

2.7 Summary

Research into flow instabilities in axial compressor, mainly rotating stall has yet to lead to a definite explanation of the mechanism of stall inception that would point the way to optimal suppression techniques. However, the stall criteria proposed by Vo et al., [8] seem to be a good candidate for tip critical rotor stall assessment and will represent therefore the conceptual framework of the present study, since they are the most experimentally corroborated stall criteria found in the open literature.

While there has only been one published work on stall suppression technology for mixed flow compressors, there has been significant research in this field for axial compressors, particularly with regard to casing treatment and tip injection. None of this research has produced any set of systematic design rules for optimizing these technologies. However, they have produced some interesting results that can be used as a starting point for the current research. The main findings are summarized below.

Casing treatment

- Slots casing treatment desensitize the impact of tip clearance in stable operability range
- Conventional casing treatments in the form of grooves and slots are well-known to be effective ways to improve the stall margin of compressors by adding momentum to the endwall flow through flow.
- Regardless to the form of conventional casing treatments, it was found in general that, the greater stall margin improvement potential, the more negative is the effect on efficiency.
- Compressibility is not essential for understanding the mechanism of casing treatment.
- Circumferential grooves are less effective than slots.
- The use of casing treatment with no loss in efficiency (or even an increase) is possible when axial skewed slots extend well upstream of the rotor leading edge.

- Recess vaned casing treatments can provide an extension of stall margin without loss in efficiency and they are used in low pressure industrial fans. But their size and complexity could be a major drawback.
- Casing recirculation endwall treatments seem to be effective devices which can deliver both stall margin improvement and gain in the isentropic efficiency in certain cases. However, the main drawback is the manufacturing complexity.

Tip air injection

- Tip injection can effectively increase the stable operating margin of compressors by adding momentum to the incoming fluid at the rotor tip to delay upstream motion of the tip clearance flow.
- Tip injection is an effective tool for recovering a compressor from fully developed stall.
- It is important to minimize the injected air to reduce the efficiency penalty on the engine cycle.
- Steady micro-air injection has the potential to significantly extend the operating range of the compressor with minimal or no loss in isentropic efficiency (even with gain in some cases).
- The best location for injection was found to be over the blade passage and not upstream of the rotor leading edge.

CHAPTER 3 METHODOLOGY

3.1 Introduction

This chapter presents a general overview of the methodology used for addressing the research objectives of this project. A computational approach using three-dimensional steady and transient computational fluid dynamics (CFD) simulations is chosen, because it allows to easily investigate the detailed flow field of the compressor rotor, as opposed to much more expensive experimental techniques which can only provide limited data on the flow field. Furthermore, CFD simulations allow for exploration of different configurations of stall suppression technology, which would be prohibitively expensive and time consuming using the experimental approach. The studied configuration is that of an aero-engine mixed flow low hub-to-tip ratio rotor, whose design parameters are presented in Table 3-1 and whose side view is shown in figure 3.1. While this transonic rotor has a design relative inlet Mach number at the tip around 1.43, the current study was carried out at 65% speed for a relative inlet Mach number at the tip around 0.95 as suggested by the industrial sponsor. This subsonic operating condition avoids dealing with the added complexity brought to the flow field by passage shocks at this early stage in the study of an already difficult problem. However, it may not affect the generality of the results since the literature review on axial compressors indicated that compressibility may not play an essential role in the mechanisms behind stall inception and casing treatment operation. The nominal tip clearance size used in the current study is 0.010 inch or 0.7% of the blade tip axial chord.

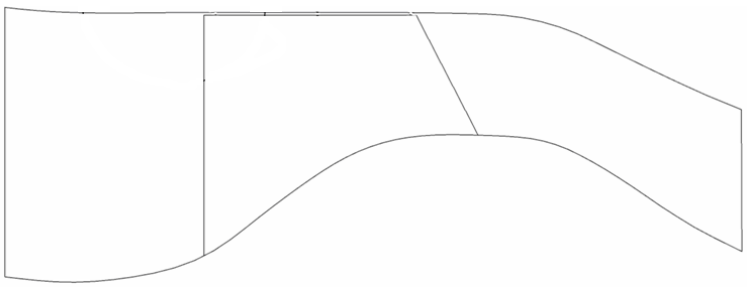

Figure 3.1: Side view of mixed flow rotor under study

Section 3.1 will give a general description of the computational tool employed. Section 3.2 describes the methodology taken to determine the stall criteria for mixed flow compressor in order to address the first objective of this research. This part will involve a brief exploration of tip injection technology as it provides a simple method to validate the stall criteria. In accordance with the second objective of this research, Section 3.3 will provide a general description of the approach taken to find the preliminary design rules for a lossless and effective casing treatment that can provide significant stall margin extension for a mixed flow compressor rotor, but that may also be applicable to axial rotors.

Table 3-1: Mixed flow rotor design parameters

Tip speed (Mach)	1.4
Total pressure ratio	2.53
Number of blades	16
Hub-tip-ratio (inlet)	0.57
Hub-to-tip ratio (exit)	0.792

3.2 Computational Tool

ANSYS CFX Version 11 was the computational fluid dynamics (CFD) tool chosen for this project. It is a Navier-Stokes commercial CFD-solver code that is commonly used for turbomachinery simulations. It is known to be a robust pressure-based code with a coupled implicit solver embedding well known turbulence models with automatic wall functions. A full steady-state convergence near choke could be reached in just a few hundred iterations without the need to initialize the flow field.

As illustrated in figure 3.1, the basic computational domain covers one blade rotor blade passage with periodic boundary conditions specified for the lateral boundaries. The single blade computational domain is justified if the rotor under study is tip critical, i.e. stall is due to tip clearance flow rather than blade boundary layer separation on the suction side over a significant

fraction of the blade span (not only near blade tip), and exhibits spike stall inception, as is the case with most modern well-designed compressor rotors. In this case, rotating stall inception starts within the blade passage and can be captured by single blade passage simulations as was shown by Vo et al. [8]. The computational domain starts from one blade pitch upstream of the rotor leading edge plane to one blade pitch downstream of the rotor trailing edge plane. The resulting upstream duct length allows for perturbation inside the blade passage of up to one blade pitch in circumferential wavelength to attenuate to zero amplitude at the computational inlet domain for the use of circumferentially uniform boundary conditions. The inlet boundary conditions consisted of a specified radial distribution of total pressure (scaled from the original radial distribution at 100% speed to 65% speed) along with a uniform total temperature. At the exit of the computational domain, a static pressure was specified which can be increased to move the operating point of the rotor up the speedline toward the stall point. The Shear Stress Transport (SST) turbulence model was used as this model has been shown by previous researchers to best capture the flow structures related to shock-boundary layer interaction [50] as better described in appendix A. Given the high Reynolds number (7×10^5) and a generally positive pressure gradient, the flow was assumed to be fully turbulent such that a transition model was not needed. An automatic wall function was applied to all solid surfaces. The remaining features of the computational setup, such as the computational domain and mesh differ for the two approaches taken to address the first and second objectives of the research and will thus be given in chapters 4 and 5.

Appendix A provides some additional details on the validation and justification of the computational setup. However, it is worth noting that the focus of the current study is on capturing the trends associated with the stall criteria and the effect of stall margin improvement technologies on these criteria and on the stall point, and not on predicting accurately the exact performance nor stall point of the compressor rotor under study. (In fact, the latter task is was not even possible since the test data for this proprietary geometry was not provided and the only feedback received from the project sponsor was an informal acceptance of the predicted performance). As such, the computational setup in this case was aimed at best practices in terms of numerical setup, such as tip mesh density and turbulence model selection, to adequately capture the flow features in the rotor tip region, mainly those associated with tip clearance flow.

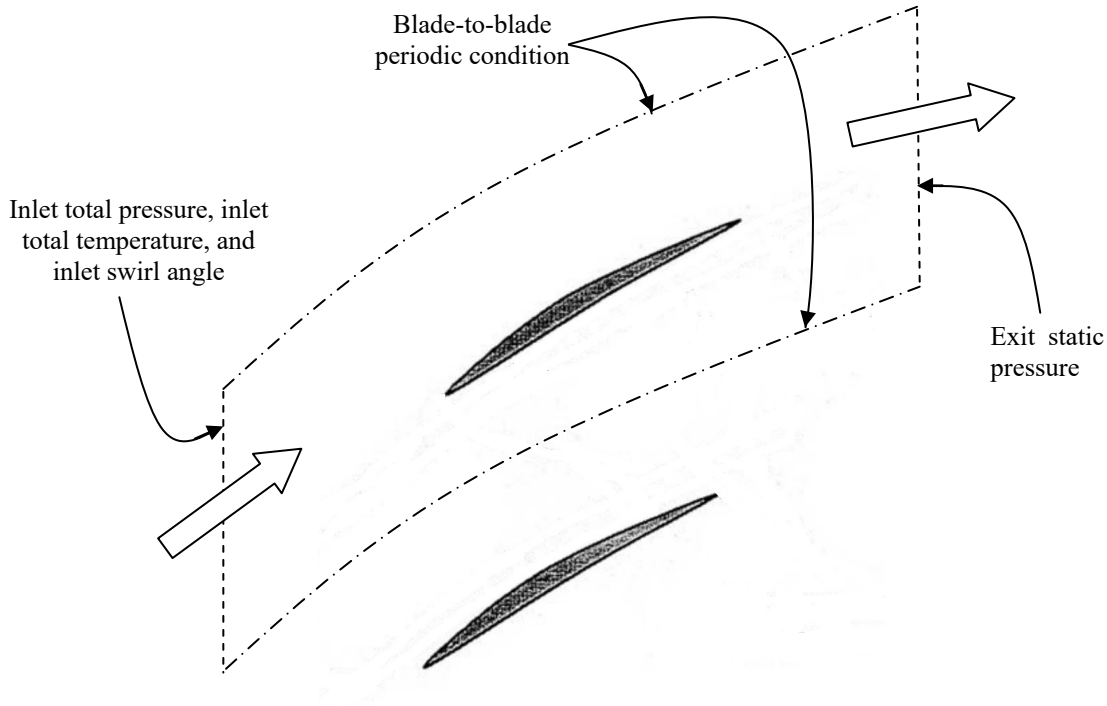

Figure 3.2: Schematic of typical computational domain (radial view)

The main post-processing tool employed was CFX-Post, which is the tool provided with ANSYS CFX. It allowed for quick evaluation of pressures and temperatures at chosen planes of the computational domain with area- and mass-averaging as well as time averaging in the case of unsteady flow field. These parameters can then be used for calculating the basic performance parameters, which are pressure ratio and efficiency. Equations (3.1), (3.2) and (3.3) were used to calculate the total-to-static pressure ratio (PR), total-to-total efficiency (η) and inlet corrected mass flow ($m_{corrected}$), where the *inlet* and *exit* subscripts represent an axial plane at the inlet and exit of the rotor, respectively, and all pressure (Pt) and temperature (Tt) parameters are mass averaged, except for static pressure (p) which is area averaged:

$$PR = \frac{p_{exit}}{Pt_{inlet}} \tag{3.1}$$

$$\eta = \frac{((\frac{Pt_{exit}}{Pt_{inlet}})^{\frac{\gamma-1}{\gamma}} - 1)}{(\frac{Tt_{exit}}{Tt_{inlet}} - 1)} \tag{3.2}$$

$$\dot{m}_{corrected} = \dot{m} \frac{\sqrt{\frac{Tt_{inlet}}{Tt_{ref}}}}{\frac{Pt_{inlet}}{Pt_{ref}}} \tag{3.3}$$

The inlet total pressure and total temperature used in the above equations are evaluated at an axial plane located at 55.6% of (axial) tip chord upstream of the blade leading edge, which is upstream of any casing treatment considered in this research. The exit total pressure and total temperature are evaluated at an axial plane located at 10.5% of (axial) tip chord downstream of the blade hub trailing edge.

3.3 Stall criteria assessment

The general approach used in determining the stall criteria for mixed flow compressor consists of two parts. The first consists of finding the stall criteria and the other to validate it using micro tip injection.

The first part is carried out by obtaining converged solutions along the pressure rise characteristics until the lowest mass flow for which a convergent solution exists, referred to as the convergence limit, which should also be the predicted stall point unless there is a numerical problem preventing convergence. This is done by first obtaining a converged solution at a stable operating point with a steady simulation. Using this solution as the initial guess, the back pressure boundary condition is set to an incrementally higher value to obtain the next solution on the speedline at a smaller mass flow. This procedure is repeated until the point where even a small increment in back pressure setting will not result in any converged solution. Instead, the mass flow dropping continuously until the simulation either crashes or ends up in a completely destroyed/meaningless flow field structure. The last converged solution is the convergence limit (in steady mode). Since flow oscillations often occur near the convergence limit which puts into doubt the accuracy of the steady simulation, an unsteady simulation is initiated at the back pressure value of the steady convergence limit using the steady solution as the initial guess and the backpressure value is increased incrementally until the unsteady convergence limit is attained. This should be the stall point of the compressor rotor.

At this point, one must first ensure that the rotor under study is tip critical and satisfies the conditions for spike stall inception under the prescribed operating conditions. For the tip-critical assessment, at the convergence limit, the flow on the blade and hub surfaces are checked for any sign of actual or imminent boundary layer separation. As a further verification, especially, if there is a sign of imminent boundary layer separation, a stall transient simulation is carried out beyond the last converged solution. Using the unsteady convergence limit as the initial solution, the stall transient is initiated by a slight increase in the back pressure value which induces a continuous drop in the mass flow through the compressor. During the initial stage of this transient, if the tip clearance flow region starts to grow before the boundary layer separates or any separation bubble grows, then the geometry is tip critical. If in addition, the total-to-static speedline has a negative slope at the convergence limit, this compressor should exhibit spike stall inception.

Next, one must look for flow features that are associated with the stall point. Since identifying the flow physics and criteria associated with stall is an entire research subject in itself, especially for a mixed flow geometry for which no such investigation has been published, we started with the hypothesis that the mechanism and criteria proposed by Vo et al., [8] for spike stall inception in axial compressor rotors, namely the leading edge spillage and trailing edge back flow of tip clearance fluid below the blade tip, apply to the mixed flow rotor. It was hoped that at least the leading edge tip clearance flow spillage criterion will apply as it has been found to be common in tip critical axial compressor rotor geometries. Thus, the flow field at the last converged solution is analyzed for the presence of the two criteria proposed by Vo et al. [8]. This analysis is carried out by plotting the parameters shown in figure 2.3, namely the entropy contours at the rotor blade tip span to show whether the incoming/tip clearance flow interface has reached the leading edge plane, and the spanwise mass flow distribution at the rotor trailing edge plane to see if the mass flow reaches zero at the blade tip (indicating imminent back flow below the blade tip).

For the second part, the rotor is simulated at the nominal (unsteady) stall point with discrete micro tip injectors. The exit static pressure is then raised to move up the speedline to see if the convergence limit can be lowered to a smaller mass flow. This exercise will allow for the assessment of the way in which tip injection affects the stall criteria both on an unsteady basis and on a time-averaged basis to validate the criteria through the fact that their suppression allows for a delay of the stall point.

3.4 Casing treatment analysis

The chosen methodology to address the second research objective starts with the establishment of the most promising casing treatment configuration for the mixed flow rotor under study based on all the knowledge accumulated from casing treatment research in axial compressors, which points to a slots casing treatment. Using this baseline geometry, a parametric study is carried out in terms of the main geometric parameters defining a slot casing treatment: axial slot location, slot skew angle, slot axial angle, open area ratio, number of slots per blade pitch and perhaps slot shape. For each configuration, a speedline from near choke to the convergence limit is obtained through CFD simulations to assess the change in the stall mass flow (stall margin improvement) and peak-efficiency with respect to the solid casing (no casing treatment) case. The same comparison and analysis is made between different slot configurations in which a parameter is

varied. The above analysis should lead to preliminary design rules that indicate the direction, and perhaps the amount, in which geometric parameters for slot casing treatment should be varied to achieve the goal of maximizing surge margin while minimizing losses (or maximizing gain) in efficiency near the design point. In addition, a new slots casing treatment geometry that combines the positive lessons learned may also be produced and assessed.

Given the fact that such an extensive parametric study for casing treatment has never been attempted for any compressor due to the computational costs, a new computational setup must be devised to comply with the constraints in computational time and resources. Furthermore, the number of simulated casing treatment configuration needs to be minimized, by constraining certain parameters to beneficial ranges. The hypothesis based on the literature review is that flow recirculation by the slots and viscous losses within the slots need to be minimized in order to reduce the negative impact on efficiency and increase the effectiveness in term of surge margin extension. Thus, the slot axial location will be confined to the front part of the blade passage, the slot area ratio will be in the small range and the slot shape is set as a semi-circular arc (as opposed to a rectangular shape that has viscous losses in the square corners).

Finally, a preliminary assessment of the flow mechanism associated with a successful casing treatment is attempted by looking at how the most successful casing treatment configuration affects the flow field in terms of the stall criteria and loss generation in the rotor tip region.

CHAPTER 4 DETERMINATION OF STALL PREDICTION CRITERIA

4.1 Introduction

This chapter aims to determine criteria for predicting stall inception in tip-critical mixed flow compressors. In this case, only the criteria for short-length scale rotating stall inception are important since modal stall inception criterion is related to the total-to-static speedline slope of the entire compression system and not any blade row. The methodology for this part of the work consists of carrying out simulations of the mixed flow rotor under study until the convergence limit to investigate the flow field at this point for tip criticality and to verify the two spike stall inception criteria proposed by Vo et al. [8] for axial compressors. Subsequently, micro tip injection is introduced as a relatively simple numerical mean to affect these criteria and delay rotating stall. This exercise will further help to validate these criteria as well as to give a preliminary assessment of the effectiveness of micro tip injection as a stall delay strategy for this type of compressor against which to compare the performance of casing treatment.

The chapter starts with the study to determine the stall criteria in section 4.2, followed by the micro tip injection assessment in section 4.3. As the mesh setup is different for each case, each section will first provide a description of the features of the mesh followed by the results. Further details of the mesh and numerical setup are provided in appendix A. The chapter concludes in section 4.4 with a summary of the findings and a discussion of possible flow physics behind the stall inception mechanism.

4.2 Stall criteria assessment

4.2.1 Mesh

The mesh used for the simulations to assess the stall criteria is a shown in figure 4.1. It is a single domain structured mesh with roughly 400,000 nodes with a dense mesh in the tip clearance gap as well as near all solid surfaces. It is generated with ANSYS Turbo-grid following the best practice in terms of tip clearance mesh density and a mesh study for this rotor, as discussed in

more detail in section A.4.1 of appendix A. Boundary conditions and simulation procedures are as described in section 3.2.

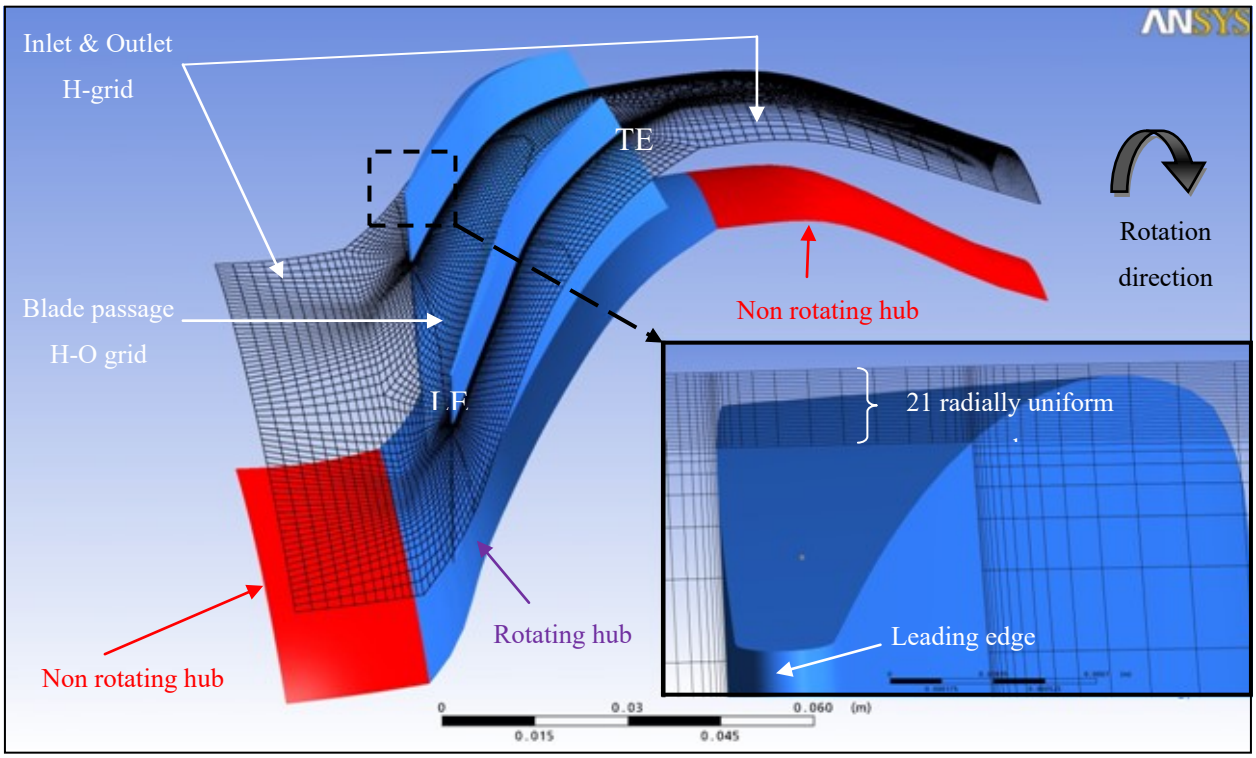

Figure 4.1: Mixed-flow rotor computational grid and tip clearance gap mesh.

4.2.2 Results

Simulations are first carried out for the computational domain described in figure 4.1 at 65% design speed to determine the speedline by increasing the exit static pressure boundary conditions until the limit of convergence. Figure 4.2 shows the resulting total-to-static pressure rise characteristics (speedline), where the unfilled symbols represent steady-state solutions. Flow oscillations appeared in the steady-state simulations close to the convergence limit (stall point), indicating the presence of flow unsteadiness. Thus, simulations for points near stall were carried out in unsteady mode with a time increment of 10 time steps per blade passing. This is the same number of time steps used by our sponsor to validate CFX for a public reference transonic axial compressor rotor geometry (NASA Rotor 37). At convergence, these simulations exhibited

oscillations in time of mass flow with constant amplitude and mean value. This time history is used to determine period associated with of the main frequency of oscillations. The time-averaged solution is obtained by restarting the time-accurate simulation in CFX for the number of iterations corresponding to the main time period of oscillations and activating the time-averaging feature. The points corresponding to these time-averaged solutions are plotted as filled symbols on figure 4.2.

The convergence limit (leftmost point in figure 4.2) is the point of focus for determining the flow criteria for predicting spike stall inception, starting from the two criteria proposed by Vo et al. [8] for axial compressors. The first criterion is the alignment at the rotor tip leading edge plane of the interface between the incoming flow and tip clearance flow, signaling onset of tip clearance flow spillage below the blade tip leading edge into the adjacent blade passage. This is evaluated by plotting the contours of entropy at the spanwise plane corresponding to the rotor blade tip. The incoming/tip clearance flow interface is represented by the large gradient line between the low-entropy incoming flow and the high-entropy tip clearance flow. Vo et al. [8] suggested that this criterion would apply on a time-averaged basis for flows with oscillations, which is the case of the convergence limit in figure 4.2 for which the time history of mass flow in figure 4.3 indicates flow oscillations of significant amplitude. Figure 4.4 plots the instantaneous entropy contours at the blade tip of the mixed flow rotor at the three time instants shown on figure 4.3, as well as that obtained from the corresponding time-averaged flow field. The instantaneous flow fields in figure 4.4 indicates oscillations in the tip clearance flow, which at time 3 seems to spill ahead of the adjacent blade leading edge. However, the time-averaged flow field shows that the time-averaged incoming/tip clearance flow interface is lined up with the leading edge plane but still inside the blade passage. In other words the tip clearance flow is on the verge of spillage into the adjacent blade passage. This indicates that the first criterion proposed by Vo et al. [8] applies to a mixed flow compressor. This criterion also seems to be the most generically observed for axial compressors.

The second spike stall inception criterion proposed by Vo et al. [8] for axial compressors is the onset of backflow of tip clearance fluid at the rotor trailing edge below the blade tip, which then impinges on the pressure side of the adjacent blade. This criterion is satisfied when the spanwise distribution of mass flow at the rotor trailing edge reaches zero at the blade tip. This distribution is thus plotted in figure 4.5 for the mixed flow rotor from the time-averaged solution at the

convergence limit. The results indicate that this criterion is not satisfied for mixed flow compressors, perhaps because the aspect ratio of mixed flow compressor rotors is significantly smaller than axial compressor rotors, leading to a much longer chord for the same span.

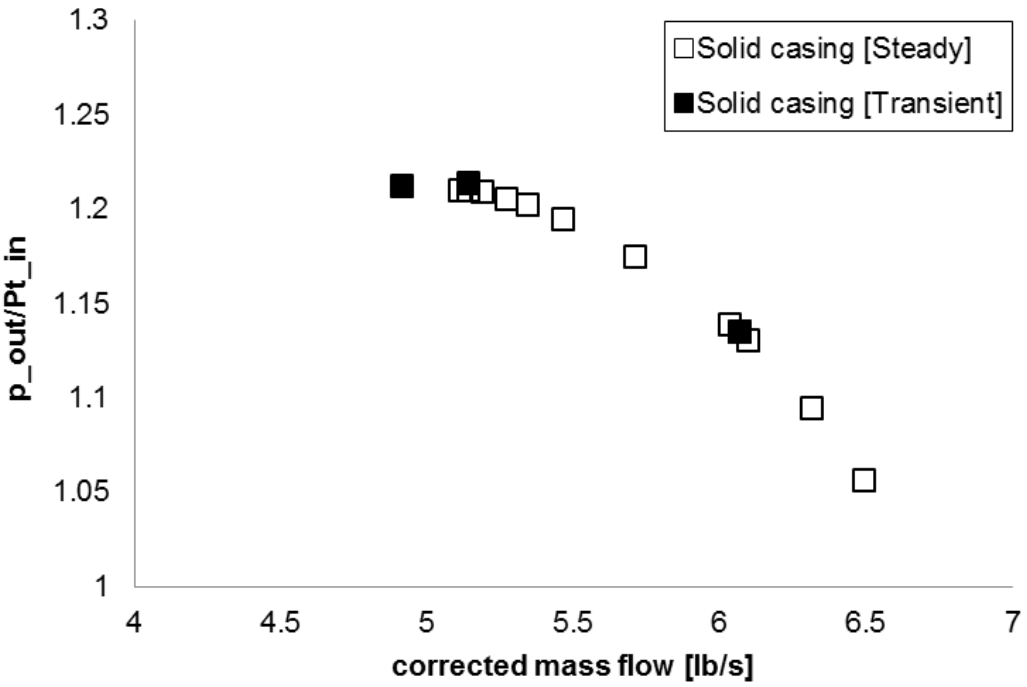

Figure 4.2: Rotor total-to-static pressure rise characteristic at 65% speed

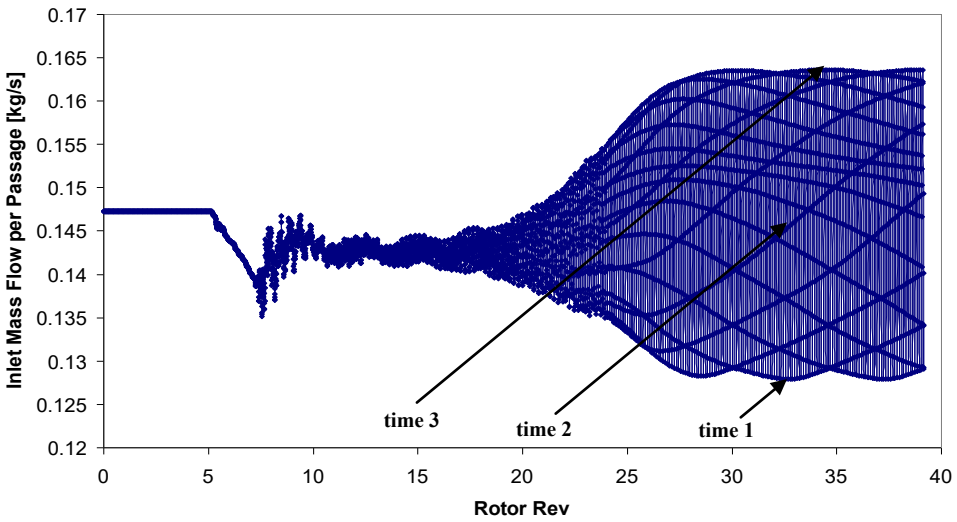

Figure 4.3: Inlet mass flow history of unsteady simulation near stall of the mixed-flow rotor at 65% speed

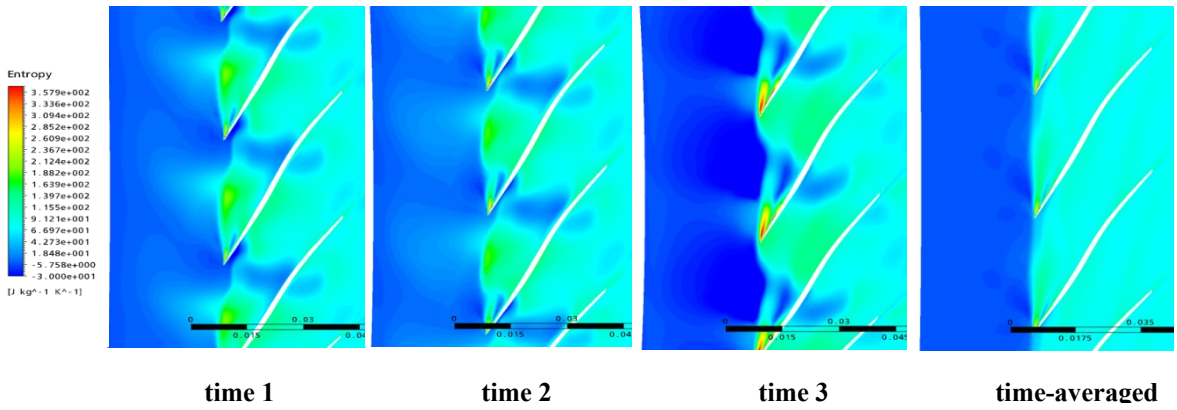

Figure 4.4: Instantaneous and time-averaged entropy contours at blade tip for the convergence limit point in figure 4.2

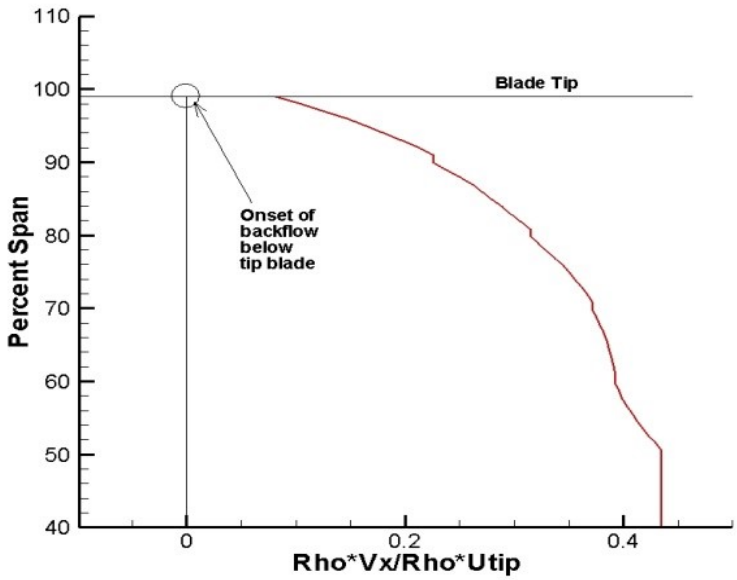

Figure 4.5: Time-averaged spanwise distribution of mass flow at the rotor trailing edge for the convergence limit point in figure 4.2

In summary, the above results indicate that the alignment of the incoming/tip clearance flow interface is a spike stall criterion for mixed flow compressors as it is for axial compressors. However, trailing edge backflow is not an applicable spike stall criterion. However, before certifying this stall criterion associated with tip clearance flow to be the source of stall, one must ensure that this mixed flow rotor is tip critical, i.e. that tip clearance flow is the cause of the convergence limit, rather than blade boundary layer separation. A transient simulation beyond the last converged solution was thus carried out to assess the behavior of the tip clearance flow and suction side boundary layer during the blade passage stall transient to confirm tip criticality. Figure 4.6-a shows the mass flow history during the stall transient as the flow field breaks down, while figures 4.6-b and 4.6-c plots the entropy contours at the blade tip and near suction-side streamlines, respectively, for a point during this transient. Figure 4.6-b shows that the incoming/tip clearance flow interface lies upstream of the leading edge plane, indicating tip clearance flow spillage criterion below the rotor tip leading edge as the source of the flow breakdown at stall as described in Vo et al. [8] for a tip axial critical compressor. At the same time, figure 4.6-c shows no sign of boundary layer separation. Thus, the results in figure 4.6 indicate that this mixed flow rotor geometry is indeed tip critical at 65% speed and also reinforces the proposed stall criterion.

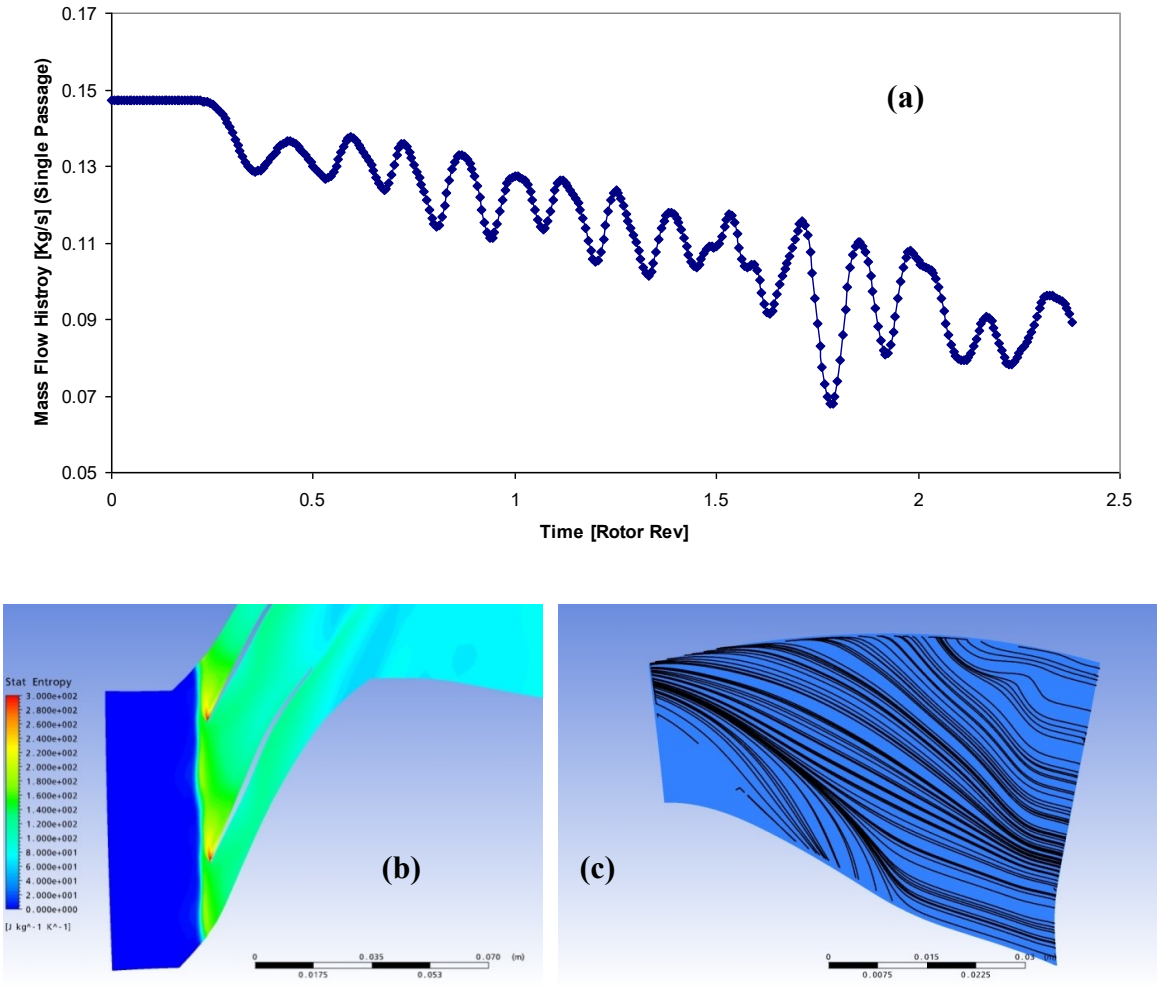

Figure 4.6: Mass flow history (a) for unsteady simulation past last converged solution in figure 4.2 along with entropy contours at the blade tip (b) and streamlines at 0.23% tip pitch from the suction side (c) for point 1 during blade passage stall transient

4.3 Effect of micro tip injection

Micro tip injection is chosen for the task of showing that the stall point can be delayed by affecting the stall criterion identifies in section 4.2.2 because it is a very localized actuation that only affects the tip clearance region. Furthermore, while casing treatment usually renders the tip region much more complex and may recirculate high entropy tip clearance fluid upstream of the blade leading edge making the detection of the incoming/tip clearance flow interface by entropy very difficult, tip injection is unidirectional and does not alter the incoming flow entropy.

4.3.1 Mesh

The addition of semi-circular micro-tip injection tubes upstream of the rotor required splitting the domain into a stationary part for the injectors and a rotating part for the rotor blade passage, separated by a sliding plane interface. However, as discussed in detail in section A.4.2 of appendix A, the use of the same mesh as for the rotor passage as that in section 4.2.1 caused excessive numerical diffusion of the injected jet across the sliding plane interface due to mesh density compatibility across the interface. Since an increase in mesh density to resolve this issue would be problematic in terms of computational time and resources, a new mesh philosophy was devised for this part of the study. As illustrated in figure 4-7, the computational domain is split into an upstream subdomain (Block 1), meshed with ICEM-CFD, that is stationary and incorporates the injector, and a downstream rotating subdomain that includes the blade passage (Blocks 2,3 and 4) and exit duct (Block 5). A sliding plane interface located just downstream of the injector exit connects the two subdomain. In order to resolve the flow region of interest where the injected air interacts with the tip clearance flow near the blade tip leading edge region, a very fine mesh has been employed within the localized Block 2. For the other parts of the blade passage (Blocks 3 and 4) and the exit duct (Block 5), at different levels of coarse mesh can be used since the boundary layers has been shown in section 4.2.2 to not play a determining factor in stall inception. This strategy allowed the mesh size of the entire computational domain to be reduced to around 95,000 nodes, which also help reduce computational time for the unsteady simulations. As shown in figure 4.8, the micro tip injector is modeled as a semi-circular tube protruding below the shroud and it is meshed with ICEM-CFD. Figure 4.9 shows the details of the mesh in the overall computational domain. It consists of a multi-block H-grid unstructured

mesh with hexahedral elements. Nine radially non-uniform nodes are dedicated to the tip clearance gap. The shroud and upstream part of the hub are specified as stationary while the other solid surfaces are rotating. The y+ values at the solid surfaces are as high as 190 and an automatic wall function condition is applied to all solid surfaces. Section A.4.2 of appendix A provides more details on this unconventional mesh including a direct visual comparison with the mesh of conventional mesh of section 4.2.1 and of their performance in capturing the stall criterion identified in section 4.2.2.

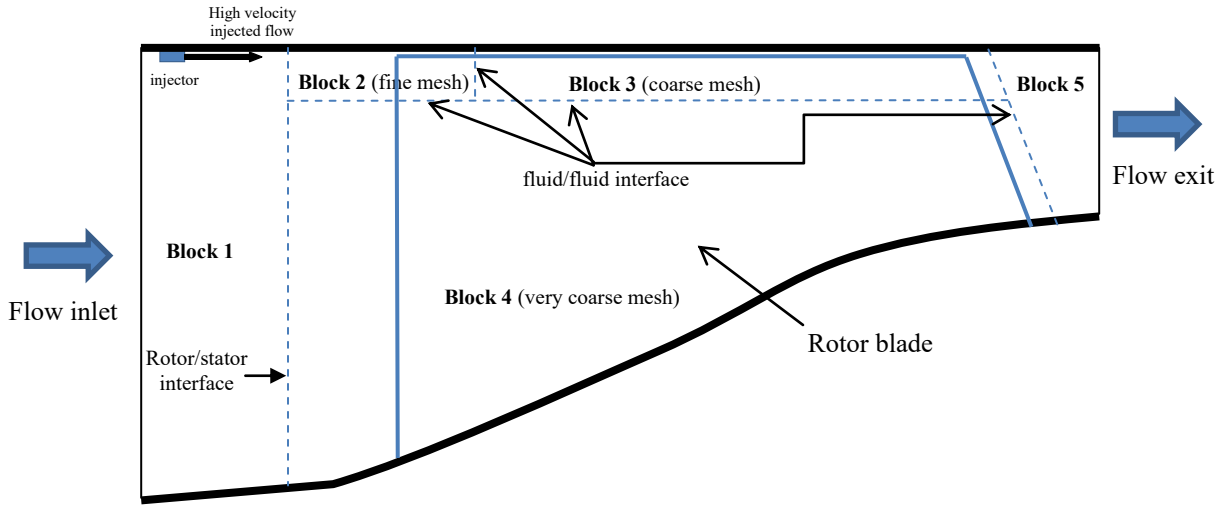

Figure 4.7: Multi-block computation domain

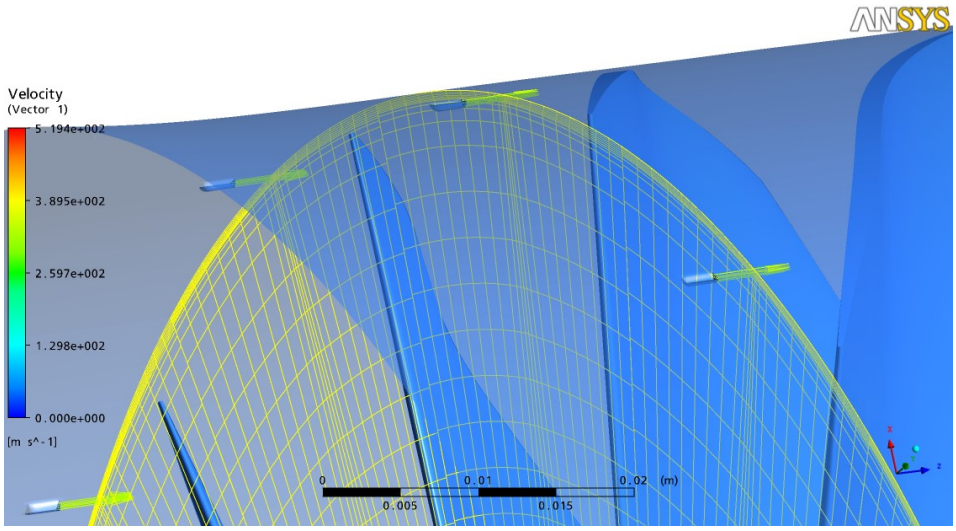

Figure 4.8: Incorporation of micro tip injectors into computational domain

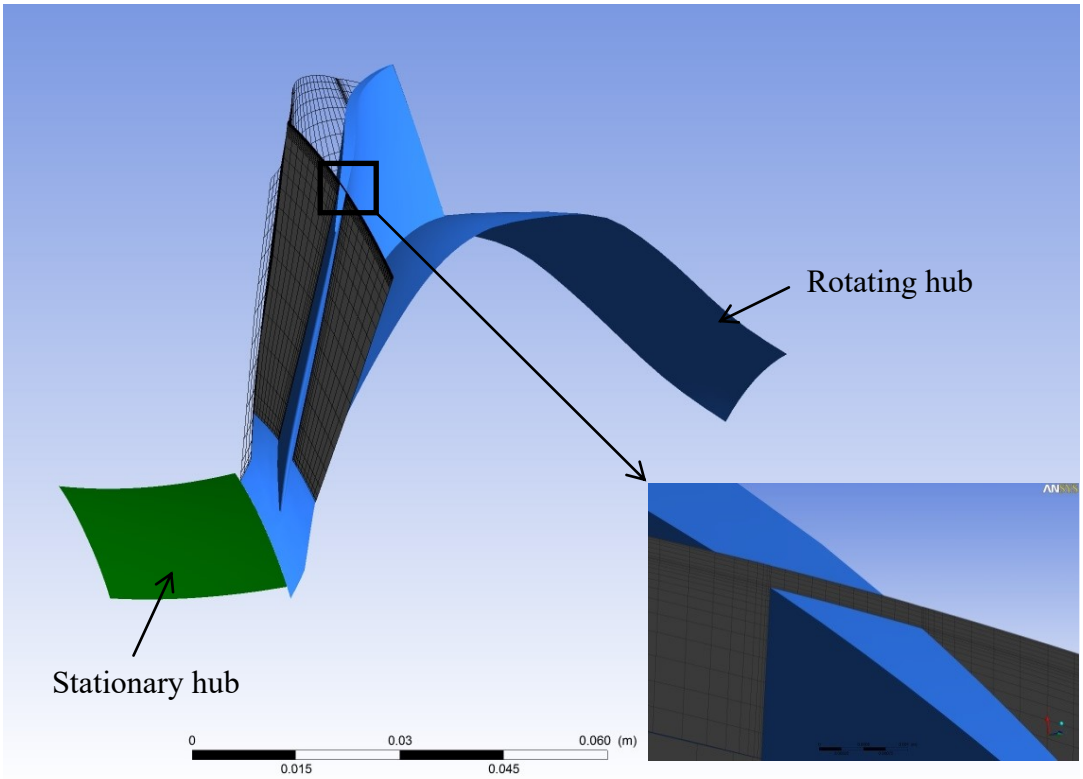

Figure 4.9: Mixed-flow rotor computational grid and tip clearance gap mesh

4.3.2 Results

The micro-injectors (one per blade passage) as shown in figure 4.8 were simulated by imposing a set total pressure as the boundary condition for the injected air. Unsteady simulations were carried out starting with initial flow fields obtained from steady runs with a mixing plane interface between the stationary and rotating subdomains. The main simulations had a jet total pressure at 1.5 times the computational domain inlet total pressure, resulting in a time-averaged injected mass flow of about 0.02% of the incoming flow and a jet velocity about four times that of the background flow.

Figure 4.10 shows the comparison of pressure rise characteristics for the mixed flow compressor at 65% speed with injection versus the reference (no injection) case. To save time, the simulations at points away from the convergence limit (unfilled symbols) were carried out in steady mode with a mixing plane interface. Simulations near stall (filled symbols) were

performed in unsteady mode with 30 time steps per blade passing. This number was used rather than 10 time steps per blade passing to allow for a more incremental movement of the micro tip injector across the blade passage to better capture the overall (time-averaged) effect from its highly localized injected flow . The results show that the micro-tip injection has very little impact on the shape of the speedline, but succeeds in delaying the convergence limit (stall point). To investigate its effect on the tip region flow field, figure 4.11 plots the time-averaged entropy contours at the blade tip at the unsteady convergence limit of the reference (no injection) case (point 1 in figure 4-10) versus injection case (point 2 in figure 4-10). As expected, the incoming/tip clearance flow interface is aligned with the blade tip leading edge plane at the no-injection convergence limit, marking the onset of tip clearance flow spillage. However, at the presence of micro-tip injection keeps this interface at the same location at a lower mass flow (point 2 in figure 4-10). In other words, tip injection has managed to delay the onset of tip clearance flow spillage to a lower mass flow where the rotor without injection would have stalled. While the simulations with injection (using an exit static pressure boundary condition) did not result in a point at exactly the same corrected mass flow as point 1 in figure 4-10 to compare the interface location without and with injection, it can be inferred that the local injection managed to push the incoming/tip clearance flow interface enough downstream on a time-averaged basis to delay stall to a lower mass flow. The above results reinforce the proposed spike stall criterion for mixed flow compressor. It also indicates that micro tip injection (with one injector per blade passage) can extend the stall mass flow on the order of 5%.

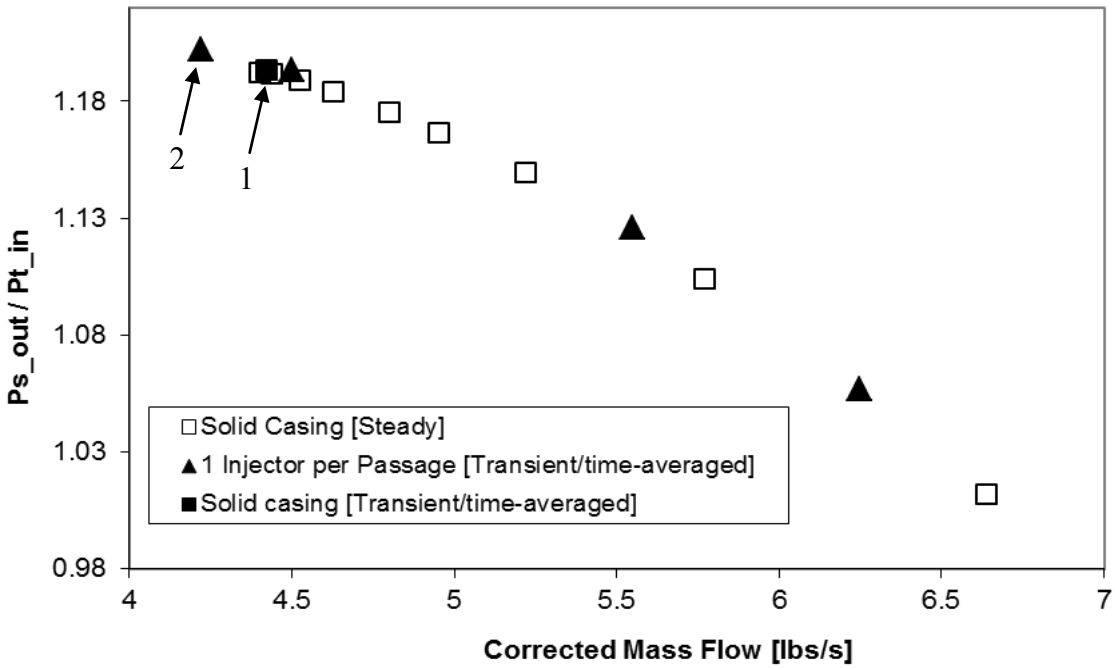

Figure 4.10: Performance comparison for mixed flow rotor without and with micro tip injection

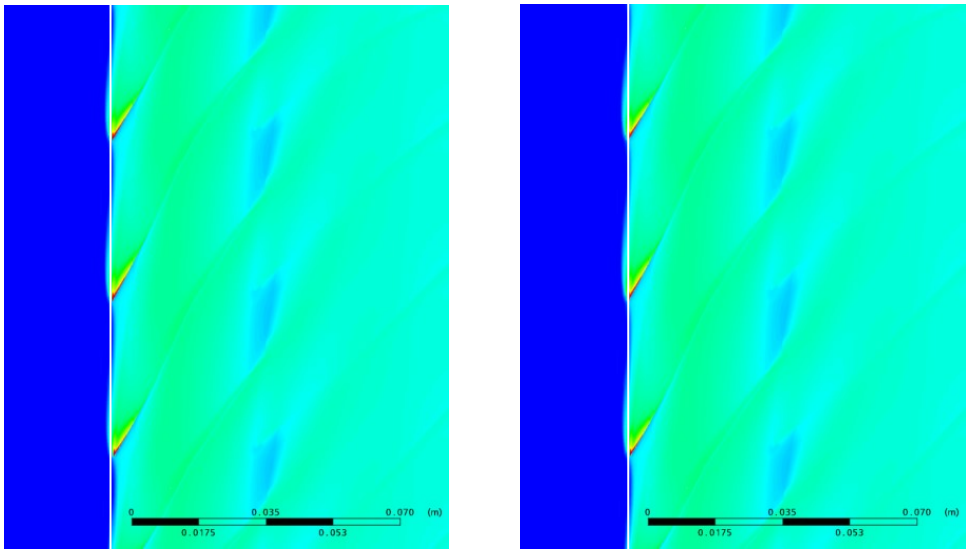

(a) (b)

Figure 4.11: Entropy contours at the mixed flow rotor tip at the last (unsteady) converged point for (a) no-injection (point 1 in figure 4-10) and (b) with micro tip injection (point 2 in figure 4-10)

4.4 Summary and discussion

Investigation of the flow field at the convergence limit at 65% speed indicates that the mixed flow rotor is indeed tip critical and the stall inception criterion for the prediction of spike stall inception for mixed flow compressors is the alignment of the incoming/tip clearance flow interface with the leading edge at the rotor tip plane on a time-averaged basis. This is consistent with what has been proposed for axial compressors by Vo et al. [8]. The proposed stall inception criterion is reinforced by simulations with micro tip injection and is the first stall prediction criterion for tip-critical mixed flow compressors. While this study was carried out on one mixed-flow rotor geometry, the probability is good that it is also generally applicable to all tip-critical mixed flow compressors since this criterion seems to be generic for axial compressors.

However, the results also show that the trailing edge tip clearance backflow criterion for spike stall inception as proposed by Vo et al. [8] for axial compressors and illustrated in figure 2.3-b does not apply to mixed flow compressors. A possible explanation can be made by drawing attention to their lower aspect ratio (i.e. larger chord for a given span) of a mixed flow compressor rotors compared to an axial compressor rotor. This feature means that the tip clearance flow has a relatively longer residence time in the blade passage as it convects downstream, which improves mixing with the core flow. Moreover, the stronger secondary flows present in such type of compressors initiated by stronger radial movement of boundary layer fluid will also reinforce this mixing. The higher mixing between the tip clearance flow and core flow within the blade passage would increase the streamwise momentum of the tip clearance flow enough by the time it reaches the trailing edge to render it unlikely to reverse back into the adjacent blade passages as was the case in figure 2.3-b. However, the spike stall inception mechanism proposed by Vo et al. [8] on the tip clearance flow requires impingement on the adjacent blade pressure side from trailing edge backflow (see figure 2.3-b). The question is thus whether this mechanism would still be relevant to spike stall inception in mixed flow compressors in the absence of the trailing edge tip clearance backflow. One can hypothesize that in a mixed flow compressor rotor the impingement of the clearance flow on the adjacent blade tip pressure-side can occur near mid-chord, as illustrated in figure 4.12. At this location, the tip clearance flow has yet to mix sufficiently with the core flow and thus still has low streamwise momentum making it likely to reach and impinge upon the adjacent blade. If this is the case, then

the spike stall inception mechanism proposed by Vo et al. [8] would still apply. Additional investigations are required to assess the validity of the above hypothesis associated with the absence of the trailing edge tip clearance backflow criterion.

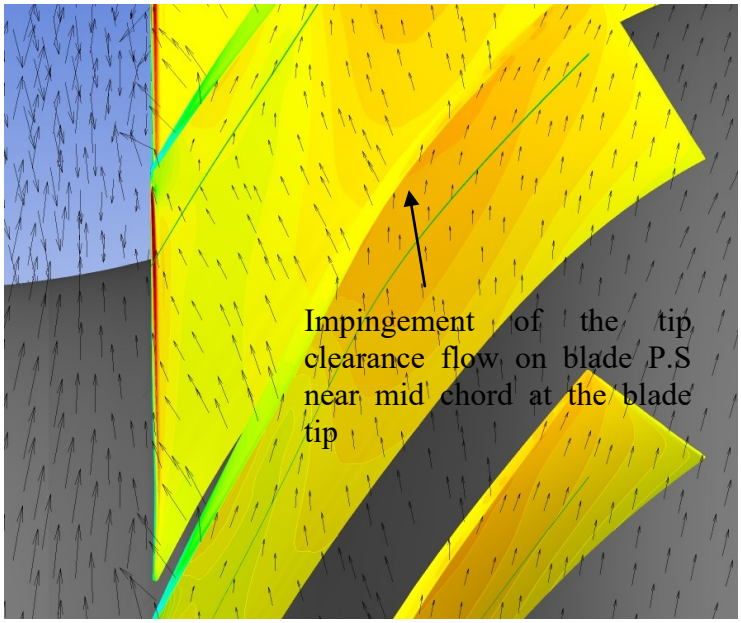

Figure 4.12: Flow impingement near mid chord at the blade tip

CHAPTER 5 EFFECTIVE LOSSLESS CASING TREATMENT DESIGN

5.1 Introduction

This chapter describes the numerical study to determine the preliminary design rules for a casing treatment for mixed flow compressors that can deliver significant stall margin improvement without penalty in peak efficiency.

The methodology essentially consists of obtaining a baseline slot casing treatment design based on the literature for axial compressors and preliminary iterations. A computational parametric study was then carried out by varying one by one different design parameters of the baseline casing treatment, namely slot axial position, open area ratio, number of slots per passage, slot skew angle, slot stagger angle, radial slot shape, meridional slot shape, slot axial length and slot depth. Simulations would be carried out to obtain the speedline of the mixed flow rotor without casing treatment (solid casing) and with each of the casing treatment configuration to evaluate the change in stall margin and peak efficiency, in order to propose, at this stage, general rules/trends for casing treatment design that would improve surge margin without efficiency penalty. However, a suitable computational strategy must be devised to make this most extensive parametric study of casing treatment to date possible at reasonable computational expense.

Section 5.2 introduces the baseline casing treatment configuration, while section 5.3 describes the computational setup specific to this study of casing treatment as well as the computational strategy. Section 5.4 presents the results with a summary of the findings given in section 5.5.

5.2 Baseline casing treatment selection

Based on the literature review for casing treatment in axial rotors covered in Chapter 2, a semi-circular axial skewed slot casing treatment placed in the leading edge region was chosen as the starting configuration as it has the best potential of producing stall margin improvement with low peak efficiency loss. This casing treatment is characterized by three axial semi-circular slots per blade passage with a skew angle of 60º, inclined in the direction of rotor rotation, as illustrated in figure 5.1. The axial length of each slot is 71% of the blade tip axial chord with half of it lying upstream of the leading edge. The open area ratio (OAR) as illustrated in figure 5.1 is 40%. From

the axial compressor literature, the semi-circular shape should minimize total pressure loss within the cavity by avoiding stagnation zones [24], the skew in the rotor rotation to improve stall margin [21] and forward positioned (axially upstream) to reduce the flow recirculation at the design point and minimize peak efficiency loss [23]. Bent skew slots as studied by Lu et al. [25], which are complex designs, were not considered in this basic parametric study into the effect of individual design parameters for slots casing treatment.

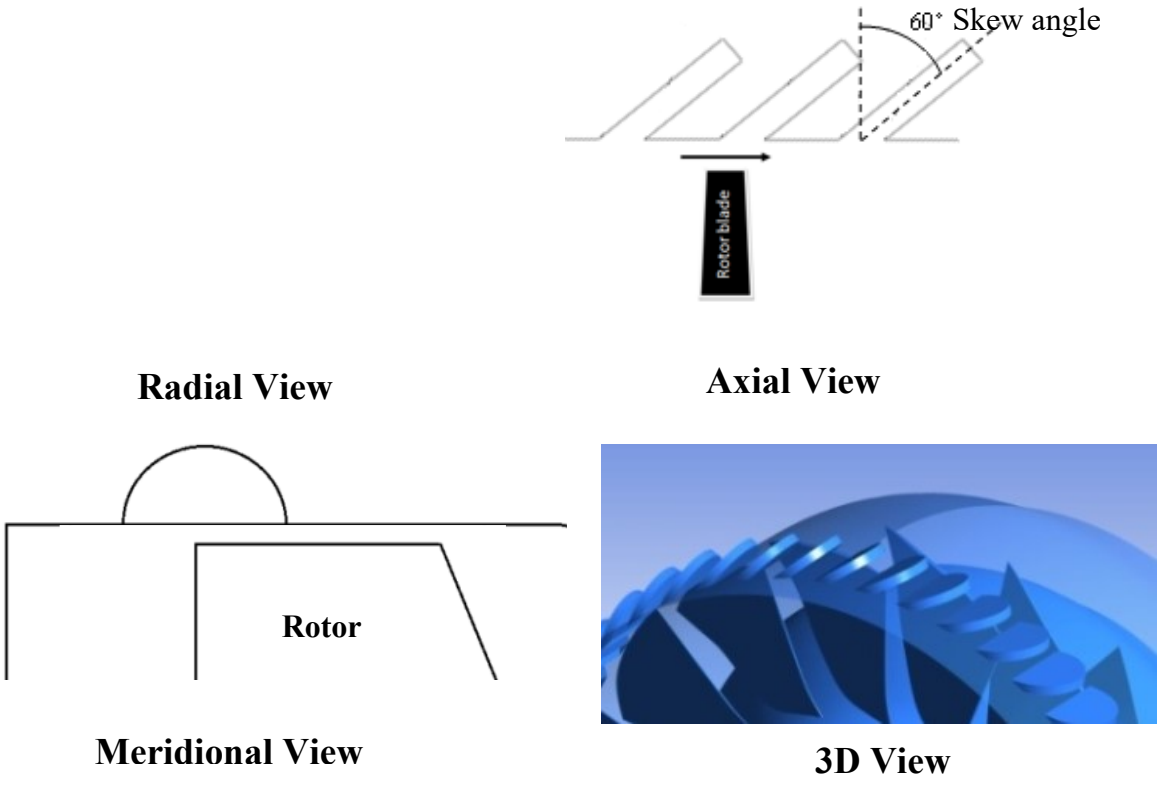

Figure 5.1: Baseline axial skewed slot casing treatment configuration

5.3 Computational setup

The mesh used for the CFD simulations was a structured mesh obtained through ICEM CFD with two domains, namely the rotor domain and the casing treatment (slots) domain. The mesh for the rotor domain is based on the mesh used in section 4.2 for the tall criteria assessment. As illustrated in the bottom of figure 5.2, the casing treatment domain extends below the shroud into the rotor domain by 25% of the tip clearance height, with a sliding plane fluid-fluid GGI interface placed between them. Details of the mesh setup for the casing treatment domain are given in section A.4.3 of Appendix A. The total number of nodes for the entire computational domain was about 600,000.

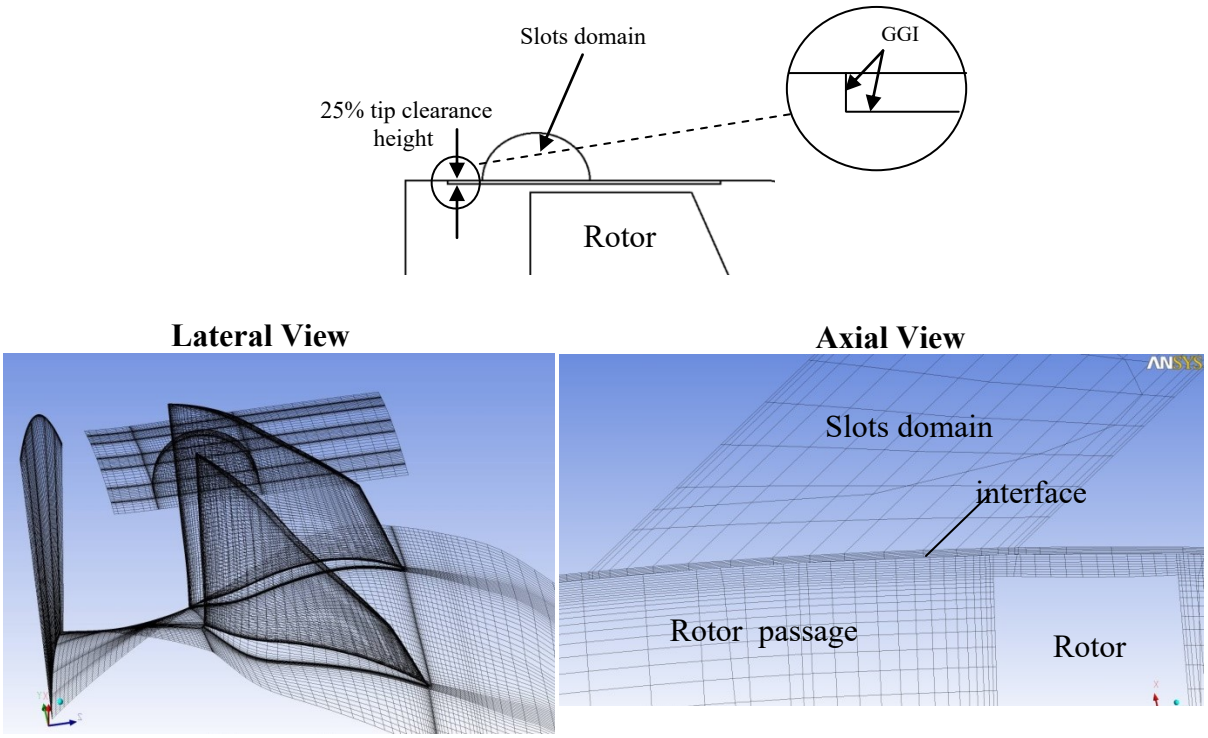

Figure 5.2: Computational domain setup and mesh

The interaction of a slots casing treatment with the rotor domain is inherently unsteady such that simulations must in principle be carried out in unsteady mode. However, one such simulation takes at least several days of computational time on a personal computer, with the convergence

time increasing as one gets closer to the convergence limit. Thus, the amount of simulation time to obtain even a single speedline as one moves point by point up the speedline in search of the stall point would be prohibitive. This is the reason why no extensive parametric study of such casing treatment has been attempted.

Given the constraints in computational time and resources, a new strategy was set up to carry out the present parametric study. This strategy was built upon steady and also in most cases, unsteady simulations. Initial trials showed that the steady simulations in CFX in frozen rotor mode, whereby the position of the slots are frozen with respect to the rotor blade, could roughly capture the speedline shape obtained with unsteady (transient) simulations while being much less time consuming. Thus, the procedure used in the parametric study to evaluate the change in surge margin and peak efficiency associated with each casing treatment configuration is illustrated in figure 5.3 for the baseline axial skewed slot casing treatment. First, the speedline (total-to-static pressure rise and total-to-total efficiency) for the solid casing (reference) case is obtained through many steady simulations (empty diamond) and a few unsteady simulations (solid diamond) to precisely locate the peak efficiency and stall points against which the casing treatment simulations will be compared. For each casing treatment configuration a large number of steady simulations (empty triangles) in frozen rotor mode were carried out to capture the entire speedline up to the stall point. In most configurations, at least two unsteady simulations (with sliding plane interface at the rotor-slots boundary) were then carried out (filled triangles), namely at the same corrected mass flow as the steady peak efficiency and stall points. Even if these points are not the exact peak efficiency and stall points, when compared with the solid casing case, these two points indicate the least stall margin extension and the largest peak efficiency loss or smallest peak efficiency gain change associated with the casing treatment configuration. This approach allowed confirmation of the trends observed in steady simulations without the excessive cost of simulating, in unsteady mode, the many points on each speedline to iterate for the peak efficiency and stall points for all casing treatment configurations.

The unsteady simulations were carried out at 25 time steps per blade passing. The justification for this time step value is provided in section A.5 of appendix A.

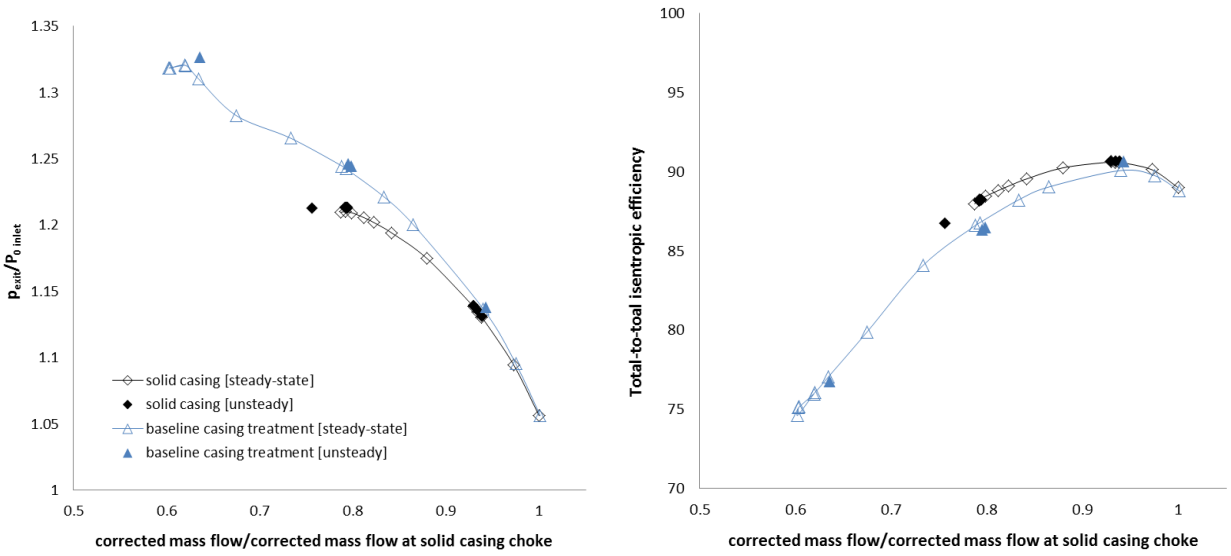

Figure 5.3: Illustration of computational strategy for parametric study using baseline axial skewed slot casing treatment

The flow properties used to calculate the pressure ratio and efficiency are obtained at 55% of axial tip chord upstream of the rotor leading edge (also upstream of the slots' leading edge) and 37% axial tip chord downstream of the rotor tip trailing edge and averaged according to Cumpsty and Horlock [49], namely work-averaged for the stagnation pressure and mass-averaged for stagnation temperature. The static pressure was area-averaged. For converged unsteady solutions, the fundamental oscillation frequency was found after performing a fast Fourier transform (FFT) on the time distribution of the exit mass flow. The simulations were then extended and the flow field time-averaged over the time period associated with this frequency. If the fundamental frequency is too small (period too large) for practical extension of the simulations, the solution is time-averaged over a practical time interval that covers as much as possible the periods of the higher frequencies.

5.4 Results

Table 1 illustrates the simulated casing treatment configurations of the parametric study and tabulates the associated change in stall margin and peak efficiency from the solid casing reference case, from both steady as well as unsteady simulations, when the latter are available. It must be reminded that the unsteady results are not meant to give the exact stall margin improvement nor peak efficiency change. Instead, they confirm the minimum surge margin improvement and indicate the worst loss or least gain in peak efficiency possible.

The stall margin improvement as given in Table 5.1 is defined by equations (5.1) and (5.2).

$$\Delta SM = \left(\frac{\Delta \dot{m}_{casing\ treatment\ stall} - \Delta \dot{m}_{solid\ casing\ stall}}{\Delta \dot{m}_{solid\ casing\ stall}}\right) * 100 \tag{5.1}$$

$$\Delta \dot{m} = \dot{m}_{peak\ efficiency} - \dot{m}_{near\ stall} \tag{5.2}$$

Below is a discussion of the results from each parametric variation with reference to the results shown graphically through speedlines and summarized for all cases in Table 5-1. It is noted that just a few unsteady simulations are missing, particular near stall, due to time constraints or convergence problem issues (they are identified as a hyphen in table 5-1).

a) Effect of slot axial position

The baseline slot of figure 5.1 is shifted axially by a quarter of its length in either upstream or downstream direction, as illustrated in figure 5.4. The results in figure 5.5 show that an axial shift that leaves part of the slot upstream of the leading edge region does not have a large impact on stall margin improvement but pointed to an optimum value lying near the 50%-50% (baseline) position. However, the steady results indicate a decrease in peak efficiency with more downstream slot position, thus confirming a trend from the literature on axial compressors that a more upstream slot position is less penalizing in peak efficiency.

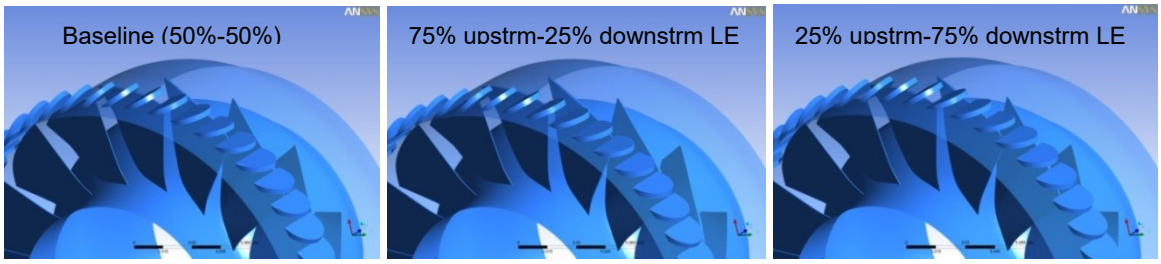

Figure 5.4: Simulated configurations with variation in slot axial position

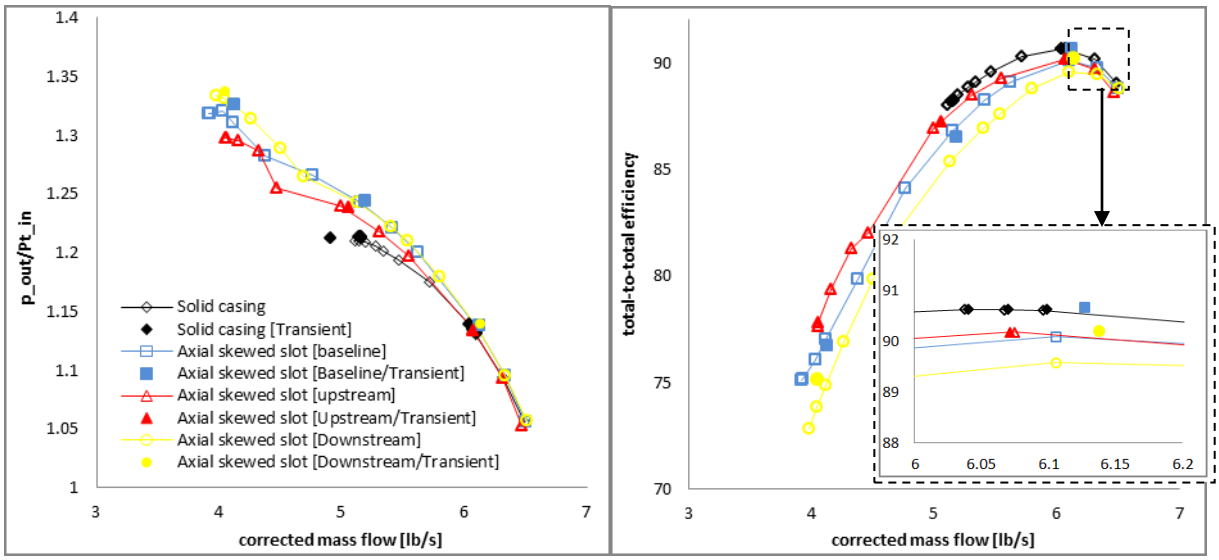

Figure 5.5: Effect of slot axial position on rotor performance

b) Effect of open area ratio (OAR)

The baseline slots' 40% open area ratio is increased to 60% and reduced to 20% (see figure 5.6). According to figure 5.7, the steady-state simulations indicate that the stall margin increases significantly with the open area ratio, while the peak efficiency initially decreases with increasing OAR but seemed to level off at least up to 60% open area ratio. However, the variation in peak efficiency is less pronounced than that associated with variation in slot axial position. The unsteady simulations confirm a significant stall margin improvement for the 60% open area ratio slot versus the baseline 40% and also point to a slightly larger gain in peak efficiency with respect to the solid casing. It is noted that there may be an upper limit in open area ratio in term of performance considerations that is not captured in the current simulations.

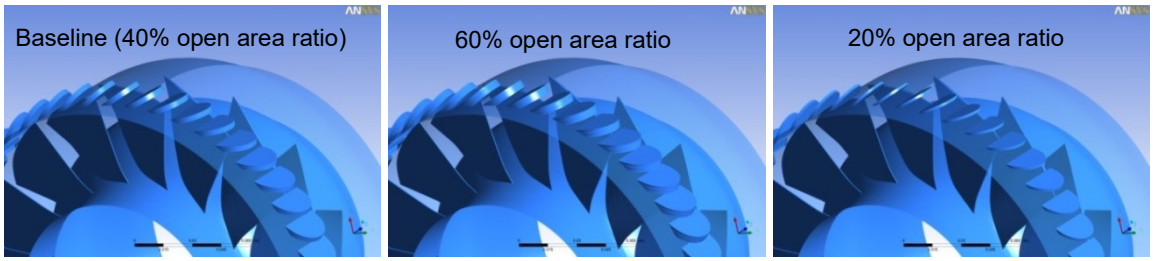

Figure 5.6: Simulated configurations with variation in open area ratio

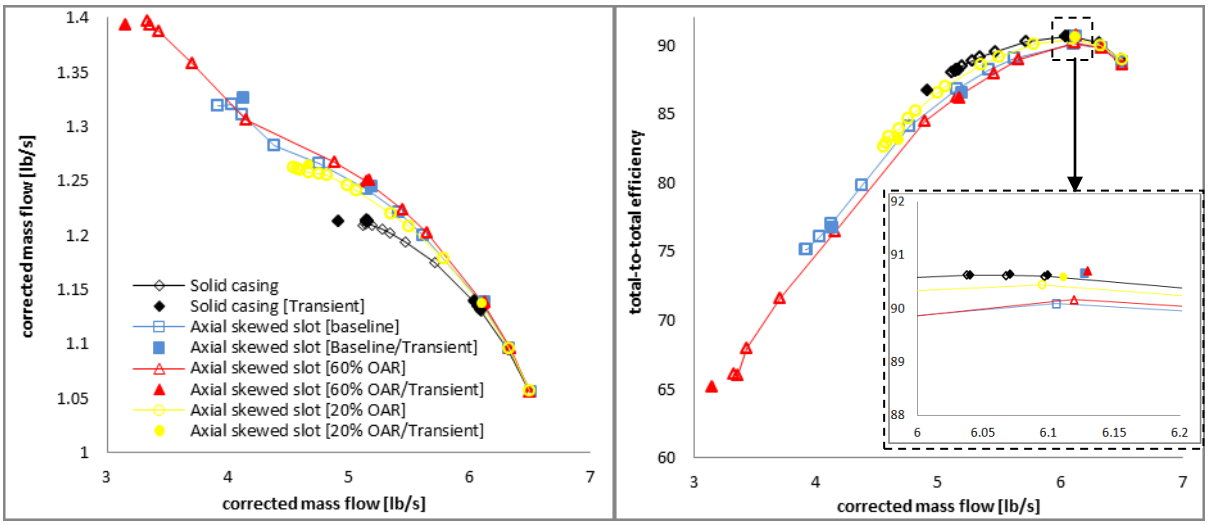

Figure 5.7: Effect of open area ratio on rotor performance

c) Effect of slot skew angle

In this case, the baseline slot skew angle with respect to the radial direction is decreased to 30º, 0º (radial slots) and -30° (opposite blade rotation), as illustrated in figure 5.8. It is worth noting that with the open area ratio held constant, the slot's volume (and its cross-flow area) increases with a decrease in the absolute value of the skew angle. The speedlines are shown in Figure 5.9. The steady-state results point to a significant drop in stall margin with a decrease in skew angle (reaching to almost zero at -30º), while the peak efficiency increases, though just slightly. The limited unsteady simulations corroborate these trends. This suggests that the skew angle should be increased as much as possible in the direction of blade rotation.

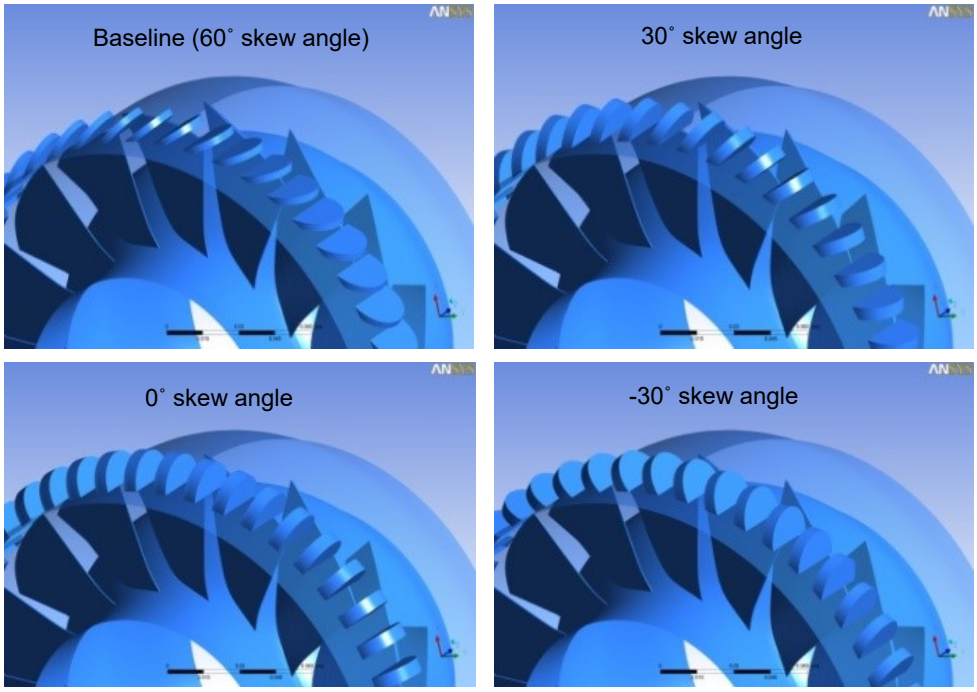

Figure 5.8: Simulated configurations with variation in slot skew angle

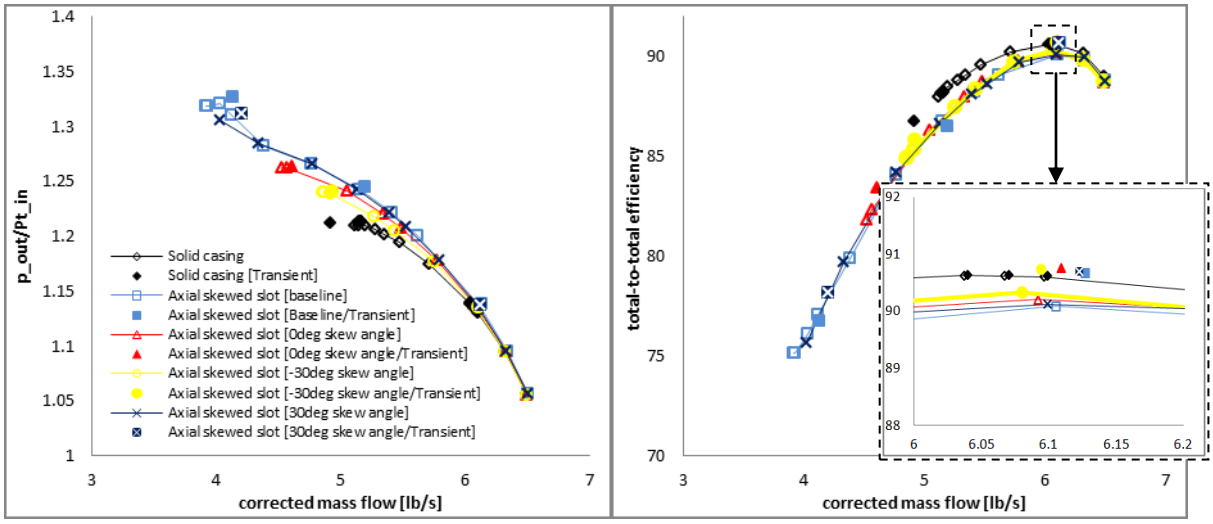

Figure 5.9: Effect of slot skew angle on rotor performance

d) Effect of number of slots per passage

With the number of slots per passage doubled from three to six while maintaining the open area ratio the same (figure 5.10), the CFD results (figure 5.11) show only a slight drop in stall margin

but a small gain in peak efficiency. These results point to a very limited influence of the number of slots on rotor performance and operability. However, it can be speculated that this parameter may have a larger impact at particular conditions if the slots passing frequency matches the natural flow oscillation frequencies in the tip region leading to resonance that may benefit the mixing of the tip clearance flow with the core flow. Nevertheless, such effect would only occur at one particular operating condition for a particular number of slots per passage.

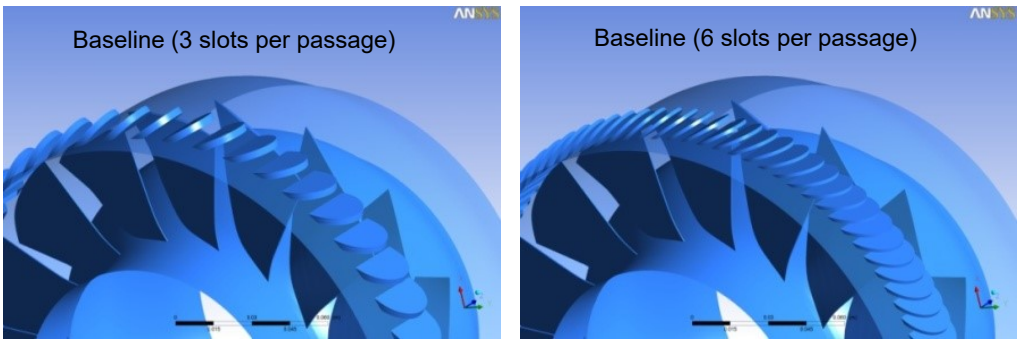

Figure 5.10: Simulated configurations with variation in number of slots per blade passage

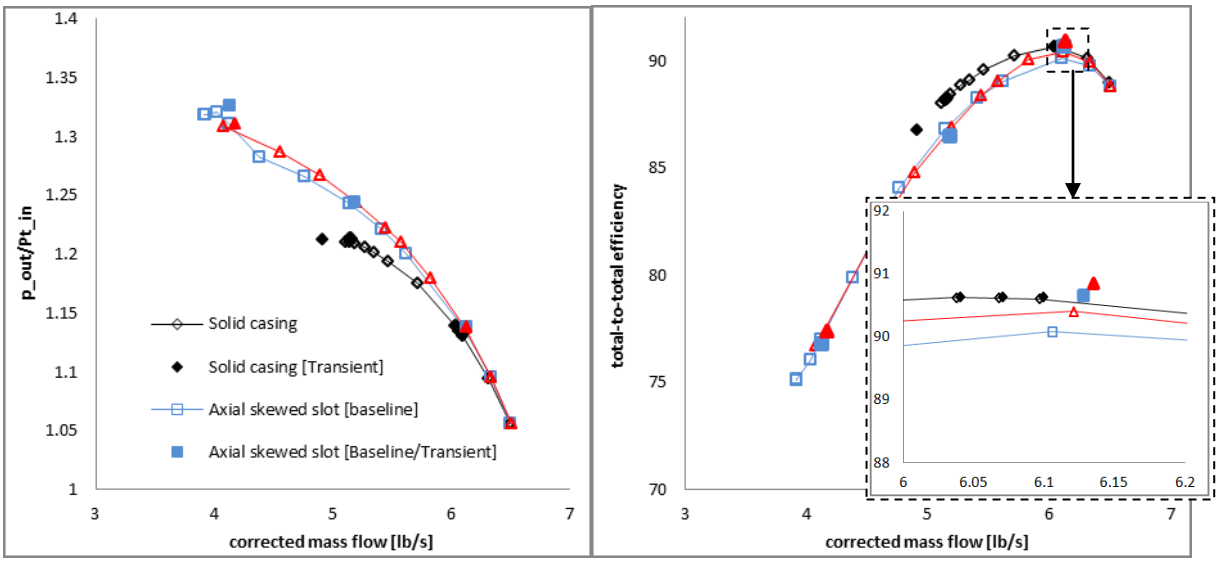

Figure 5.11: Effect of number of slots per blade passage on rotor performance

e) Effect of slot stagger angle

In this case, the angle of the slot with respect to the axial direction is changed. As illustrated in figure 5.12, the "blade angle skew slots" configuration approximately matches the blade tip stagger angle while the "anti-blade angle skewed slots" configuration has the opposite stagger angle. With the circumferential area ratio, axial extent and slot depth unchanged, the slots lateral shape changes from a semi-circle to a semi-ellipse with narrower slot width. As shown in figure 5.13. The results from steady simulations show that changing the slot the stagger slot angle toward that of the blade increases loss in peak efficiency while skewing it in the other direction has the opposite effect. In terms of stall margin, the left most steady points shown in figure 5.13 are not the convergence limits because the actual convergence limits are at a very positive slope making their validity questionable since the exit static pressure boundary condition cannot handle a turnover in back pressure. As such, one cannot make conclusions at this time of the effect of slots stagger angle of the slots on stall margin.

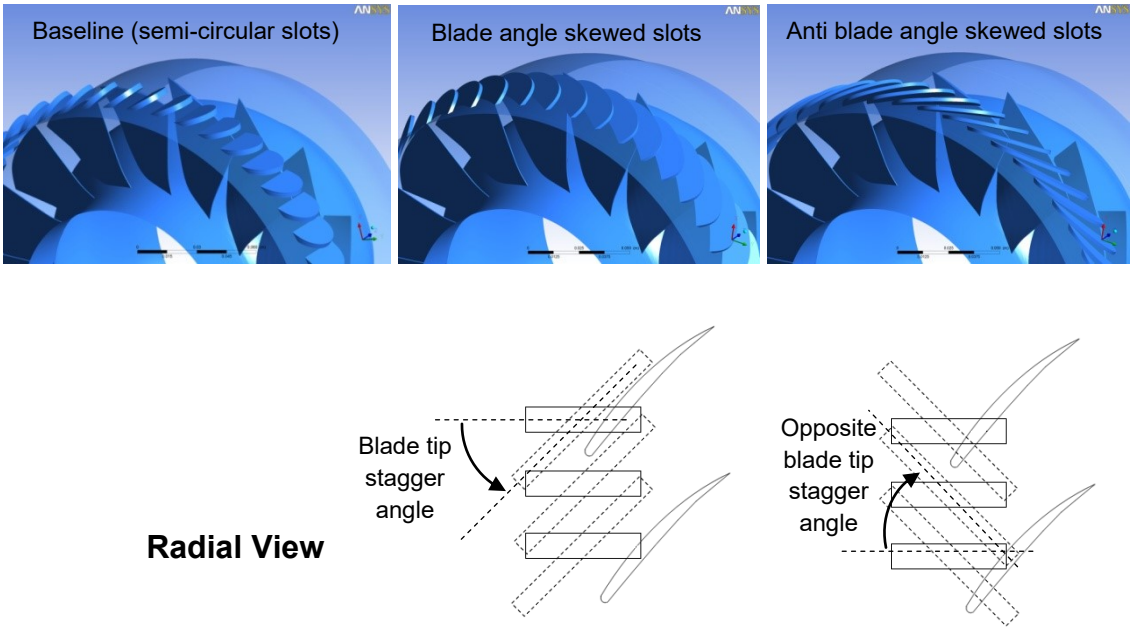

Figure 5.12: Simulated configurations with variation in slot stagger angle

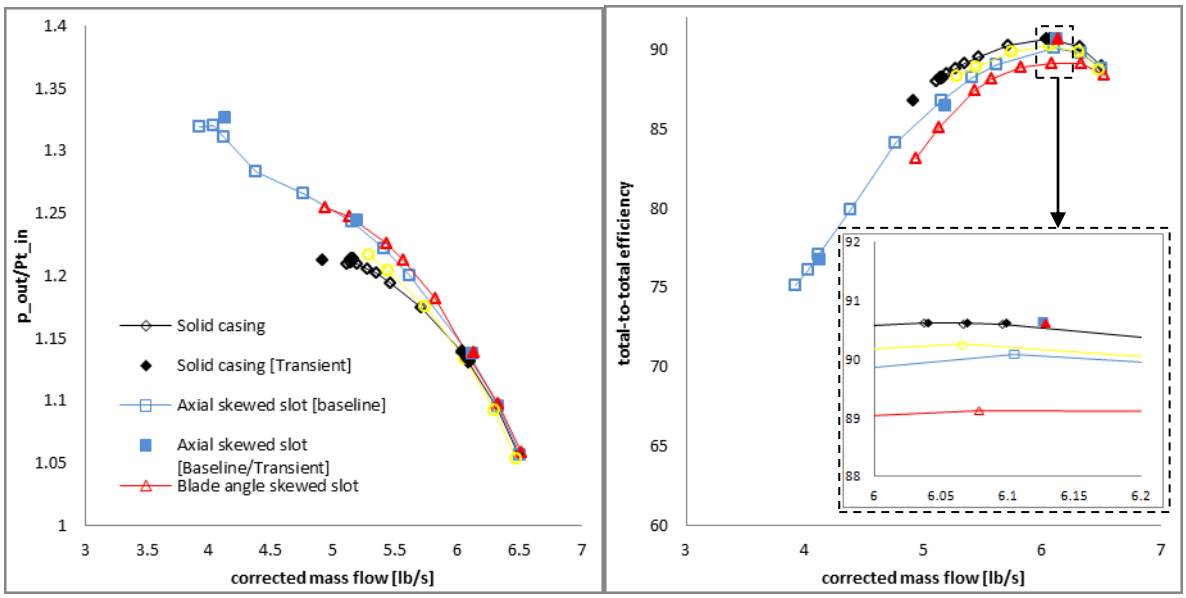

Figure 5.13: Effect of slot stagger angle on rotor performance

f) Effect of radial slot shape

For this parameter, the width of the slot is either decreasing with depth to produce an outwardly convergent slot or increases with depth for an outwardly divergent slot, as illustrated in figure 5.14. The results in figure 5.15 point to this parameter only having a minor positive impact on both stall margin improvement and peak efficiency in either direction of change when compared to the baseline configuration.

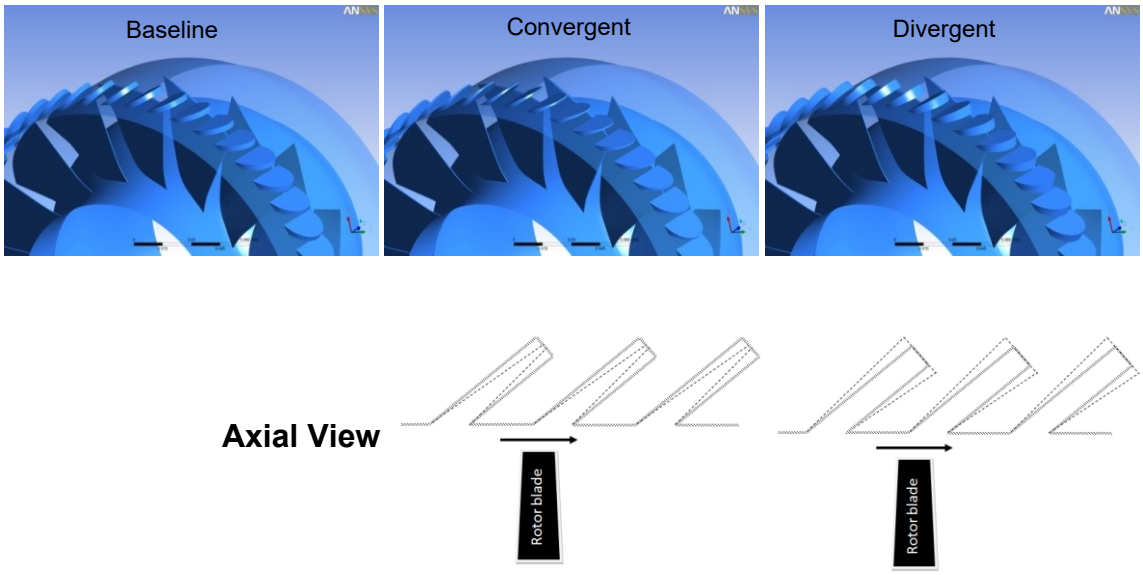

Figure 5.14: Simulated configurations with variation in radial slot shape

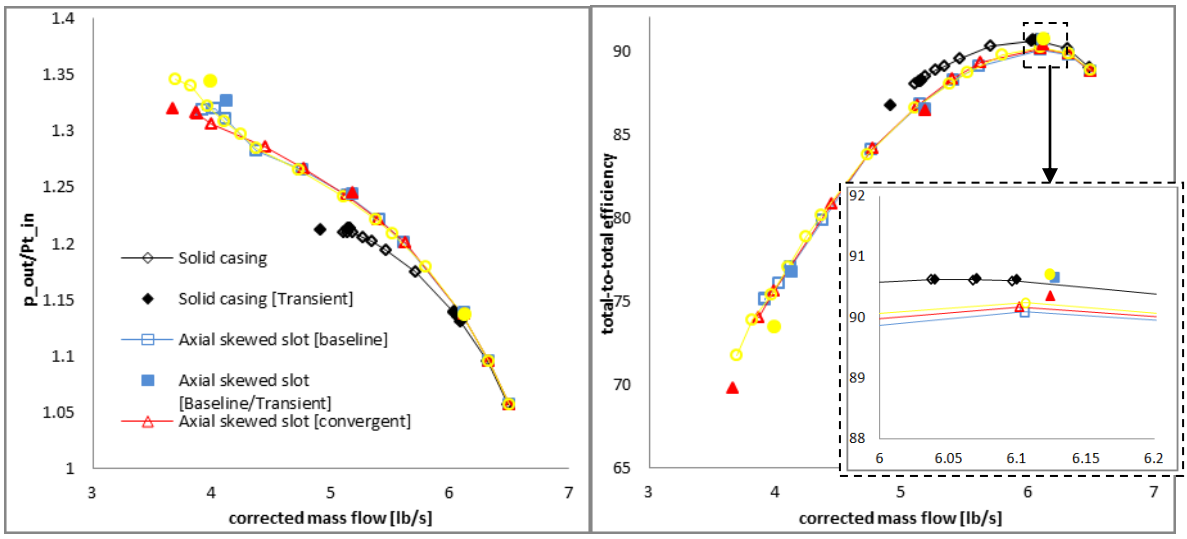

Figure 5.15: Effect of radial slot shape on rotor performance

g) Effect of the lateral slot shape

In this case, the lateral shape of the axial slot is modified from a semi-circle to a rectangle, keeping the slot width and volume constant, which implies a slight decrease in slot depth. The CFD data indicates that this parameter does not have a significant impact on surge margin improvement nor peak efficiency change, at least if the slot symmetry is kept. In the current change from semi-circular to rectangular shapes, the stall margin and efficiency drops a little bit as expected considering the viscous losses from flow recirculation in the corners of the rectangular slots. Whether a smooth non symmetrical slot can more significantly alter the performance is an open question, but the current results point to keeping the slot semi-circular.

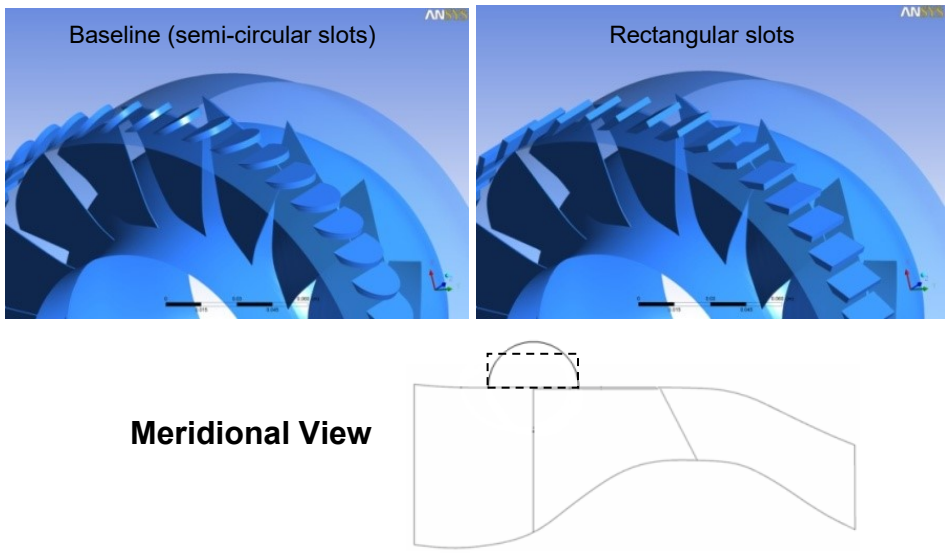

Figure 5.16: Simulated configurations with variation in meridional slot shape

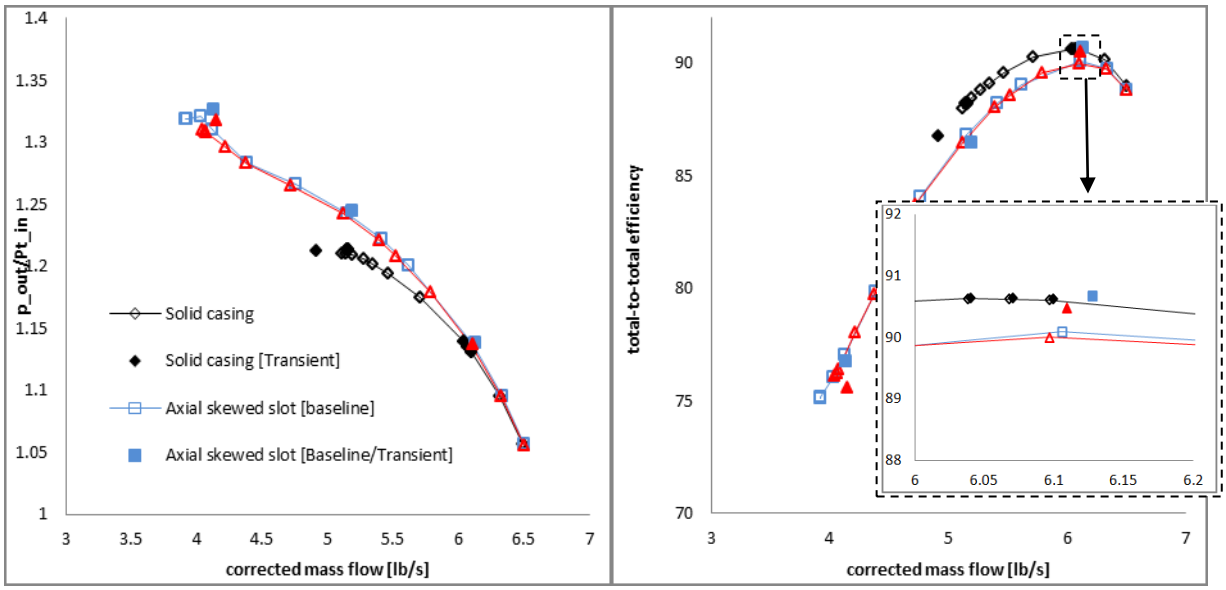

Figure 5.17: Effect of meridional slot shape effects on rotor performance

h) Effect of the slot axial length

To assess the effect of this parameter, the baseline slot length is decreased and increased by 50% while keeping both the mean axial position and the depth constant, thus transforming the lateral shape of the slot from semi-circular to rectangular-semi-circular and semi-elliptical, respectively, as shown in figure 5.18. The data in figure 5.19 shows that the stall margin improvement increases significantly with axial length. Nevertheless, peak efficiency seems to decrease slightly in either direction implying the existence of an optimum slot axial length, which in this case should be around the value of the baseline configuration.

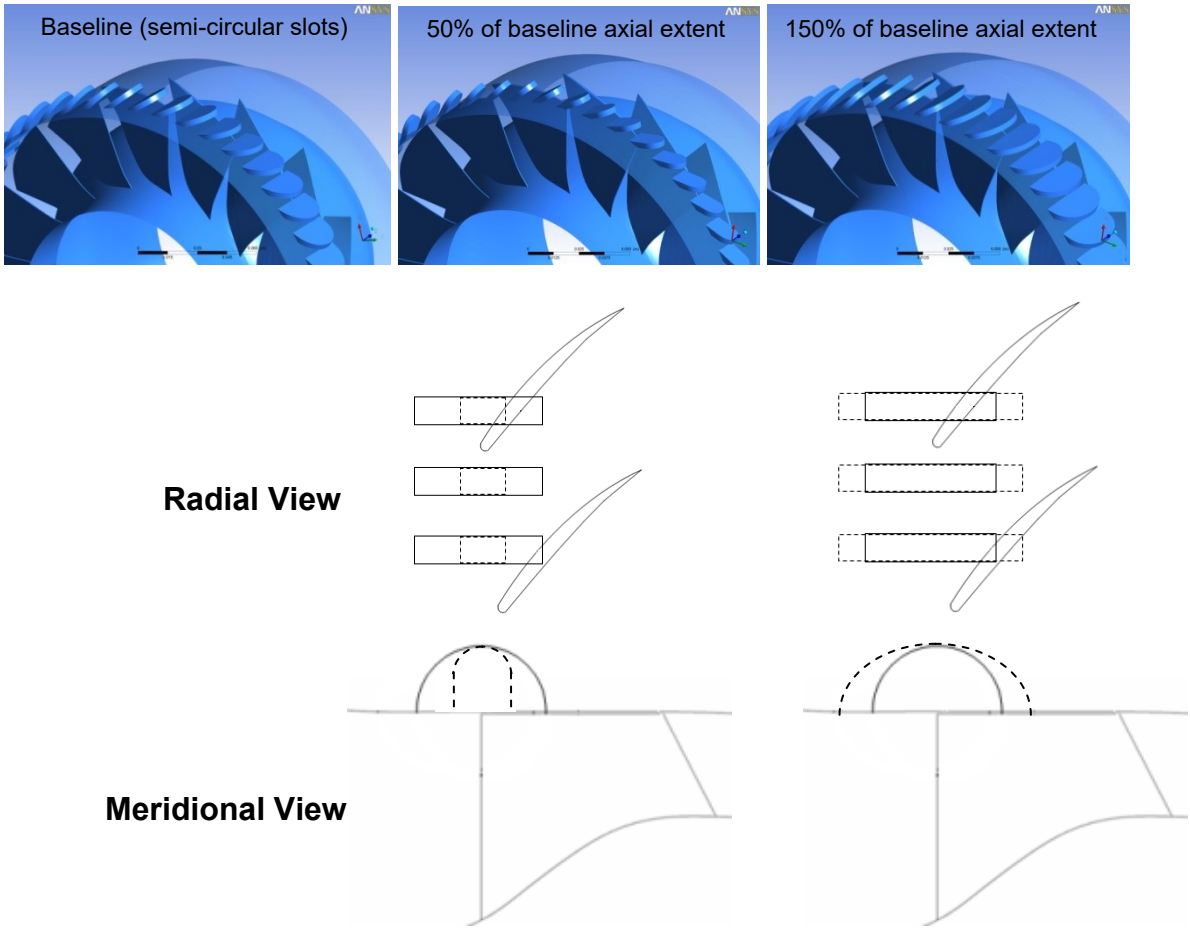

Figure 5.18: Simulated configurations with variation in slot axial length

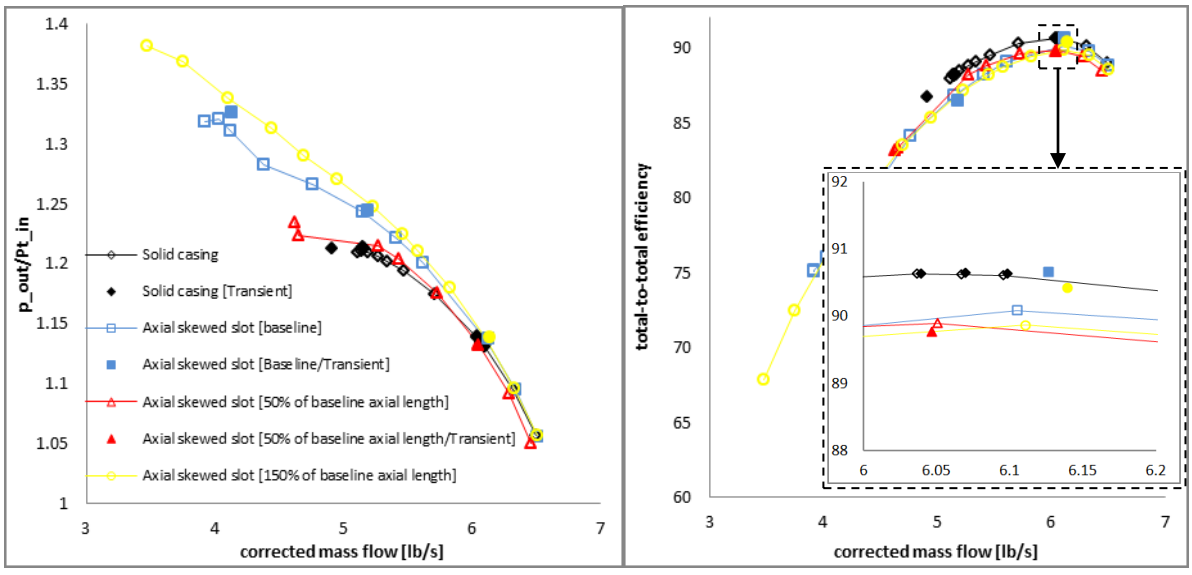

Figure 5.19: Effect of slot axial length on the rotor performances

i) Effect of the slot depth

For depth variation, the two cases with reduced and increased axial length are used as references, as indicated and illustrated in Table 5-1, rather than the baseline skewed slots casing treatment. For the reduced depth case, the reduced axial length casing treatment configuration is reduced in depth by half to bring the rectangular-semi-circular to a semi-circular lateral slot shape with half the nominal (baseline) slot radius. For the increased depth case, the extended axial length casing treatment is increased in depth by 50% to bring it from an elliptical to a semi-circular lateral slot shape with 150% of the nominal (baseline) slot radius. When compared with their respective reference casing treatment configurations, the steady-state CFD results in Table 1 for these new configurations in Table 1 indicate that a decrease in slot depth results in a moderate increase in stall margin improvement and vice-versa. However, the slot depth has virtually no impact on change in peak efficiency.

Table 5-1: Parametric study of casing treatment geometry effects on SM and efficiency (part 1)

Parameter	Configuration	Schematic	Steady		Unsteady	
			ΔSM* [%]	peak efficiency [%]	ΔSM* [%]	peak efficiency [%]
-	Baseline		129.10	-0.53	72.70	0.02
Slot axial position	More upstream		112.19	-0.44	-	-0.47
	More downstream		122.64	-1.04	80.69	-0.43
Open area ratio	60% open area	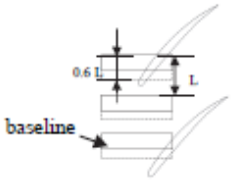	194.09	-0.45	157.58	0.07
	20% open area	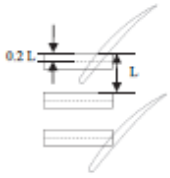	61.89	-0.17	24.65	-0.05

Table 5-2: Parametric study of casing treatment geometry effects on SM and efficiency (part 2)

Parameter	Configuration	Schematic	Steady		Unsteady	
			ΔSM* [%]	peak efficiency [%]	ΔSM* [%]	peak efficiency [%]
Slot skew angle	30° skew angle slots	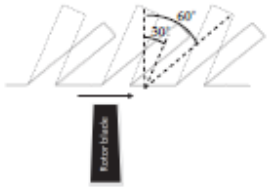	117.57	-0.50	69.73	0.06
	0° skew angle (radial slots)	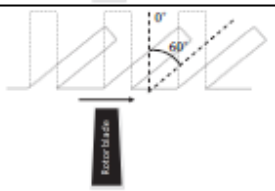	64.11	-0.41	65.86	0.12
	-30° skew angle slots	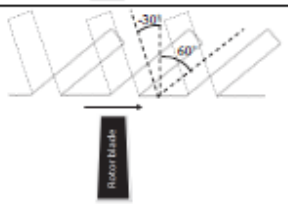	28.64	-0.29	29.97	0.10
Number of slots per blade passage	6 slots per blade passage	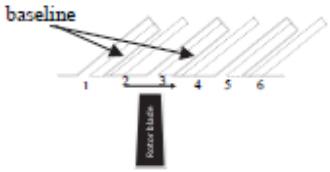	114.28	-0.22	1.59	0.22
Slot stagger angle	Blade angle slots	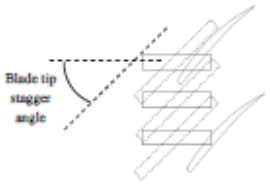	-	-1.49	-	-0.02
	Anti blade angle slots	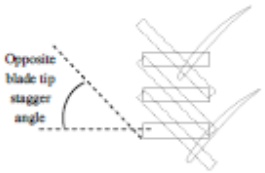	-	-0.36	-	-

Table 5-3: Parametric study of casing treatment geometry effects on SM and efficiency (part 3)

Parameter	Configuration	Schematic	Steady		Unsteady	
			ΔSM* [%]	peak efficiency [%]	ΔSM* [%]	peak efficiency [%]
Radial slot shape	Convergent slots	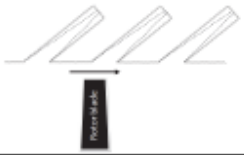	134.00	-0.45	112.31	-0.28
	Divergent slots	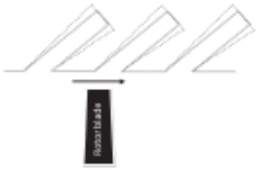	152.90	-0.38	84.39	0.08
Lateral slot shape	Rectangular slots		115.18	-0.62	69.84	-0.16
Slot axial length	50% axial length	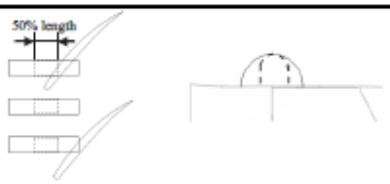	49.40	-0.73	-	-0.87
	150% axial length	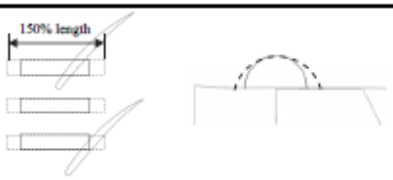	176.05	-0.76	-	-0.22
Slot depth	50% depth (reference: 50% axial length)		74.67	-0.78	-	-0.80
	150% depth (reference: 150% axial length)	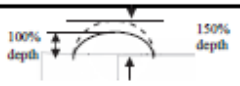	140.89	-0.76	-	-0.31

5.5 Summary and discussion

The main observations from this rather extensive parametric study of slot casing treatment are given below with the most important parameters underlined. These observations provide preliminary rules for optimal slot casing treatment design.

i) Open area ratio: The larger the open area ratio, the more increase in stall margin, accompanied by an initial decrease but then levelling-off in peak efficiency (at least up to 60% open area ratio for this rotor)

ii) Slot skew angle: The larger the skew angle (in the direction of blade rotation) the larger the surge margin improvement but as well as the decrease (though relatively small) in peak efficiency

iii) Slot axial length: The larger the axial length, the larger the improvement in stall margin. Although the effect on peak efficiency is very small, there may be an optimum value for slot axial length in terms of efficiency.

iv) Slot axial position: The impact on the stall margin is minor, but the more downstream the location, the larger the drop in peak efficiency.

v) A decrease in slot depth has a moderate positive impact on stall margin and a negligible impact on peak efficiency change.

vi) Slot shape: either radial or lateral, seems to only have very minor impact on stall margin and peak efficiency.

vii) The results for slot stagger angle variation are not conclusive in term of real stall margin improvement because of speedline turnover. However, the inverse (or anti-blade angle slot has a significant positive impact on peak efficiency change.

For the studied mixed flow rotor, the parametric study yielded a small variation of the baseline casing treatment design, namely the 60% AOR axial skewed slot casing treatment, with a large stall margin improvement (about 20% reduction in stalling mass flow) combined with at least a small gain in peak efficiency both confirmed by unsteady simulations.

A preliminary analysis into the effect of the best casing treatment configuration on the flow field in the rotor tip region was carried out. It indicates that the casing treatment slots increases stall

margin by pushing the incoming/tip clearance flow interface downstream of the rotor tip leading edge plane. It is noted that for the case with casing treatment, the interface can only by seen through the tip clearance flow streamlines because the entropy of the upstream (incoming flow) is corrupted (increased) by high-entropy tip clearance flow recirculated by the slots. Consequently, entropy contours are not a reliable way to show the incoming/tip clearance flow interface. Figure 5.20 plots the time-averaged streamlines emanating from the tip gap at the blade tip surface for the 60% OAR slots casing treatment at the stalling mass flow of the solid casing case. The results clearly show that the incoming/tip clearance flow interface has been displaced downstream into the blade passage by the slots casing treatment.

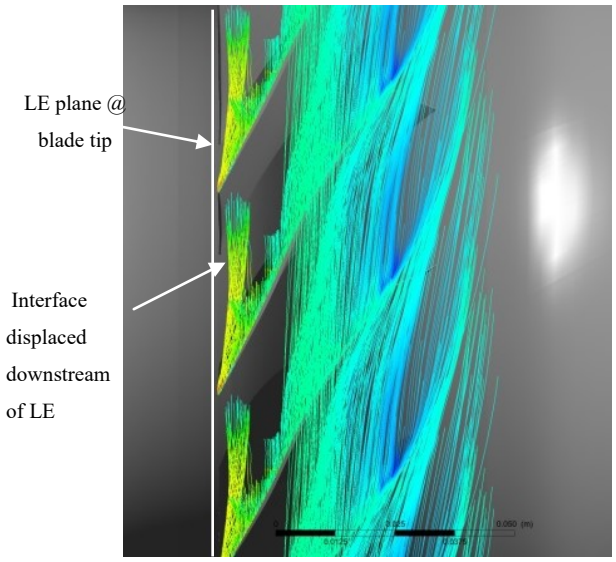

Figure 5.20: Time-averaged tip clearance flow streamlines at blade tip plane for 60% AOR slots casing treatment at solid casing stalling mass flow

However, preliminary quantitative analysis shows a complex unsteady flow with fluctuation in fluid injection and suction at the slots opening. A pattern with regard to the momentum transfer between the slots and rotor blade passage and stall margin improvement/efficiency penalty and the correlations of these factors with the changes in the studied parameters are not immediately obvious. Further work is required to elucidate the details of the flow mechanism associated with stall margin improvement and efficiency penalty/improvement by slots casing treatment and how this mechanism is affected by the design parameters of the slots.

In the absence of the flow mechanism, one can still envision the wider applicability of the results presented in this chapter from an engineering perspective. The parametric study did replicate some of the trends reported in past limited studies of slots casing treatment for axial compressors in terms of the effect of certain parameters, such as axial slot position, skew angle, open area ratio, on stall margin improvement and peak efficiency. This indicates that the preliminary design rules listed above may be generally applicable to both mixed flow and axial compressors.

In terms of the practicability of the proposed strategy as laid out in section 5.3 for extensive parametric study of slots casing treatment to any rotor geometry, one can estimate the reduction in computational time and resources in comparison to traditional method employing strictly unsteady simulations. For the configurations presented in this chapter, a converged solution obtained from an unsteady simulation took on the order of a month on an intel quad-core Pentium processor, whereas the equivalent steady simulation (with frozen-rotor interface) was about up to one hundred times faster. A parametric study of slots casing treatment would require a speedline for the baseline case and two speedlines per parameter studied, and on the order of 10-12 points per speedline. As such, a study such as the one in this chapter, would involve around 200 simulations or 1.5×10^5 CPU-hr if only unsteady simulations were carried out. The proposed method which would involve 10-12 steady simulations and two unsteady simulations would require about 80% less computational time making it much for feasible to do. Furthermore, the ability to practically carry out such extensive parametric study to parameter-related gradients for both stall margin improvement and the loss in peak efficiency that can be used as inputs for an optimizer. This adds to the power of the proposed strategy for practical use in the design of an optimal casing treatment for any compressor geometry on an engineering industrial environment.

CHAPTER 6 CONCLUSION AND RECOMMENDATIONS FOR FUTURE WORK

6.1 Conclusions and contributions

A set of computational studies were carried out on an industrial (aero-engine) mixed flow compressor rotor to determine rotating stall prediction criteria and preliminary design rules for effective casing treatment without peak efficiency penalty in this type of compressor. The main conclusions are provided below:

- For a tip critical mixed flow compressor, the alignment of the incoming/tip clearance flow interface with the leading edge at the rotor plane evaluated on a time-average basis can be used as a prediction for spike rotating stall inception.

- The delay of this criterion delays the stall point in mixed flow compressors

- It is possible to design a casing treatment with substantial stall margin improvement without loss (even small gains) in peak efficiency for tip-critical subsonic mixed flow compressors.

- The slots casing treatment design parameters with the largest impact on stall margin improvement and peak efficiency are: open area ratio, slot skew angle, slot axial length and slot axial position. Larger open area ratio, slot skew angle (in the direction of rotor rotation) axial length tend to increase stall margin. However, larger slot skew angle and more downstream axial location of the slots have negative impact on peak efficiency.

- The slots depth and slot shape seem to have only limited influence on stall margin improvement and peak efficiency.

- Given the similarity in one of the two the stall criterion between axial and mixed flow compressor, it is possible that the above preliminary design rules for slots casing treatment may also be applicable to axial compressors.

- A strategy using many low-cost steady RANS CFD simulations with a *frozen-rotor interface* between the rotor and casing treatment domain coupled with only a few high-cost unsteady URANS CFD simulations to confirm stall margin improvement and peak efficiency change is an effective way to carry out at relatively low cost an extensive parametric study for optimizing casing treatment on any compressor.

The contributions of this research are:

1) Determination of a rotating stall prediction criterion for mixed flow compressors.

2) Establishment of preliminary design rules for a lossless effective casing treatment for a subsonic mixed flow compressor through the most extensive casing treatment parametric study ever attempted.

3) Establishment of a new strategy to carry out extensive parametric study at relatively low cost for casing treatment optimizing.

6.2 Suggestions for future work

Based on the highly promising results of the work above, the list of suggested future work includes the following items:

- Detailed analysis of the stall inception mechanism in mixed flow compressors to see why the other stall prediction criterion did not apply

- Detailed analysis of the effect of casing treatment on the flow in the tip region to elucidate the flow mechanism behind stall margin improvement and peak-efficiency gain/loss and how it is affected by the different casing treatment design parameters

- Extend the casing treatment study to transonic flow regimes

- Perform the casing treatment parametric study on axial compressors to validate the applicability of the proposed design rules to this type of compressors

BIBLIOGRAPHY

[1] N. A. Cumpsty. *Compressor Aerodynamics*. New York: Longman Group, 1989.

[2] B. Lakshminarayana. *Fluid Dynamics and Heat Transfer of Turbomachinery*. John Wiley and Sons, 1996.

[3] F. K. Moore and E. M. Greitzer. *A Theory of Post-Stall Transients in Axial Compression Systems. Part 1: Development of Equations*. *ASME Journal of Engineering for Gas Turbines and Power*, 108(1), 1986.

[4] H. D. Vo. *Role of Tip Clearance Flow in Stall Inception*. Phd Thesis, Massachusetts Institute of Technology, 2001.

[5] J. M. Haynes, G. J. Hendricks, and A. H. Epstein. *Active Stabilization of Rotating Stall in a Three-Stage Axial Compressor*. ASME Journal of Turbomachinery, 116(2), 1994.

[6] H. J. Weigl, J. D. Paduano, L. G. Fréchette, A. H. Epstein, E. M. Greitzer, M. M. Bright, and A. J. Strazisar. *Active Stabilization of Rotating Stall and Surge in a Transonic Single Stage Axial Compressor*. ASME Journal of Turbomachinery, 120(4), 1998.

[7] I. J. Day. *Stall Inception in Axial Flow Compressors*. ASME Journal of Turbomachinery, 115(1), 1993.

[8] H. D. Vo, C. S. Tan, E. M. Greitzer. *Criteria for Spike Initiated Rotating Stall*. ASME Journal of Turbomachinery, 130(1), 2008.

[9] K. L. Suder, M. D. Hathaway, S. A. Thorp, A. J. Strazisar, and M. B. Bright. *Compressor Stability Enhancement Using Discrete Tip Injection*. ASME Journal of Turbomachinery, 123(1), 2001.

[10] C. Nie, G. Xu, X. Cheng, and J. Chen. Micro Air *Injection and Its Unsteady Response in a Low-Speed Axial Compressor*. ASME Journal of Turbomachinery, 124(4), 2002.

[11] A. Deppe, H. Saathoff, and U. Stark. *Spike–Type Stall Inception in Axial–Flow Compressors*. Proceedings of the 6th European Conference on Turbomachinery - Fluid Dynamics and Thermodynamics, Lille, France, 2005.

[12] X. Q. Qiang, M. M. Zhu, and J. F. Teng. *Effect of Circumferential Grooves Casing Treatment on Tip Leakage Flow and Loss in a Transonic Mixed-Flow Compressor*. PTMTS Journal of Theoretical and Applied Mechanics, 51(4), 2013.

[13] J. M. Haynes, G. J. Hendricks, and A. H. Epstein. *Active Stabilization of Rotating Stall in a Three-Stage Axial Compressor*. ASME Journal of Turbomachinery, 116(2), 1994.

[14] Y. Gong, C. S. Tan, , K. A. Gordan, and E. M. Greitzer. *A Computational Model for Short Wavelength Stall Inception and Development in Multi-Stage Compressors*. ASME Journal of Turbomachinery, 121(4), 1999.

[15] D. A. Hoying, C. S. Tan, H. D. Vo and E. M. Greitzer. *Role of blade passage flow structures in axial compressor rotating stall inception*. ASME Journal of Turbomachinery, 121(4), 1999.

[16] U. Stark and H. Saathoff. *Passive and Active Methods to Enhance Axial-Flow Compressor Aerodynamics*. In SPRINGER-VERLAG Notes on Numerical Fluid Mechanics and Multidisciplinary Design, 102(Hermann Schilchting – 100 years), 2009.

[17] J. D. Cameron. *Stall Inception in a High-Speed Axial Compressor*. PhD Thesis, University of Notre Dame, 2007.

[18] C. Hah, J. Bergner, and H. P. Schiffer. *Short Lenght-Scale Rotating Stall Inception in a Transonic Axial Compressor – Criteria and Mechanims*. ASME Turbo Expo, Barcelona, Spain, 2006.

[19] D. C. Prince, D. D. Wisler, and D. E. Hilvers. *Study of Casing Treatment Stall Margin Improvement Phenomena*. NASA CR–134552, 1974.

[20] H. Fujita and H. Takata. *A Study of Configurations of Casing Treatment for Axial Flow Compressors*. Bulletin of JSME, 27(230), 1984.

[21] H. Takata and Y. Tsukuda. *Stall Margin Improvement by Casing Treatment—Its Mechanism and Effectiveness*. ASME Journal of Engineering for Power, 99(1), 1977.

[22] G. D. J. Smith and N. A. Cumpsty. *Flow Phenomena in Compressor Casing Treatment.* ASME Journal of Engineering for Gas Turbines and Power, 106(3), 1984.

[23] P. A. Seitz. *Casing Treatment for Axial Flow Compressors*. PhD Thesis, Cambridge University, 1999.

[24] I. Wilke, H. P. Kau, and G. Brignole. *Numerically Aided Design of a High-Efficient Casing Treatment for a Transonic Compressor*. ASME Turbo Expo 2005, GT2005-68993, June 6-9, Reno-Tahoe, Nevada, USA, 2005.

[25] X. Lu, L. Zhu, C. Nie, and W. Huang. *The Stability-Limiting Flow Mechanisms in a Subsonic Axial-Flow Compressor and its Passive Control with Casing Treatment*. ASME Turbo Expo, Berlin, Germany, 2008.

[26] F. Lin, F. Ning, and H. Lui. *Aerodynamics of Compressor Casing Treatment. Part 1: Experiment and Time-Accurate Numerical Simulation*. ASME Turbo Expo, Berlin, Germany, 2008.

[27] R. Emmrich, H. Hönen, and R. Niehuis. *Time resolved investigations of an axial compressor with casing treatment. Part 1: Experiment. Part 2: Simulation*. ASME Turbo Expo, Montreal, Canada, 2007.

[28] G. Brignole, F. C. T. Danner, and H. P. Kau. *Time Resolved Simulation and Experimental Validation of the Flow in Axial Slot Casing Treatments for Transonic Axial Compressors*. ASME Turbo Expo, Berlin, Germany, 2008.

[29] V. Nezym. *Parametric Investigation of Entire Annular Recess Casing Treatment on Compressor Stable Operation*. ELSEVIER Experimental Thermal and Fluid Science, 29(2), 2005.

[30] M. W. Muller, H. S. Schiffer, and C. Hah. *Effect of Circumferential Grooves on the Aerodynamic Performance of an Axial Single-Stage Transonic Compressor*. ASME Turbo Expo, Montreal, Canada, 2007.

[31] H. Zhang and H. Ma. *Study of Sloped Trench Casing Treatment on Performance and Stability of a Transonic Axial Compressor*. ASME Turbo Expo, Montreal, Canada, 2007.

[32] X. Huang, H. Chen, and S. Fu. *CFD Investigation on the Circumferential Grooves Casing Treatment of Transonic Compressor*. ASME Turbo Expo, Berlin, Germany, 2008.

[33] V. Mileshin, I. Brailko, and A. Startsev. *Application of Casing Circumferential Grooves to Counteract the Influence of Tip Clearance*. ASME Turbo Expo, Berlin, Germany, 2008.

[34] M. D. Hathaway. *Passive Endwall Treatments for Enhancing Stability*. NASA/TM-2007-214409, 2007.

[35] H. Yang. *Unsteady Simulation of a Transonic Compressor Coupled with Casing Treatment*. 11th Annual Conference of the Computational Fluid Dynamics Society of Canada, Vancouver, B. C., Canada, 2003.

[36] H. Behesthi, G. Kaveh, F. Bijan, J. A. Teixeira, and P. C. Ivey. *A New Design for Tip Injection in Transonic Axial Compressors*. ASME Turbo Expo, Barcelona, Spain, 2006.

[37] H. Khelaghi, A. M. Tousi, M. Boroomand, and J. A. Teixeira. *Recirculation Casing Treatment by Using a Vaned passage for a Transonic Axial-Flow Compressor*. Proceedings of the IMechE, Part A: Journal of Power and Energy, 221(8), 2007.

[38] R. G. Giffin and L. R. Jr Smith. *Experimental Evaluation of Outer Case Blowing or Bleeding of Single Stage Axial Flow Compressor. Part 1: Design of Rotor and Bleeding and Blowing Configurations*. NASA CR-54587, 1966.

[39] H. A. Epstein, J. E. F. Williams, and E. M. Greitzer. *Active suppression of aerodynamic instabilities in turbomachines*. AIAA Journal of Propulsion and Power, 5(2), 1989.

[40] Z. S. Spakovszky, C. M. van Schalkwyk, H. J. Weigl, J. D. Paduano, and M. M. Bright. *Rotating Stall Control in a High-Speed Stage with Inlet Distortion*. *Part 1: Radial Distortion*. *Part 2: Circumferential Distortion*. ASME Journal of Turbomachinery, vol. 121(4), 1999.

[41] M. Kefalakis, and K. D. Papailiou. *Active Flow Control for Increasing the Surge Margin of an Axial Flow Compressor*. ASME Turbo Expo, Barcelona, Spain, 2006.

[42] G. Cassina, B. H. Beheshti, K. Albert, and R. S. Abhari. *Parametric Study of Tip Injection in Axial Flow Compressor Stage*. ASME Turbo Expo, Montreal, Canada, 2007.

[43] H. Khaleghi, M. Boroomand, J. A. Teixeira, and A. M. Tousi. *A Numerical Study of the Effects of Injection Velocity on Stability Improvement in High-Speed Compressors*. Procedings of the IMechE Part A: Journal of Power and Energy, 222(2),2008.

[44] B. Roy and S. Veraarapu. *Stability Enhancement and Hysteresis Improvement of Axial Flow Fan by Discrete and Distributed Tip Injection Schemes*. ASME Turbo Expo, Berlin, Germany, 2008.

[45] B. Dobrzynski, H. Saathoff, G. Kosyna, C. Clemen, and V. Gümmer. *Active Flow Control In A Single-Stage Axial Compressor Using Tip Injection And Endwall Boundary Layer Removal*. ASME Turbo Expo, Berlin, Germany, 2008.

[46] X. Lu, W. Chu, J. Zhu, and Z. Tong. Numerical and Experimental Investigations of Steady Micro-Tip Injection on a Subsonic Axial-Flow Compressor Rotor", HINDAWI International Journal of Rotating Machinery, 2006.

[47] S. A. Khalid, A. S. Khalsa, I. A. Waitz, C. S. Tan, E. M. Greitzer, N. A. Cumpsty, J. J. Adamczyk, and F. E. Marble. *Endwall Blockage in Axial Compressors*. ASME Journal of Turbomachinery, 121(4), 1999.

[48] M. Çevik, , O. Uzol, and I. Yavrucuk. *A Robust Design Optimization of a Mixed-Flow Compressor Impeller*. ASME Turbo Expo, Florida, USA, 2009.

[49] N. A. Cumpsty, and J. H. Horlock. *Averaging Nonuniform Flow for a Purpose*. ASME Journal of Turbomachinery, 128(1), 2006.

[50] R. Biollo. *Systematic Investigation on Swept and Leaned Transonic Compressor Rotor Blades*. PhD Thesis, Padova University, 2008.

[51] D. E. Van Zante, A. J. Strazisar, J. R. Wood, M. D. Hathaway, and T. H. Okiishi. *Recommendations for Achieving Accurate Numerical Simulation of Tip Clearance Flows in Transonic Compressor Rotors*. ASME Journal of Turbomachinery, 122(4), 2000.

[52] A.N. Aksyonov and A.B. Shabarov. *Modelling of turbulent flows in transonic axial-flow compressor NASA Rotor 37 with local weak-equilibrium damping of eddy viscosity coefficient*. Springer, Thermophysics and Aeromechanics, 16(4), 2009.

APPENDIX A: VALIDATION OF THE COMPUTATIONAL TOOL SET-UP

A.1 Introduction

This appendix provides additional details on the numerical setup used to carry out the research. It starts with a justification of the selection of the CFD code (ANSYS-CFX) and the turbulence model through published validation results. It is followed by a detailed account of the process followed to obtain the meshes used in chapters 4 and 5. The appendix concludes with the sensitivity study for the number of time steps used in unsteady simulations for this rotor. While the effort was made to apply best practices to get as accurate a solutions as possible, it is worth re-iterating that the aim of the present work is geared toward capturing the trends associated with the stall inception criteria and the overall effect of casing treatment slots geometry variation rather than accurately resolving the spatial and temporal fine details with finer meshes along with the extra computational resources which is, at some level of mesh density, limited by turbulence models.

A.2 Code selection

The main reason for choosing ANSYS-CFX as the CFD tool for carrying out this research was that it was suggested by the industrial sponsor. However, CFX is an efficient and well-known tool for turbomachinery CFD simulations as proven by its extensive use in both industry and academia. CFX has been validated for different types of rotating turbomachinery by many research groups against experiments, especially on a transonic rotor [50, 52] which is more relevant to this study. Figures A.1 and A.2 compares the CFD simulations by Biollo [50] using CFX (with two common turbulence models) for a transonic compressor rotor, known as NASA Rotor 37, with experimental measurements of relative Mach number at 70% and 95% span near the design point. These results demonstrates clearly the capacity of CFX to capture quite well important flow structures, namely the normal shock-boundary layers (BL) interaction as well as the interaction between the tip leakage (TL) flow and shock waves inside the blade passage.

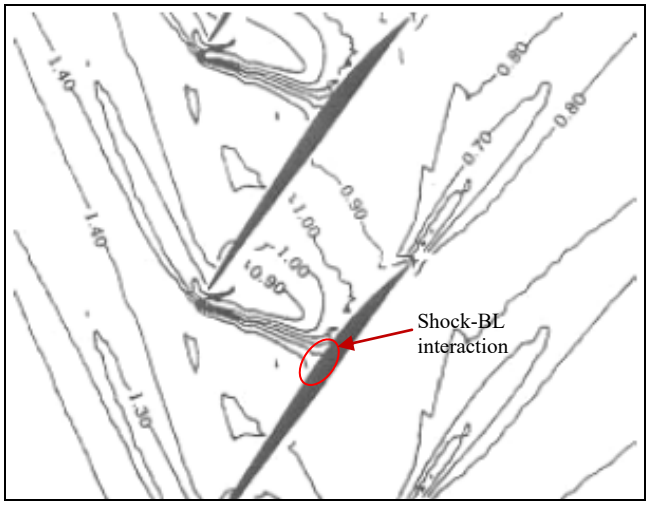

a) Experimental results (Suder 1998)

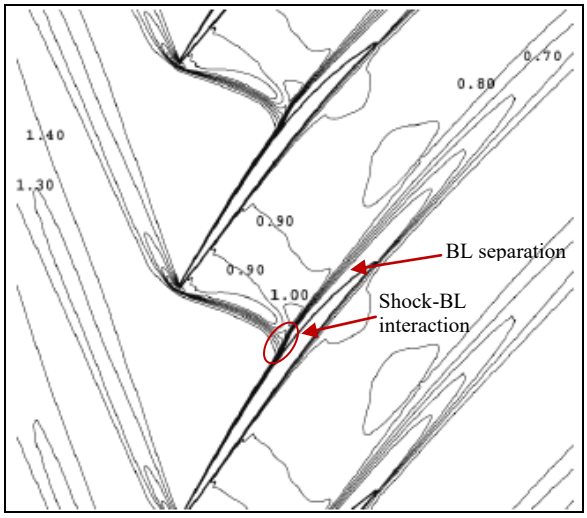

b) K-ε turbulence model

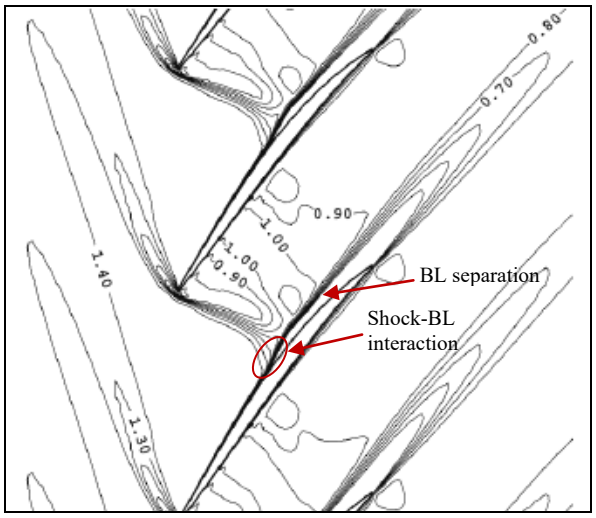

c) SST k-ω turbulence model

Figure A.1: Contours of relative Mach number at 70% span, 92% of choked mass flow operating point (near-stall point) [50]

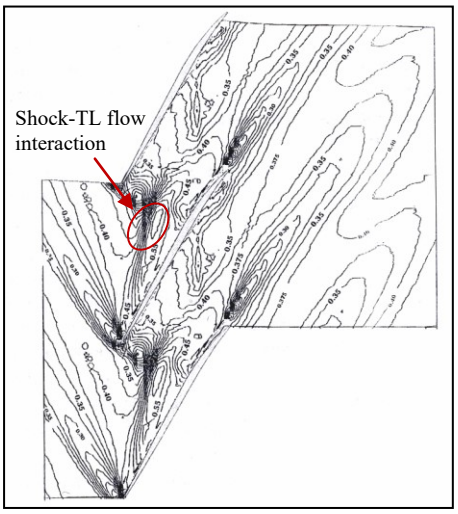

a) Experimental results

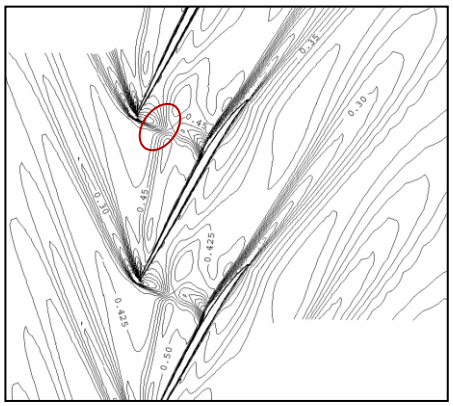

b) k-ε turbulence model

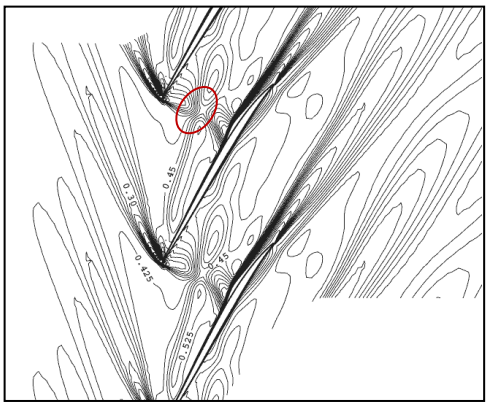

c) k-ω SST turbulence model

Figure A.2: Contours of relative Mach number at 95% span, 98% of choked mass flow operating point (near peak efficiency point) [50]

A.3 Turbulence model selection

Figures A.1 and A.2 also provide an assessment of the two main two-equations, and commonly used, turbulence models available in ANSYS-CFX, namely k-ε and Shear Stress Transport k-ω (SST). The SST turbulence model is well known to be relatively accurate to predict the separated boundary layer under adverse pressure gradients. Figure A.1 shows that the SST turbulence

model better captures the flow deceleration after the shock as indicated by the resulting relative Mach number contours downstream of the shock, which better match the experimental results when compared to those predicted by the k-ε turbulence model.

On the other hand, the flow in the blade tip region is dominated by the interaction between the high-turning tip leakage flow with the shock wave, which is quite challenging for two-equations turbulence models known for their limited ability to capture curvature and rotation effects [2]. However, figure A.2 shows that both turbulence models capture this effect quite well. Based on these results, the SST turbulence model was selected for the current work as it performs as well in the tip region and better than the k-ε turbulence model at lower spans.

A.4 Mesh setup

This section describes the procedure and reasoning followed to arrive at the different meshes used in chapters 4 and 5. It starts with the mesh study that led to the original mesh used for the stall criteria assessment simulations. It follows with the setup of the mesh for the micro tip injection study. Finally, it describes the process leading to the mesh used for the casing treatment simulations.

A.4.1 Mesh for stall criteria assessment

A mesh study was carried out at the start of the project to produce a mesh suitable for the research. It was carried out at 100% speed prior to the shift of the computational study to 65% speed. A single computational domain containing the rotor passage with upstream and downstream ducts as described in section 3.2 was meshed using Turbo-grid. Since the tip clearance flow is a central feature of this study, the mesh in the tip clearance region was produced in consideration of the work by Van Zante et al. [51]. These authors recommended refining the mesh near the shroud, as shown in figure A.3, by radially clustering the grid toward the casing for adequate resolution of the wall-bounded shear layer which results from a difference in the direction between the tip clearance jet and the shroud-wall velocity in the relative reference frame, as depicted in figure A.4, which is found to have a major impact on the trajectory of the primary clearance flow. They also concluded that the clearance gap itself is not important to include and a simple model of non-gridded tip clearance is sufficient with smaller gap-height to simulate the vena-contracta effect due to viscous boundary layer blockage at the blade tip, since

the leakage flow through the gap does not experience a significant loss in the relative total pressure or direction change due to the small blade tip thickness of the high speed compressors. In the end, Van Zante et al. used 12 radial nodes for a tip clearance gap of 0.014 inch (compared to a tip clearance of 0.010 inch for the present rotor)

Following the above approach, four different mesh sizes were generated for the mesh study, having 800K, 400K, 200K and 100K nodes, as shown in Table A.1. In the tip clearance, the radial mesh is clustered near the casing, as suggested by Van Zante et al.. However, instead of guessing the value of the vena-contracta effect to produce an effective small tip clearance, it was decided to also cluster the mesh near the blade tip surface in order to have the physical tip clearance size and let the simulation capture this effect.

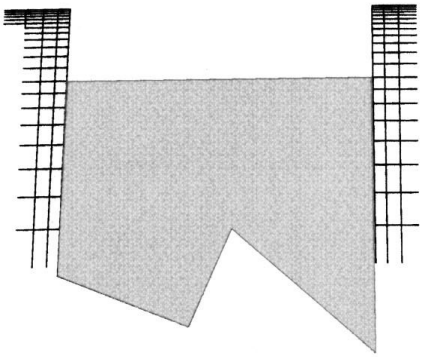

Figure A.3: Mesh resolution near the casing shroud [51]

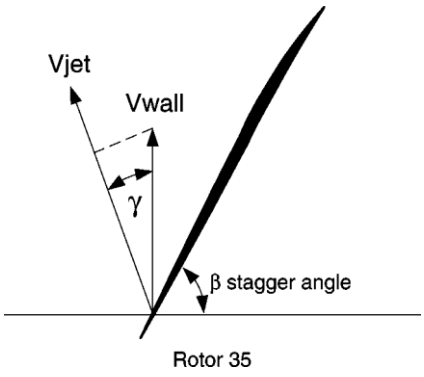

Figure A.4: Difference between the tip clearance jet and the wall speed [51]

Figure A.5 plots the speedlines for the four meshes as obtained from steady-state simulations. In addition, figure A.6 compares the circumferentially mass-averaged total pressure and total temperature profiles at the trailing edge plane for the last converged point on the speedline for each mesh. The results show an asymptote occurring at about 400K nodes. Thus, the 400K mesh in Table A.1 served as the basis to generate the new mesh shown in figure 4.1 to assess the spike stall inception criteria. In this new mesh, the number of radial nodes in the tip clearance was increased significantly above the mesh density used by Van Zante et al. [51] to ensure highly accurate capture of the tip clearance flow behavior.

Table A-1: Different blade passage and tip clearance mesh densities

Total number of nodes	Radial nodes in the tip clearance	Grid distribution
100K	7	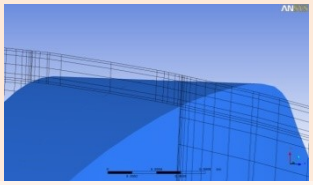
200K	7	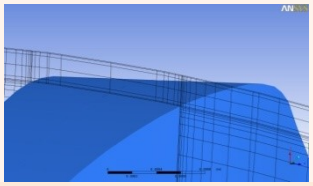
400K	9	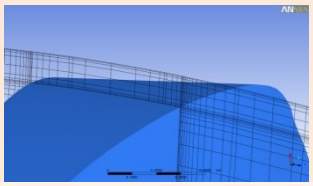
800K	13	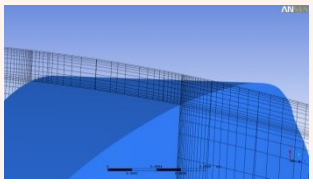

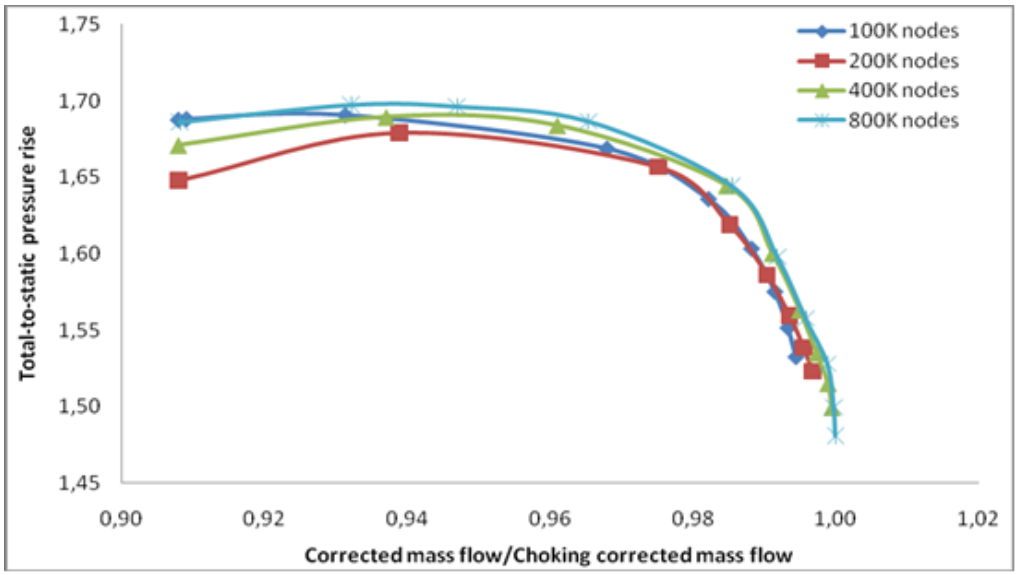

Figure A.5: Total-to-static characteristic of the mixed flow rotor at design speed with different mesh densities

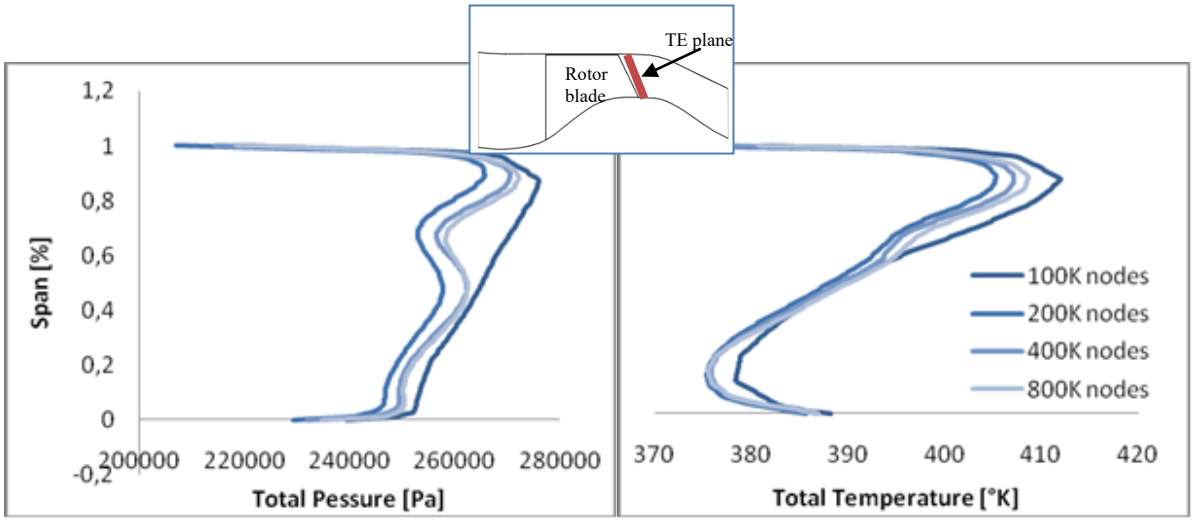

Figure A.6: Circumferentially mass-averaged total pressure and total temperature profiles at the trailing edge plane with different meshes at near stall

A.4.2 Mesh setup for micro tip injection

Initial attempt at micro tip injection were carried out with a mesh that combined an upstream stationary subdomain containing the micro-injectors and a rotating downstream rotor subdomain using a Turbo-grid mesh based on the 400K mesh from section figure 4.1, with a sliding plane

interface between them. The mesh of the rotor subdomain has a high mesh density near the blades but much lower near the middle of the passage, whereas the mesh density on the upstream subdomain was highest around the tip injector. Consequently, there is a significant discontinuity in circumferential mesh density between the two subdomain when the injector is not in front of the blade leading edge, as illustrated in figure A.7, resulting in unacceptable numerical diffusion of the flow across the interface. However, an increase in the circumferential mesh density of both domains to resolve this problem would make an already long simulation even less manageable in terms of time and resources.

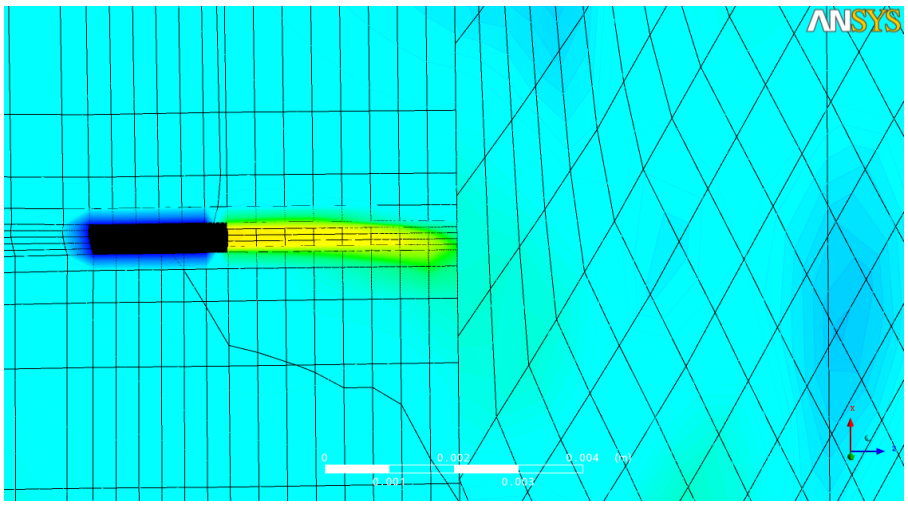

Figure A.7: Axial velocity contour and mesh near interface between injector and rotor subdomains

To remedy this situation, a new mesh philosophy was created with higher mesh density only in the region where it is needed to capture the pertinent flow physics, namely the rotor leading edge tip region. Since it was previously determined that this rotor is tip critical at 65% speed, with no hub nor blade boundary layer separation, the computational domain was divided into many blocks as was shown in figure 4.7 (the discontinuity between the mesh at the boundary of the blocks being managed by the GGI interface method), with high density grid applied only to the blocks associated with the injector and blade tip leading edge while the grid in the rest of the domain is kept as coarse as possible. The goal is to minimize the total mesh size to save

computational time, which is pivotal for the time-consuming transient numerical studies. With Turbo-grid incapable of creating such an unconventional grid, the mixed-flow rotor was re-meshed using ICEM-CFD of ANSYS. A structured multi-block topology consisting of I-blocks for the inlet and outlet and a main H-grid girdling an O-block was used for the rotor blade passage. The result is an unconventional mesh with about 95,000 nodes. Figure A.8 compares the initial conventional mesh shown in figure 4.1 with the new unconventional mesh obtained here for micro tip injection simulations. The new mesh was almost three times faster to run than the conventional 400K mesh. The computational cost associated with the many GGI interfaces between the blocks could explain why the new mesh does not run four times faster despites have about 25% of the node count.

Figure A.9 compares the entropy contours at the blade tip for the last converged solutions with the unconventional mesh with those of the conventional mesh from section A.4.1. The results show that the stall criterion identified in section 4.2, namely that the incoming tip/clearance flow interface lines up with the leading edge plane, is captured by the new mesh. This means that the new mesh is adequate to be used for evaluating the impact of tip micro jet injection on the stall criterion and the stall point.

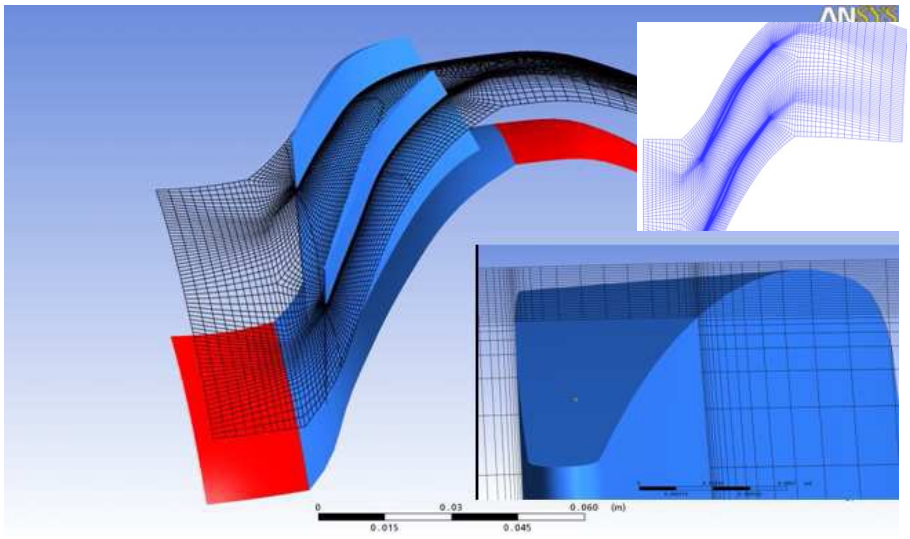

a) Conventional mesh

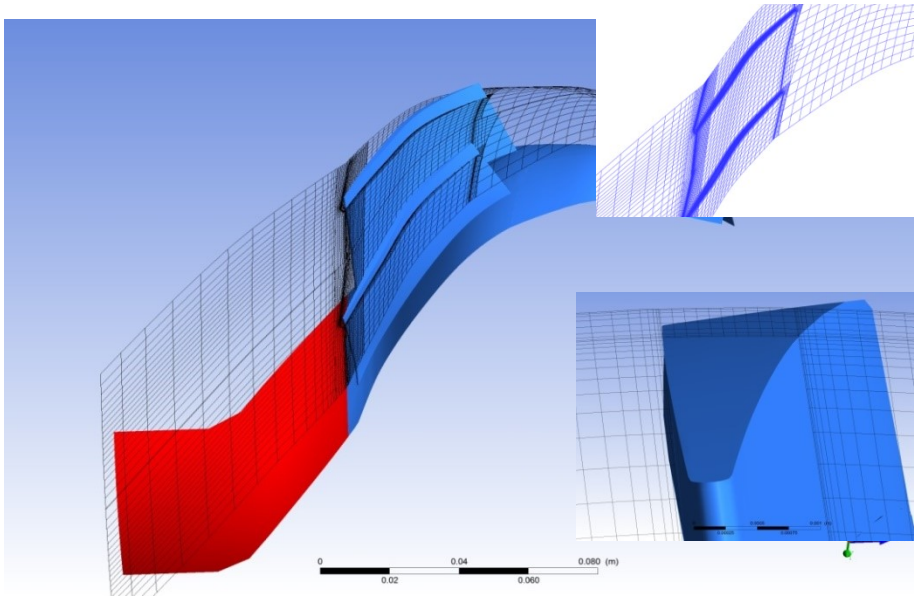

b) Unconventional mesh

Figure A.8: Blade passage and clearance gap mesh details for both conventional (400K nodes) versus new unconventional (95K) preliminary and simulated meshes

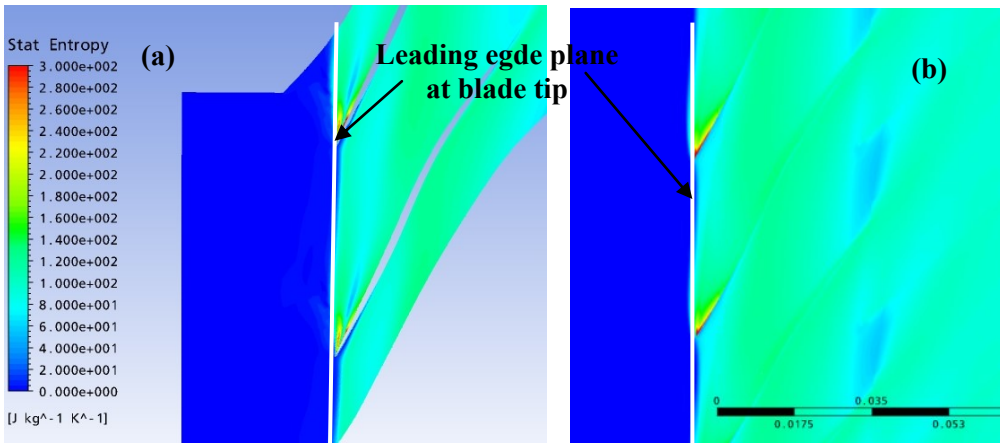

Figure A.9: Entropy contours at the mixed flow rotor tip with new mesh at the last converged point (a) with conventional mesh and (b) with the new unconventional mesh

A.4.3 Mesh setup for casing treatment study

The simplest computational domain strategy for the casing treatment simulations would have been to place meshed slots over the unconventional rotor domain mesh described in section A.4.2 with a fluid-solid-fluid interface (similar to what was done in reference [35]) where the slots sub-domain slides directly on the casing shroud surface in the relative frame. However, preliminary trials showed problems with adequate transfers of momentum between the two sub-domains. Consequently, a safer strategy was selected in which the slots/rotor interface was offset 25% of tip clearance height inward from the shroud such that a fluid-fluid interface can be used between the two sub-domains, as illustrated in figure 5.2. In addition, the use of a fine mesh in the rotor sub-domain based on the 400K nodes conventional mesh in figure 4.1 ensured that there is enough mesh density everywhere to adequately capture the flow interaction between the slots and rotor passage which covers a larger spatial extent that was the case for the localized micro tip injectors. Both sub-domains used structured meshes that were generated with ICEM-CFD. The grid topology for this mesh is already described in chapter 5. Figure A.10 shows the mesh in the tip gap which has 16 radial nodes, which is a bit less than the number of radial nodes (21) in the mesh of figure 4.1 but still surpasses the mesh density used by Van Zante et al. [51].

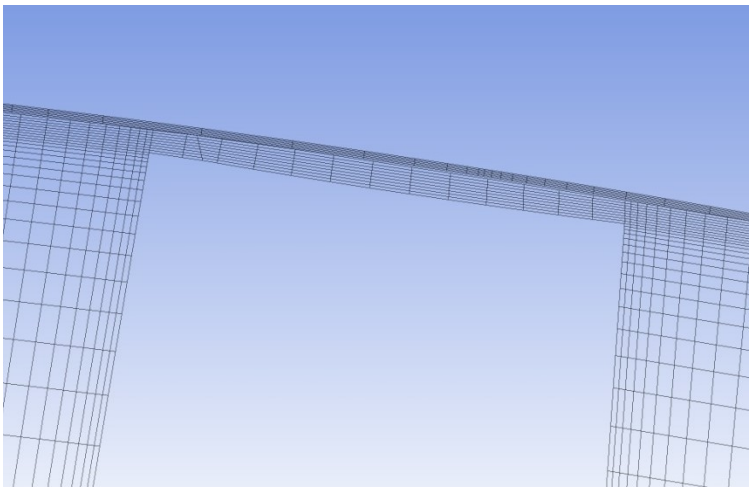

Figure A.10: Radial nodes distribution in the tip gap for the mesh used for casing treatment study

In choosing a meshing strategy for the mesh inside the slots, an O-H-grid type is preferred over the simpler O-grid to avoid severe mesh cells skewness present at the center of the slots. The mesh is clustered toward the slanted walls to capture the viscous boundary layers developing in the flow through the slots. Figure A.11 shows the mesh for slots corresponding to the 60% OAR case in chapter 5. It must be noted that the slots are designed to be manufactured with a milling disk cutting at an angle to the casing. This is the reason for observation from figure A.11b that the leading and trailing edges of the casing slots are not straight lines.

While an explicit mesh study was not carried out for the slots, it was ensured that the final mesh had adequate y+ values at the walls of the slots to correctly capture the viscous shear layers near the slots wall. Figure A.12 plots the y+ contours at the walls of the slots and show that it is around 10, which is less than the y+ values for the walls in the blade passage.

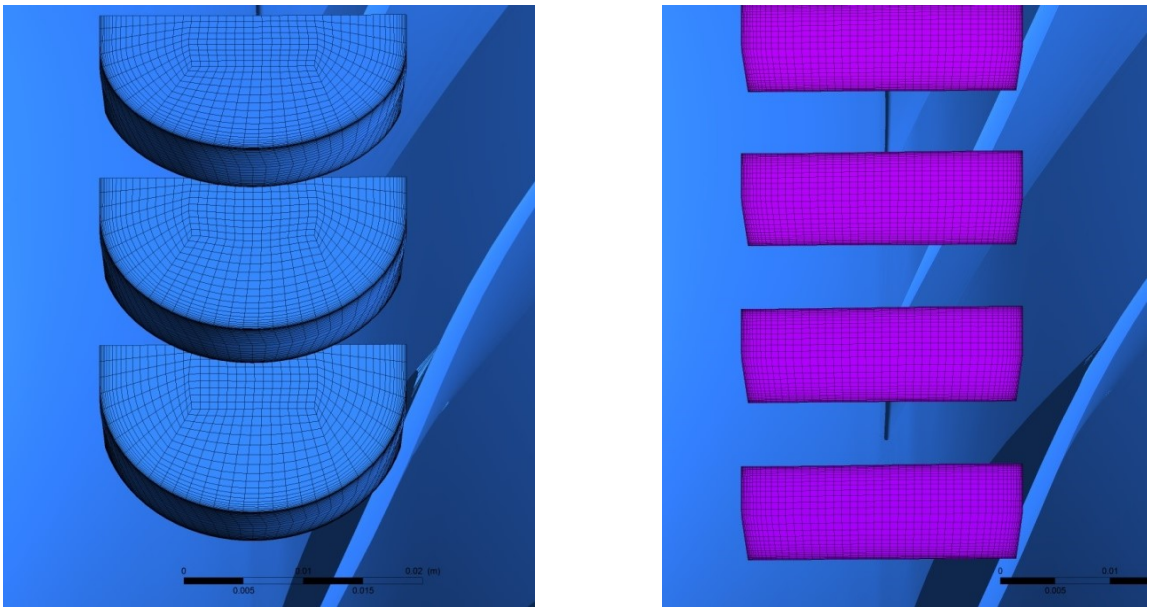

a) Slots' side wall mesh (top view)

b) Slots' opening mesh (bottom view)

Figure A.11: Meshing of the casing treatment slots

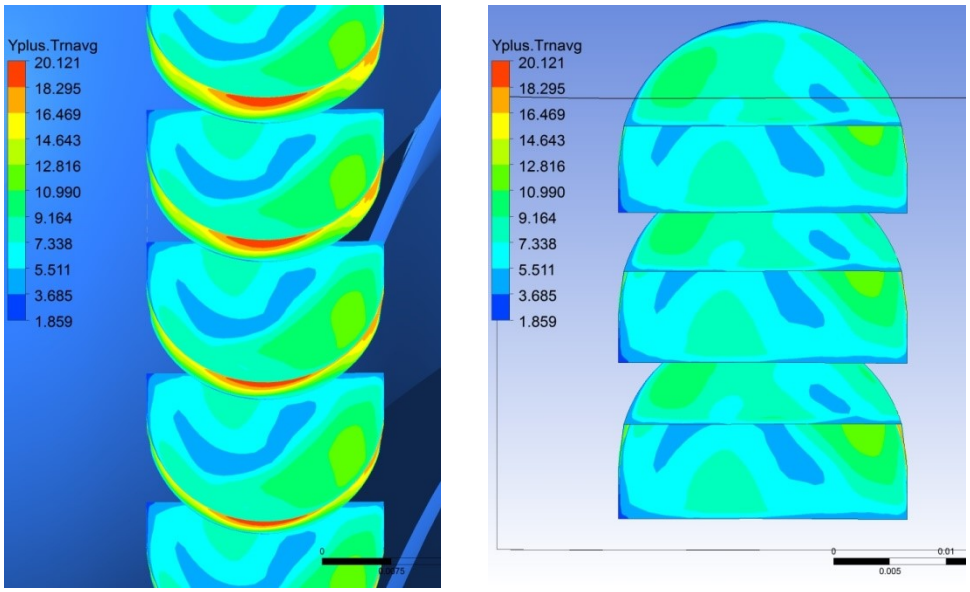

b) Top view

a) Bottom view

Figure A.12: Contours of y+ on casing treatment slot walls

A.5 Time step selection

There are two dominant time scales when simulating non-axisymmetric casing treatments. The first is the blade passing period which is equal to the time for a given blade to rotate one blade pitch. The second is the slot passing time which is equal to the time for a given blade to rotate over one slot pitch. The latter time scale is more critical as the number of slots is usually greater than the number of rotor blades (the slot passing time is lower than the blade passing time).

The initial time step selection was based on published casing treatment simulations validated against experimental data. Lu et al. [25], used 6.66 time steps for each slot passing time (40 time steps per blade passing period with 6 slots for each blade pitch) for simulating casing treatment over a subsonic axial compressor. Their predicted loss in peak efficiency and increase in stall margin match experimental data quite well. Emmerich et al. [27] computed a highly subsonic axial compressor using 8 time steps per slot passing time (144 slots for 16 rotor blades) and predicted the measured loss in peak efficiency. These results suggests that about 8 time steps per slot passing is adequate to capture the overall effects of casing treatments compressor performance. Given that the main casing treatment configuration in this study has three slots per blade passage, a round number of 25 time steps were selected.

To further ensure the adequacy of the selected time step, a parametric study was carried with 25, 50 and 100 time step per blade passing for the 60% OAR case at the peak efficiency point. Figures A.13 and A.14 plots the numerical pressure signal taken at two points inside a slot over two blade passing periods (the location of the points are illustrated on the upper right corner of each figure). The results demonstrate that the pressure is almost insensitive above 25 time steps per blade passing. It is thus concluded that 25 time steps per blade passing period (8.33 time steps per slot passing time) is adequate.

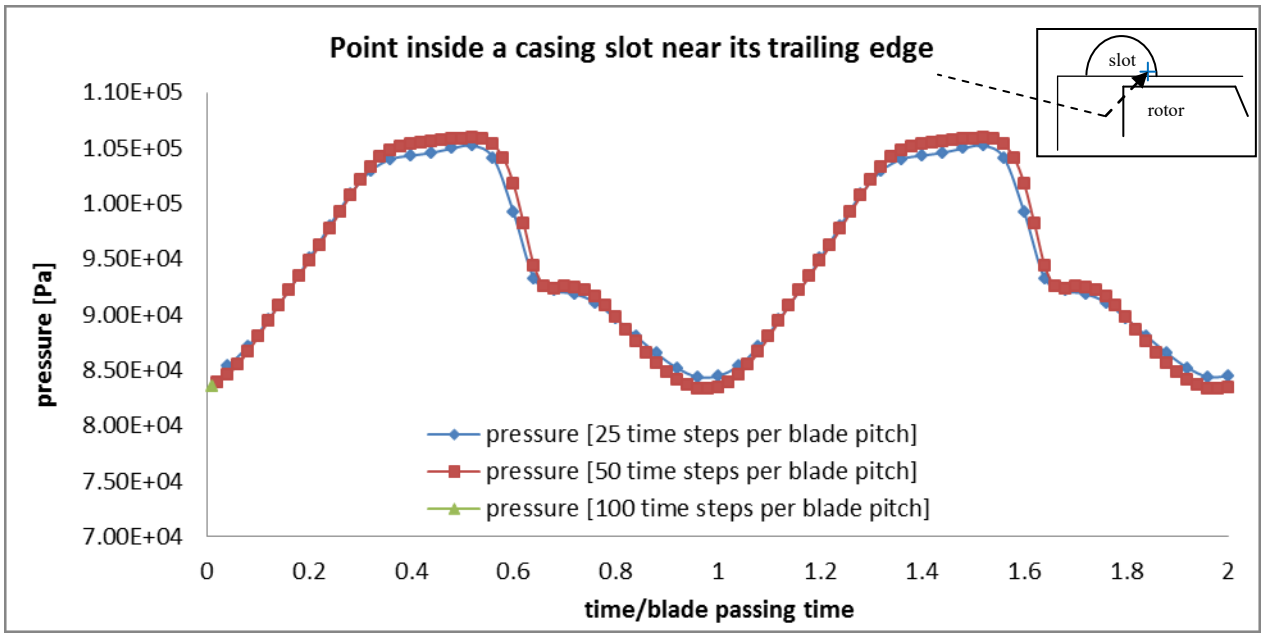

Figure A.13: Temporal pressure signal from one spatial point located inside the casing slot near its leading edge

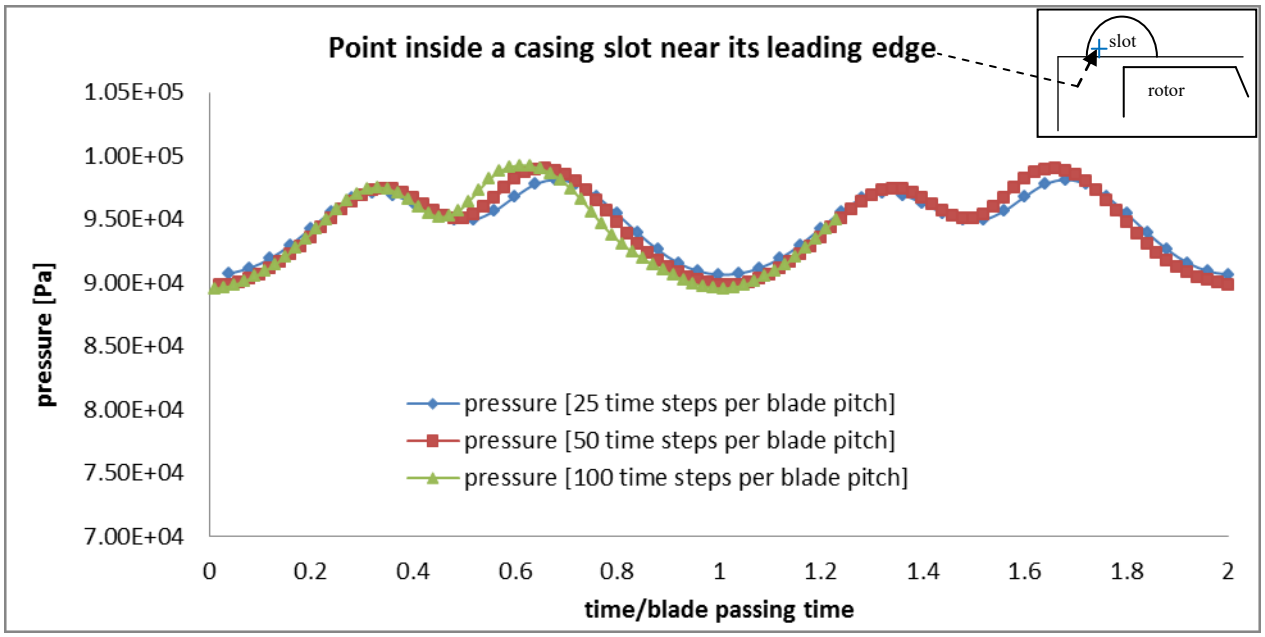

Figure A.14: Temporal pressure signal from one spatial point located inside the casing slot near its leading edge